UARI Research Report No. 64

DETERMINATION OF MODAL DAMPING FOR LAUNCH VEHICLES USING EXPERIMENTAL DATA

by

R. R. Reed

THE APOLLO STRUCTURAL DAMPING STUDY

Final Technical Report

This research work was supported by the
National Aeronautics and Space Administration
under contract NAS8-21110"B"

University of Alabama Research Institute

Huntsville, Alabama

February 1969

UARI Research Report No. 64

DETERMINATION OF MODAL DAMPING FOR LAUNCH VEHICLES USING EXPERIMENTAL DATA

by

R. R. Reed

THE APOLLO STRUCTURAL DAMPING STUDY

Final Technical Report

This research work was supported by the
National Aeronautics and Space Administration
under contract NAS8-21110"B"

University of Alabama Research Institute
Huntsville, Alabama

February 1969

ABSTRACT

During the dynamics tests of the Saturn V - Apollo vehicle sufficient data was obtained to evaluate the modal damping forces. However, the use of this data was limited to the choice of a linear damping force. The result was that variations in the computed values of linear damping from different tests could not be explained. In this study both linear and nonlinear damping forces are investigated. To accomplish this required the development of analytical and empirical techniques not presently available in the literature. It also required some conditioning of the raw experimental data. The conclusion is that a nonlinear damping force will yield results much more consistent than those using linear damping. Numerical values are given for the first two modes of two Saturn V - Apollo configurations. Considerable differences between resonant amplitudes using linear damping compared with nonlinear damping are noted when the results are extrapolated to force levels above those used in the tests. Linear viscous damping is shown to be very conservative as far as the structure is concerned.

TABLE OF CONTENTS

		Page
List of Tables		ii
List of Figures		iii
Nomenclature		v
Chapter I.	Introduction	1
Chapter II.	The Saturn V Vehicle and Its Dynamic Parameters	3
	2.1 The Saturn V Tests	4
	2.2 Modal Equations of Motion	10
	2.3 Modal Damping and Energy Dissipation	15
	2.4 Hysteretic Representations of Damping	18
	2.5 Modal Versus Sub-system Damping	23
Chapter III.	Analysis of Test Data and Linear Damping Force	25
	3.1 Conditioning of Experimental Test Data	26
	3.2 Linearized Data and Damping Coefficient	48
Chapter IV.	Determination of a Nonlinear Damping Force	57
	4.1 From Variable Linear Damping Coefficients	58
	4.2 From Amplitude Versus Frequency Plots	65
	4.3 From an Equivalent Energy Dissipation Function	84
Chapter V.	An Empirical Method to Determine Damping Force	91
	5.1 The Polynomial Representation of Energy Loss per Cycle	92
	5.2 Program to Compute Damping Coefficients	95
	5.3 Numerical Results for Empirical Damping	99
Chapter VI.	Summary and Conclusions	107
	6.1 Modal Damping Force Summary	107
	6.2 Experimental Test Data Summary	110
	6.3 Conclusions	112
References		115

LIST OF TABLES

Table		Page
2.I	Analytical Representation of Damping	16
2.II	Energy Losses - Sinusoidal Response	17
3.I	Conversion of Raw Test Data to Nodal Displacements	28
3.II	Modal Parameters from Tests	35
3.III	Second Mode Amplitude and Phase Angle	40
3.IV	Pitch and Yaw Second Mode Values and Linear Damping Coefficient	55
4.I	Saturn V Vehicle Yaw Tests (Configuration II)	60
4.II	Damping Coefficient, Amplitude, and Energy Loss for First and Second Modes	61
4.III	Damping Term for Different Cases of Damping	69
4.IV	Errors in Using Damping Coefficients Obtained from One Sweep to Predict Other Amplitudes - First Mode	82
4.V	Percent Variation in Damping Coefficients Calculated from Various Sweeps - First Mode	83
5.I	Damping Coefficients from Energy Terms	94
5.II	Numerical Results for Check-out Data	101
5.III	Computed Energy Loss and Percent Deviation for Rough Modal Data	104
5.IV	Computed Energy Loss and Percent Deviation for Principle Pitch Data	106

LIST OF FIGURES

Figure		Page
2.1	Saturn V, 500-D Pitch Test Time Point 2 (Configuration I) Typical Displacement Configuration Determined For First Mode	8
2.2	Saturn V, 500-D Yaw Test Time Point 11 (Configuration II) Typical Displacement Configuration Determined for First and Second Modes	9
2.3	N-Degree-of-Freedom Mathematical Model	11
2.4	Hysteresis Loops for Typical Linear and Nonlinear Damping Characteristics	20
2.5	Analytical Approximation of Slip Damping Hysteresis by Velocity Squared Damping	22
3.1	Accelerometer Record of the Configuration I Vehicle Tip Motion During Pitch Testing	27
3.2	Tail Displacements Versus Frequency - Second Mode	31
3.3	Sine of Tail Phase Angle Versus Frequency - Second Mode	32
3.4	Rigid-Body Rotation of Vehicle	37
3.5	Tail Node and Second Mode Phase Angles	41
3.6	Modal Amplitude Versus Frequency - Second Mode	42
3.7	Single-Degree-of-Freedom Model with Planar Coupling	43
3.8	Rotation to Principle Pitch and Yaw Axes	49
3.9	Energy Input Per Cycle - Second Mode	54
3.10	Principal Pitch and Yaw Modal Amplitudes Versus Frequency-Second Mode	56
4.1	Linear Damping Coefficient as a Function of Resonant Amplitude - First Mode	63
4.2	Linear Damping Coefficient as a Function of Resonant Amplitude - Second Mode	64
4.3	Typical Amplitude Versus Frequency Ratio Curve	68
4.4	Displacement Versus Frequency Ratio Squared, Cases I - IV.	72

Figure | Page

4.5 Displacement Versus Frequency Ratio Squared, Case V . . . 73

4.6 Phase Angle Versus Frequency Ratio Squared 74

4.7 Horizontal Difference (δ) Versus Amplitude - First Mode . 76

4.8 Vertical Difference (ϵ) Versus Amplitude - First Mode . . 77

4.9 Maximum Percent Error at Constant Amplitude Between Damped and Undamped Curves 81

4.10 Resonant Force Versus Amplitude 87

5.1 Energy Loss Versus Amplitude and Frequency 94

NOMENCLATURE

A	amplitude of any one modal displacement
A_1	limiting amplitude before slip occurs
A_j	modal amplitude in the j^{th} mode
$A_{j\bar{p}}$	modal amplitude in principal pitch plane, j^{th} mode
$A_{j\bar{y}}$	modal amplitude in principal yaw plane, j^{th} mode
A_m	resonant amplitude at any one mode
A_{mj}	resonant amplitude at the j^{th} mode
A_{mr}	resonant modal amplitude for the r^{th} modal force
C	damping coefficient for planar motion
C_i	coefficients of the i^{th} damping force
C_{tj}	rigid-body and adjacent mode tail amplitude correction, j^{th} mode
E	computed input energy supplied to the system
$\bar{E}$	actual input energy supplied to the system
F_d	symbolic representation of damping force
F_e	any one equivalent modal force amplitude
F_{ej}	equivalent force amplitude for the j^{th} mode
F_{er}	resonant equivalent modal force
F_p	input force in the vehicle pitch plane
$F_{\bar{p}}$	input force in the principal pitch plane
$F(t)$	time varying forcing function
$F_{\bar{y}}$	input force in the principal yaw plane
$\underset{\sim}{F}$	nodal force matrix
$\underset{\sim}{F_e}$	equivalent modal force matrix
I	rigid-body rotational inertia
K	slope of slip hysteresis curve initially

K_1	slope of slip hysteresis curve after slippage
K_j	modal stiffness of j^{th} mode
K_p	modal stiffness in vehicle pitch plane
$K_{\bar{p}}$	modal stiffness in principal pitch plane
K_T	rigid-body spring stiffness
K_y	modal stiffness in vehicle yaw plane
$K_{\bar{y}}$	modal stiffness in principal yaw plane
K_{py}, K_{yp}	coupled stiffness terms between pitch and yaw
$\mathcal{L}_i$	normalized damping coefficient
M	any one modal mass
M_j	modal mass of j^{th} mode
Q	any one modal displacement
$\underset{\sim}{Q}$	modal displacement vector
Q_j	modal displacement in the j^{th} mode
R	distance from center of rotation to tail node
S	the Laplace transform variable
X	amplitude of any nodal point
X_t	pitch amplitude at the vehicle tail
X_t^R	amplitude of rigid-body tail node displacement
Y	any nodal amplitude in yaw
Y_t	yaw amplitude at the vehicle tail
a_i	coefficients of energy terms in the energy polynomial
f_n	natural forcing frequency in cycles per second
g	acceleration due to gravity at sea level
[k]	stiffness matrix
[m]	matrix of nodal masses m_i

p	vehicle pitch axis or plane
$\bar{p}$	principal vehicle pitch axis or plane
$p(t)$	modal displacement in vehicle pitch plane
r_j	ratio of forcing to natural frequency, j^{th} mode
$r_{j\bar{p}}$	frequency ratio for principal pitch motion, j^{th} mode
$r_{j\bar{y}}$	frequency ratio for principal yaw motion, j^{th} mode
t	the independent variable time
$\underset{\sim}{x}$	nodal displacement vector
x_i	displacement of the i^{th} node
x_t^B	bending displacement of the tail node
x_t^R	rigid-body displacement of tail node
y	vehicle yaw axis or plane
$\bar{y}$	principal vehicle yaw axis or plane
$y(t)$	modal displacement in vehicle yaw plane
Γ	gamma function
Δw	energy loss or input energy
θ, β	the angles between vehicle axes and principal axes
Φ	phase angle between force and displacement
Φ_j	phase angle for the j^{th} mode
Φ_{2t}	phase angle for tail node near the 2^{nd} mode
$\Psi_n(t)$	harmonic functions to approximate $Q(t)$
α	coefficient of damping force, $C_5 = C_1\alpha$
β, B	a ratio of gamma functions

γ	rigid-body rotation angle
δ	horizontal difference on amplitude frequency curve
ϵ	vertical difference on amplitude frequency curve
$\eta = r_j$	ratio of forcing frequency to natural frequency
ξ_j	linear damping factor for the j^{th} mode
$[\phi]$	mode shape or transformation matrix
ϕ_{ij}	modal displacement of m_i in the j^{th} mode
$\phi_k(Q_j)$	the energy loss functions in the computer program
ω	frequency of the input force
ω_j	natural modal frequency for the j^{th} mode
$\omega_{j\bar{p}}$	natural frequency in principal pitch plane, j^{th} mode
$\omega_{j\bar{y}}$	natural frequency in principal yaw plane, j^{th} mode
ω_n	any one natural modal frequency
ω_p	natural frequency in vehicle pitch plane
$\omega_{\bar{p}}$	natural frequency in principal pitch plane
$\omega_{py} = \omega_{yp}$	natural frequency from coupled stiffness terms
ω_R	natural frequency of rigid-body rotation
ω_y	natural frequency in vehicle yaw plane
$\omega_{\bar{y}}$	natural frequency in principal yaw plane

CHAPTER I

INTRODUCTION

The purpose of this report is to investigate the system damping of a large launch vehicle with its payload; in particular the Saturn V - Apollo system. No logical explanation has been given to the reported damping values previously obtained from dynamic test and analysis. There are reasons for this. First, the experimental test data has not been conditioned or modified. Only the test records that are accurate should be used. Secondly, engineers have not accounted for sources of damping other than the linear viscous damping commonly used. Finally, the analytical techniques for determining the system damping from experimental data have not been perfected to the point that a rigorous analysis of the data can be performed. Each of these reasons for the reported inconsistent values of damping are eliminated in this final report.

The particular vehicle configurations that were studied are discussed in the second chapter. They are the Saturn V - Apollo vehicles; Configuration I at time point two and Configuration II at time point eleven, as simulated in the dynamic test tower at the Marshall Space Flight Center. The lumped parameter or modal approach for studying this continuous system is reviewed and the fundamentals of energy dissipation and hysteretic damping are introduced in this chapter.

Conditioning of the experimental test data is explained in the third chapter. It is shown that test records occur which may contain undesirable effects, and the desirable data must be filtered or separated out. Test records containing principal pitch and yaw modal coupling are conditioned so that uncoupled data is obtained. With data which has been conditioned, one can determine modal damping coefficients that are more accurate than those previously available. These coefficients are still based on linear viscous damping and are shown to be frequency dependent.

To be able to decide what analytical representations of damping (including nonlinear forms) can best describe modal damping, additional test data must be used. The energy loss per cycle,or energy dissipation, is easily obtained for this purpose. In chapter four the energy loss per cycle is used along with other test records on amplitude and frequency to obtain nonlinear representations of damping. This requires new analytical techniques to be used with the resulting nonlinear modal equations. Three such techniques are introduced and discussed in detail.

An empirical method to determine modal damping is shown in chapter five. This technique uses a polynomial in amplitude and frequency to describe modal energy loss per cycle. Terms of this polynomial are directly related to modal damping forces, and damping coefficients are easily determined from the coefficients of the energy loss polynomial. Energy loss coefficients are obtained from a computer program which fits the polynomial to the set of energy loss values obtained from tests.

A summary of analytical results and the resulting conclusions are discussed in chapter six.

CHAPTER II

THE SATURN V VEHICLE AND ITS DYNAMIC PARAMETERS

It is the purpose of this chapter to place in perspective the type of vehicles of concern,and what analytical techniques can be used on such vehicles. One must constantly be aware of what type of test data has been collected and how it can best be utilized. However, if a particular analytical approach appears to be useful, it will be explored with the hope that desirable experimental test data may be available in the future.

From the standpoint of expense and time involved with obtaining test data, a maximum amount of information is desired from a minimum amount of test data. Thus, only a few dynamic parameters are obtained from the tests. How these parameters interface with analytical techniques is quite important. Of particular interest is the interface that permits one to determine the damping of the vehicle system.

Furthermore, it is desirable to see whether linear viscous damping is a reasonable approximation to system damping. Other nonlinear representations of damping are known to exist and may be predominant. Energy dissipation is a dynamic parameter directly related to system damping; and this fact is utilized to a great extent throughout this study. Also, it is desirable to know the sub-system or component damping based on what the total vehicle damping is.

2.1 The Saturn V Tests.

The dynamic test vehicle (DTV) is the Saturn V vehicle. The Saturn V Dynamic Test Program was conceived by the George C. Marshall Space Flight Center at Redstone Arsenal in 1962. The primary objective of this program was to obtain structural dynamic data from a test specimen,the 500-D vehicle, representingas closely as possible the Saturn V vehicle and its flight environment. A knowledge of these structural dynamic characteristics was required for the flight control system design, for the determination of vehicle loads, and for the verification of propulsion system stability on the Saturn V flight models. The test was also intended to verify the analytical methods and results used in flight simulation analyses of the Saturn V vehicle.

The vehicle was supported in a semi-free condition using a unique six degree of freedom oil/gas suspension system with restraining springs for rigid body lateral and roll stability. This gave the vehicle essentially no restraint in the horizontal direction and very soft spring support in the vertical direction. In addition to the hydrodynamic supports, the vehicle support system included two sets of lateral stabilizing springs. Both sets were located as close as possible to the mean nodal point locations so that they would restrain the vehicle as little as possible during flexible body bending modes. The upper stabilizing system consisted of 16 springs attached tangentially so that they would also provide the roll restraint necessary to keep the vehicle centered during roll testing. The entire vehicle was enclosed in a 400 foot steel tower to provide access to the vehicle and to minimize the effects of the weather on the test. The vehicle was excited using 10,000 pound capacity electrodynamic shakers oriented to excite pitch, yaw, roll, and longitudinal motions. Accelerometers and rate gyros were used for the primary data instrumentation.

At the conclusion of each test, rapid data validation was achieved by use of the digital computer for data reduction. Analysis of the data was immediately performed to declare the test data valid or to declare the need for retest.

The final step in the Test Program was the correlation by The Boeing Company of the test data with their analytical data and the subsequent projection of the dynamic characteristics to flight control design [1].*

The test vehicle itself was a full scale Saturn V vehicle (500-D) built to flight vehicle specifications. Where deviations from these specifications occurred, the deviations were designed so as not to change the overall dynamic response of the vehicle. For example, the engine mass simulators were designed to represent the mass and center of gravity location of the flight article very closely (within five percent). The vehicle consists of (1) the propulsion stage, the booster rocket containing the S-IC, S-II, and S-IVB stages, (2) the instrument unit (IU) which houses the primary flight control and guidance systems, (3) the payload which consists of the command and service modules, and (4) the lunar excursion module simulator. The full test vehicle was approximately 365 feet high with a base diameter of 33 feet. The physical size of the test specimen and the liquid propellants it contained required testing the vehicle in the vertical position.

Based on analytical studies, the dynamic characteristics of the free-free, cryogenic flight vehicle were simulated by filling the S-IC fuel and liquid oxygen tanks with water. The upper stage tanks were left empty for

*See Reference Page 115.

lateral testing. This is referred to as "Configuration I", see Fig. (2.1).

During lateral tests a single shaker was used and during longitudinal and roll testing two shakers were used. Only lateral bending modes are investigated in this study, but the analysis in general is not limited to only lateral motion.

Accelerometers and rate gyros were used to define the primary vehicle dynamic characteristics such as the vehicle mode shapes and structural characteristics in the IU flight sensor location. A typical test employed about 120 instruments which fed their outputs directly into the data acquisition system. The instrument outputs were continuously monitored, recorded, and visually displayed by the data acquisition system during testing.

The data acquisition system automatically controlled the frequency sweeps by monitoring the instrumentation outputs continuously to insure that the vehicle transients had settled to an acceptable level prior to recording data. Each time the system checked or recorded data, it took a full three cycles at the rate of 900 data points per second from each of the 120 sensors simultaneously.

All data, including raw test output frequency response plots, curve fit frequency response plots, and vehicle mode shapes, were plotted on high speed plotters for visual analysis.

At the conclusion of testing, a very large package of data had been collected. Test records for a specimen of this size have not been previously available. These data afford an excellent opportunity to compare analytical and test dynamic parameters for very large space vehicles.

In addition to the complete vehicle test information, particularly useful information on a truncated version of the vehicle was available. This is the same vehicle minus the first booster stage,or the S-IC stage. This is referred to as Configuration II, as shown in Fig. (2.2). Data for the test of this vehicle was available for time point 11. This is for a time when certain maximum loads are imposed and the propulsion tanks are at a certain fill condition, which was simulated by water. Data collected for this Configuration II was obtained directly from the Boeing Company[2].

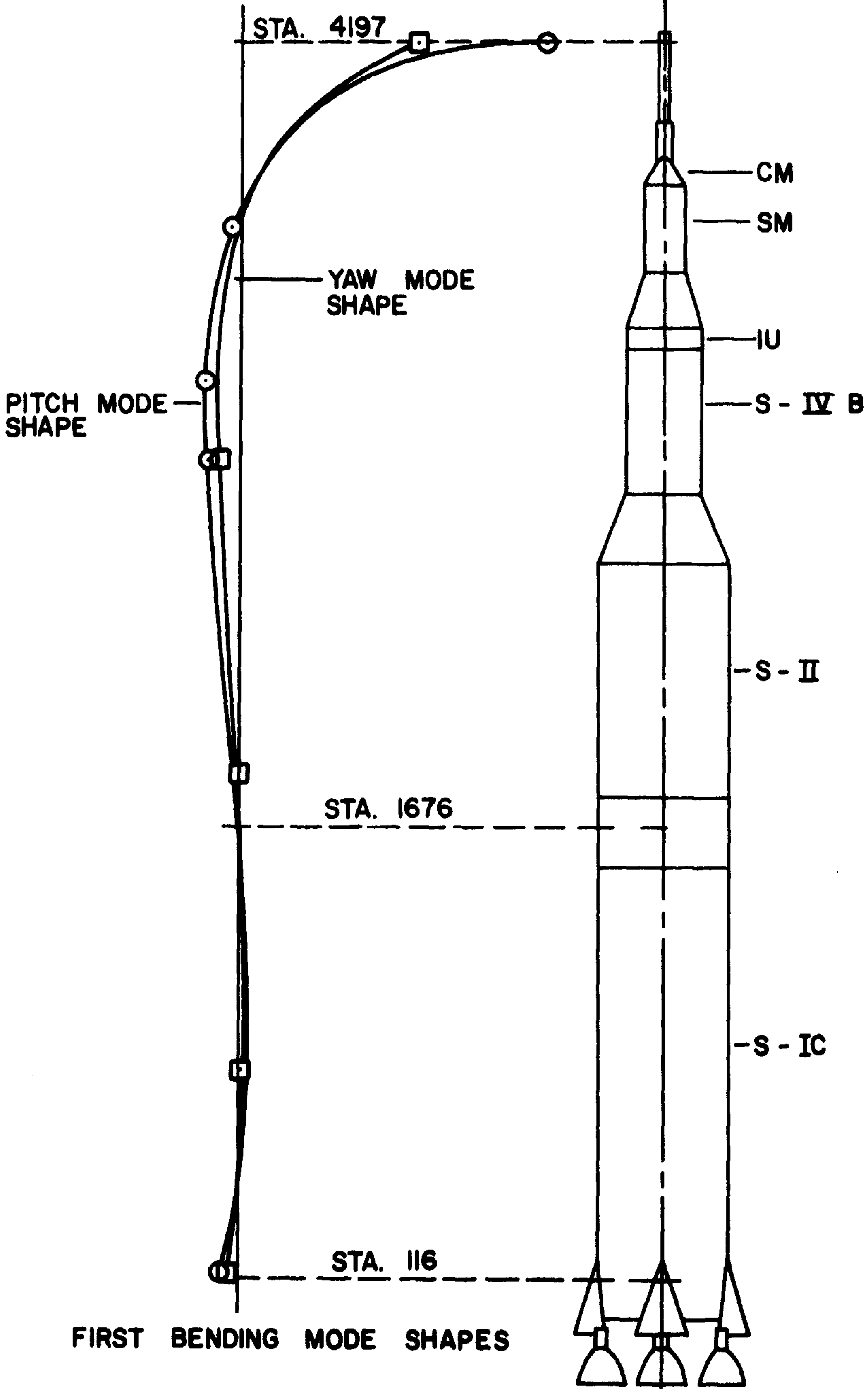

FIG. 2.1 SATURN V, 500-D PITCH TEST TIME POINT 2 (CONFIGURATION 1)
TYPICAL DISPLACEMENT CONFIGURATION DETERMINED, FIRST MODE

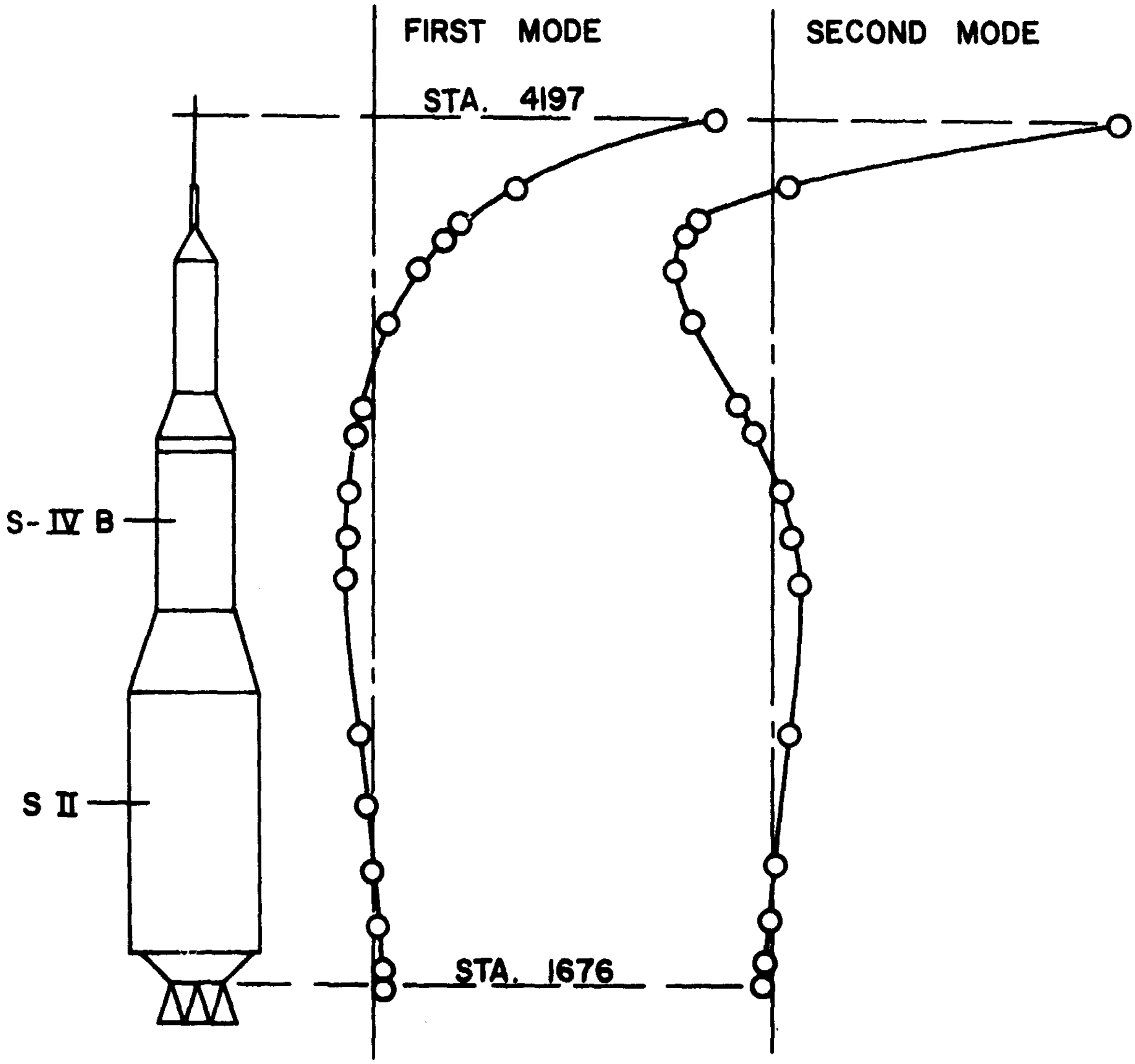

FIG. 2.2 SATURN V, 500-D YAW TEST TIME POINT 11 (CONFIGURATION II) TYPICAL DISPLACEMENT CONFIGURATION DETERMINED FOR FIRST AND SECOND MODES.

2.2 Modal Equation of Motion.

To be able to extend the test results to other configurations and to permit design changes to be checked and verified, it is necessary to develop an analytical technique that allows one to use test results to determine system parameters in the mathematical model of the vehicle. The collection of test data was based on a pre-test analysis. Thus, further analysis is limited in scope to what was done prior to testing the vehicles. The technique commonly applied to this complex continuous free-free vibrating beam like system is the normal mode, or modal, technique. This technique is based on the ability to approximate a continuous system by a N-degree-of-freedom model as shown in Fig. (2.3).

It is rather easy to calculate the response amplitudes of systems having two or three degrees of freedom. The analysis of a large system with perhaps more than one hundred degrees of freedom is simplified by the application of modal techniques. This technique utilizes four properties of the system, (1) natural modal frequencies, (2) resonant amplitudes or amplitude frequency plots, (3) mode shapes, and (4) energy dissipation per cycle. With these four things known, any system can be considered to be an equivalent single degree of freedom system. The amplitude of an arbitrarily chosen nodal mass is taken as the reference for a vibrational mode. The amplitudes of all other nodal masses are ratios of the reference mass in calculating amplitude, so that the mode shape becomes normalized for the mode. Generalized mass is actually the equivalent mass of the total system in one of its primary or normal modes. The four properties make up what is referred to as the "dynamic characteristics" of the system; they are all that is necessary to perform a dynamic analysis.

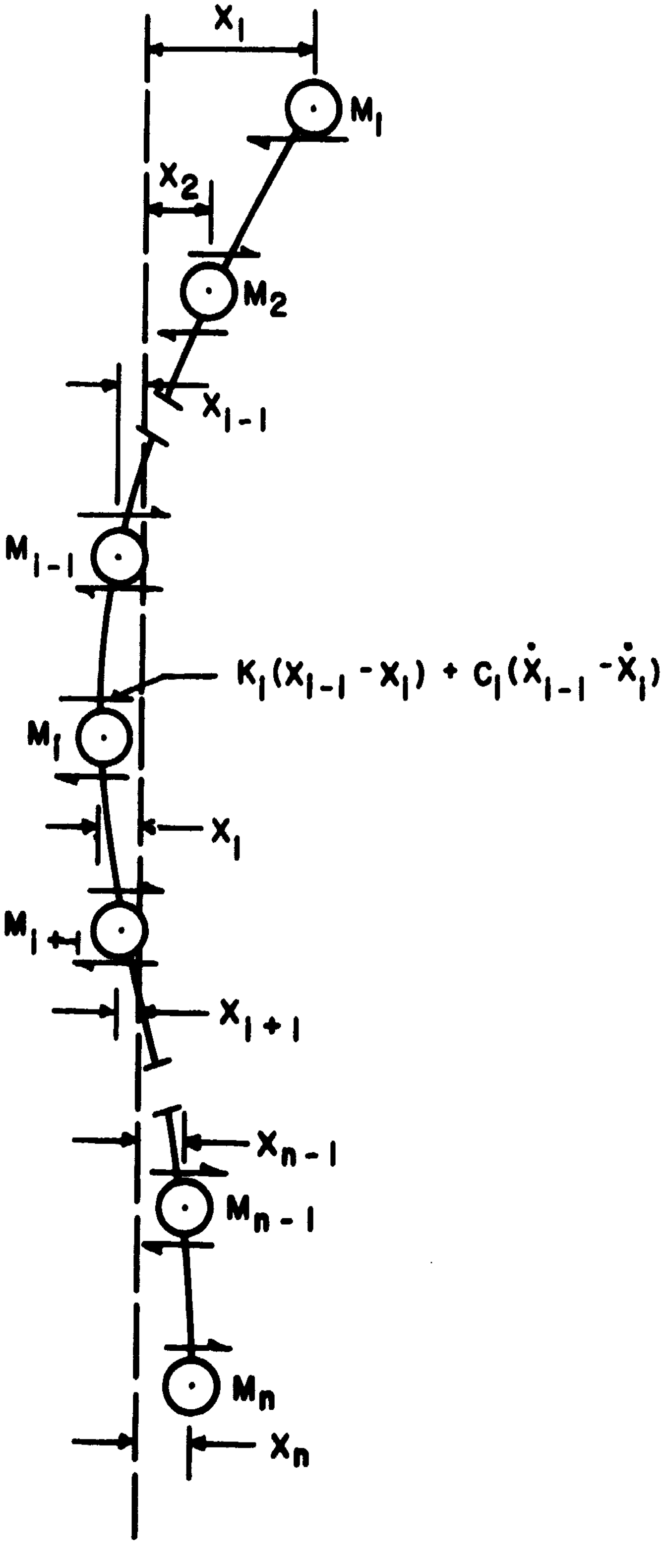

FIG. 2.3 N-DEGREE-OF-FREEDOM MATHEMATICAL MODEL

A distributed mechanical system can be investigated as a system of nodal points with the mass lumped at these nodes, and the displacement of the nodes as dependent variables in the ordinary differential equations of motion, see Fig. (2.3). For many systems the damping terms in the equations of motion can be neglected. Such is the case for many of the launch vehicles used in our present space efforts. Chang[3] states that if damping is small the natural modes of vibration should not differ significantly from those predicted neglecting the damping.

To place the idea of a modal equation of motion in prospective it is desirable to review its classical formulation. The equations of motion for the undamped lump-mass system in vector-matrix notation are

$$[m]\ddot{\underset{\sim}{x}} + [k]\underset{\sim}{x} = \underset{\sim}{F} \qquad (2.2.1)$$

To uncouple the equations let

$$\underset{\sim}{x} = [\phi]\underset{\sim}{Q}$$

where $[\phi]$ is the matrix of mode shapes which uncouples the equations of motion and $\underset{\sim}{Q}$ are the principal coordinates. Substituting into Eq. (2.2.1) and premultiplying by the transpose gives

$$[\phi]^T[m][\phi]\ddot{\underset{\sim}{Q}} + [\phi]^T[k][\phi]\underset{\sim}{Q} = [\phi]^T\underset{\sim}{F} \qquad (2.2.2)$$

If the proper $[\phi]$ matrix is chosen, each coefficient matrix is diagonalized. Thus

$$[\phi]^T[m][\phi] = [\ulcorner M_j \lrcorner]$$

$$[\phi]^T[k][\phi] = [\ulcorner K_j \lrcorner] = [\ulcorner \omega_n^2 M_j \lrcorner]$$

where $\omega_n^2 = \dfrac{K_j}{M_j}$.

For example, consider four lumped masses and consider only two modes. Thus

$$[\phi_{ij}] = \begin{bmatrix} \phi_{11} & \phi_{12} \\ \phi_{21} & \phi_{22} \\ \phi_{31} & \phi_{32} \\ \phi_{41} & \phi_{42} \end{bmatrix}$$

where ϕ_{ij} is the normalized modal displacement of the i^{th} mass in the j^{th} mode. Substituting

$$\lfloor M_j \rfloor = \begin{bmatrix} \phi_{11}^2 m_1 + \phi_{21}^2 m_2 + \phi_{31}^2 m_3 + \phi_{41}^2 m_4 & 0 \\ 0 & \phi_{12}^2 m_1 + \phi_{22}^2 m_2 + \phi_{32}^2 m_3 + \phi_{42}^2 m_4 \end{bmatrix}$$

provided $\lfloor m \rfloor$ is diagonal with m_i being the i^{th} lumped mass.

With the force applied only at the r^{th} lumped mass point, say at the $i = 4$ mass, then

$$[\phi]^T \underset{\sim}{F} = \begin{bmatrix} \phi_{11}\phi_{21}\phi_{31}\phi_{41} \\ \phi_{12}\phi_{22}\phi_{32}\phi_{42} \end{bmatrix} \begin{bmatrix} 0 \\ 0 \\ 0 \\ F(t) \end{bmatrix}$$

$$= \begin{bmatrix} \phi_{41} & F(t) \\ \phi_{42} & F(t) \end{bmatrix} = \underset{\sim}{F_e}$$

With a sinusoidal forcing function

$$F(t) = F \sin \omega t$$

the modal forcing functions become

$$F_{ej} \sin \omega t$$

where $F_{ej} = \phi_{4j} F$. In general

$$F_{ej} = \phi_{rj} F \tag{2.2.3}$$

with the load at the r^{th} mass point.

Making the appropriate substitutions into Eq. 2.2.2 yields

$$\left[\ulcorner M_j \lrcorner\right] \ddot{\tilde{Q}} + \left[\ulcorner K_j \lrcorner\right] \tilde{Q} = \tilde{F}_e \qquad (2.2.4)$$

which can be separated into n separate uncoupled equations. Each equation represents a different mode of vibration. Looking at any one of the modes and dropping the subscripts

$$M\ddot{Q} + KQ = F_e \text{ Sin } \omega t$$

This equation describes the modal response as long as the forcing frequency ω is not near the natural frequency $\omega_n = \sqrt{K/M}$. When this occurs the modal amplitude is large and damping must be included. Thus, the modal equation of motion becomes

$$\ddot{Q} + \frac{1}{M} g[Q, \dot{Q}] + \omega_n^2 Q = \frac{F_e}{M} \text{ Sin } \omega t \qquad (2.2.5)$$

where $g[Q, \dot{Q}]$ is the modal damping. Methods to determine the appropriate damping terms is the object of this study.

From test information the system parameters in Eq. (2.2.5) can be found. That is, the natural modal frequency yields ω_n, the mode shapes as shown in Figs. (2.1) and (2.2) yield the columns in the transformation matrix $[\phi]$, and the generalized mass is calculated knowing the actual mass. The form of the damping term and the magnitude of the damping coefficients are determined from energy dissipation per cycle, resonant amplitudes, and the shape of the amplitude versus frequency curves.

2.3 Modal Damping and Energy Dissipation.

When the Apollo-Saturn V structural system has no damping, it will continue to oscillate without an external driving force to add energy to the system. However, many sources of damping are present and energy is removed from the system. The analytical representation of damping is different for the different sources of damping. Consider the modal damping force function of Eq. (2.2.5) as

$$\text{Modal Damping Force} = g\,[Q, \dot{Q}] \qquad (2.3.1)$$

Some of the typical analytical representations of damping are shown in Table 2.I; see Reference [4]. The possible source of each case is also shown.

As mentioned above, a useful technique in studying different analytical representations of damping is to make a comparison of energy dissipation per cycle, ΔW/cycle. This is obtained by integrating the force times the displacement over a vibration cycle. As mentioned above, only the damping forces will remove energy from the system. Thus,

$$\Delta W/\text{cycle} = \int_{\text{cycle}} [g(Q, \dot{Q})]\, dQ \qquad (2.3.2)$$

Consider the input force F(t) to be a type which maintains a constant response amplitude. The response may be approximated by

$$Q = A \sin(\omega t - \Phi), \qquad (2.3.3)$$

where A is the amplitude, ω is the frequency, and Φ is the phase angle. This amplitude, frequency, and phase may be determined by using the method of W. Ritz discussed in Section 4.2. The velocity becomes

$$\frac{dQ}{dt} = A\,\omega \cos(\omega t - \Phi). \qquad (2.3.4)$$

TABLE 2.I. ANALYTICAL REPRESENTATION OF DAMPING

Case	$g\left(\frac{dQ}{dt}, Q\right)$	Source
I	$C_1 \frac{dQ}{dt}$	Viscous or environmental
II	$C_2 \mid Q \mid \left(\text{sign} \frac{dQ}{dt}\right)$	Material or slip
III	$C_3 \left(\frac{dQ}{dt}\right)^2 \left(\text{sign} \frac{dQ}{dt}\right)$	Environmental
IV	$C_4 \mid Q \mid \frac{dQ}{dt}$	Material
V	$C_1 (1 + \alpha Q^2) \frac{dQ}{dt}$, $C_1 \alpha = C_5$	All Sources

Substituting any of the damping functions of Table 2.I into Eq. (2.3.2), with displacement and velocity given by Eqs. (2.3.3) and (2.3.4), the energy loss per cycle is obtained by integrating between the limits of Φ/ω and $2\pi + \Phi/\omega$. The energy content is similarly obtained from

$$\psi = \frac{\Delta W/\text{cycle}}{M(\dot{Q}_{max})^2} \tag{2.3.5}$$

The results for each damping function shown in Table 2.I are shown in Table 2.II.

TABLE 2.II. ENERGY LOSSES - SINUSOIDAL RESPONSE

Case	ΔW/cycle	$\psi = \Delta W/2W$
I	$C_1 \pi A^2 \omega$	$\frac{C_1 \pi}{M\omega}$
II	$2C_2 A^2$	$\frac{2C_1}{M\omega^2}$
III	$\frac{8}{3} C_3 A^3 \omega^2$	$\frac{8C_3 A}{3M}$
IV	$\frac{4}{3} C_4 A^3 \omega$	$\frac{4C_4 A}{M\omega}$
V	$C_5 \pi A^2 \omega + \frac{\pi}{4} A^4 \omega C_5 \alpha$	$\frac{C_5 \pi}{M\omega} + \frac{C_5 \pi \alpha A^2}{4M\omega}$

Most authors consider the damping to be from a single source when investigating a dynamic system. This is sufficient when the damping is small and/or when one has a simple sub-system of a more complex system. Furthermore, many authors consider only viscous damping, Case I. The present basis for determining the modal damping of the Saturn V is also based on viscous damping. By observing the resonant amplitudes of a response curve the viscous damping coefficient is obtained. The coefficient for other cases can also be computed to give this resonant amplitude. When a response curve is observed, there is an equal reason to believe that damping is characterized by any other case rather than viscous damping. This dilemma may be solved by observing the response curves for a different force amplitude. It is noted from Table 2.II that energy losses per cycle vary with different powers of amplitude. Thus, with the change in response amplitude, using the same damping coefficients, response curves will now show a difference. This is illustrated in Chapter IV.

Extending the idea that no complex dynamic system can have a single source of damping, or that one analytical representation may or may not be better than another, a method to allow all possible sources or analytical representations of damping is shown in Chapter V. If all sources are present the total energy loss per cycle is the sum from each source.

2.4 Hysteretic Representations of Damping.

Regardless of the particular damping mechanism involved, all materials exhibit multi-valued load-deflection curves under cyclic loading. These curves form the familiar hysteresis loops used in defining the constitutive relationships of materials. Also, interfacial slip joints produce similar hysteresis loops. Typical hysteresis loops for linear and nonlinear damping characteristics are shown in Fig. (2.4).

The area between the loading and unloading branches of the hysteresis loop is proportional to the energy dissipated by the system during one cycle of motion. Thus, the area inclosed by the hysteresis loop is a measure of the damping capacity of the system.

Mathematically, the energy dissipated per cycle (ΔW) is given by

$$\Delta W = \int F_d dQ \tag{2.4.1}$$

where F_d is the symbolic representation of linear or nonlinear force, and

Q is the mechanism deformation.

Many investigators have employed hysteresis relationships in their study of the damping properties of materials and structural systems. Notable contributions to structural analysis techniques have been made by Chang [3], and Lazan [5]. In this study , an analytical representation of damping will be used to define the nonlinear damping functions. The analytical representation of slip damping is discussed in the following paragraphs.

When an external load is applied to a built-up structure, microscopic relative displacements occur along the interface. This mechanism is the principle contributor to the damping of the system.

As the applied load goes through its growth phase, the force-deflection plot is of a constant slope, proportional to the structural stiffness. At the onset of relative displacements along the mating surfaces, referred to as interfacial slip, there is an abrupt change in stiffness, which causes the force-deflection curve to change radically to a less steep slope. This reduced slope now remains constant until the applied load reaches its maximum. The curve then becomes the same as during load initiation, but in the negative direction. It does not change until the shear force system along the interface created by the load increasing toward its positive maximum has been completely cancelled, and an equal and opposite system has been established. At this point, slip again occurs, giving rise to a slope change on the force-deflection diagram which is of the same magnitude but opposite in direction to the "slip slope" obtained during positive load phase. When the load reaches its minimum, force-deflection slope takes on the same value and direction as with load initiation, however, it will intercept the x-axis on the negative side of the origin.

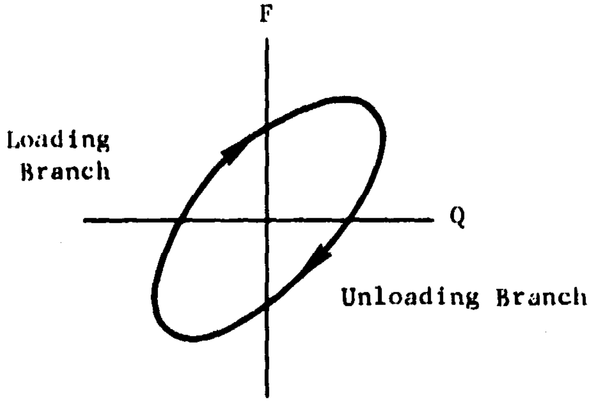

(a) Linear Viscous Damping Characteristic

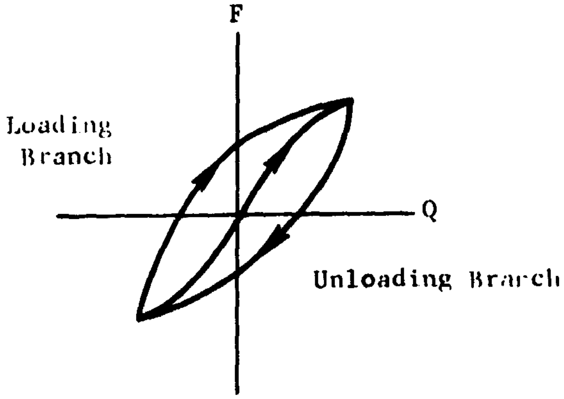

(b) Material Damping Characteristic

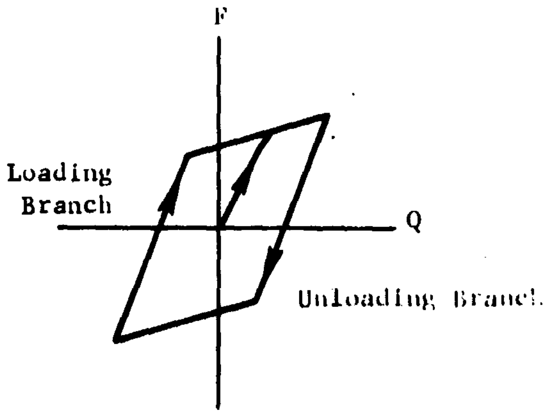

(c) Slip Damping Characteristic

FIG. 2.4 HYSTERESIS LOOPS FOR TYPICAL LINEAR AND NONLINEAR DAMPING CHARACTERISTICS

After the cancellation and re-establishment of a sufficiently large inter-facial shear force system increasing in the positive direction, slip will again occur. Progression along this force-deflection slope closes the curve.

This reasoning has been used to conclude that the force-deflection hysteresis path describes a parallelogram. The longitudinal axis of the parallelogram is anti-symmetric about the x-axis and is inclined from the y-axis due to the force contribution by the spring, see Fig. (2.4c).

It is a well-known fact that a measurement of the system damping is equal to the area enclosed by the force-deflection hysteresis curve. It would be desirable to analytically represent the damping force by a function of terms involving displacement and velocity.

After trying several combinations of displacement and velocity in search of a hysteresis curve of suitable shape, it was found that a function $g(Q, \dot{Q}) = \overline{C}_3\dot{Q}^2(\text{sign}\,\dot{Q})$ is a good simple simulation of the damping force. For increasing and decreasing load the slopes are equal and very nearly constant. However, the velocity-square plot exhibits a lobe at top and bottom rather than a straight line. This is illustrated in Fig. (2.5).

Therefore, slip damping can be represented by Case III in Table I which has an energy loss per cycle

$$\Delta W/\text{cycle} = \frac{8}{3}\,\overline{C}_3\overline{A}^3\omega^2 \qquad (2.4.2)$$

Including Case III as part of the gross vehicle damping would allow for slip damping as well as environmental damping (vortex shedding in aerodynamic studies). Static tests are conducted to determine hysteresis loops for slip damping; however, these loops are not frequency dependent. No good test information or analysis is available to justify frequency independence. Thus,

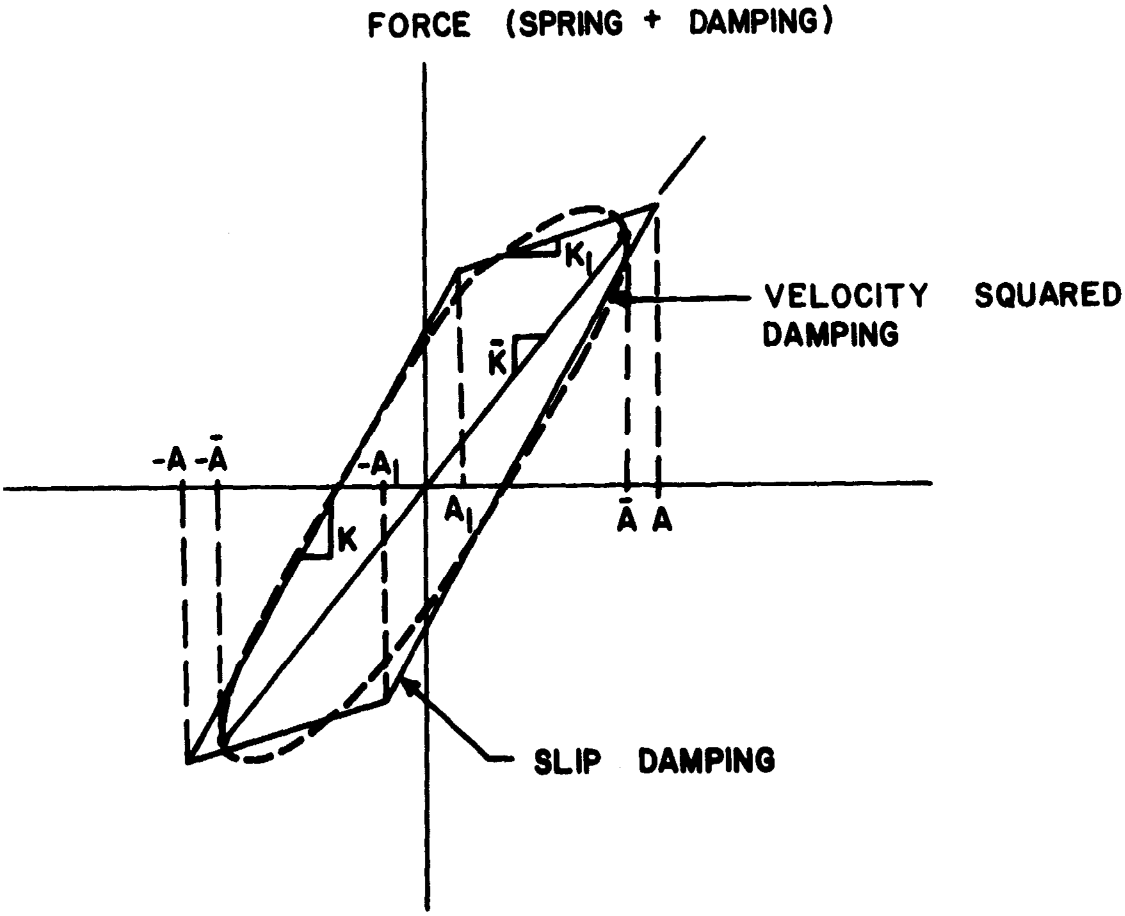

FIG. 2.5 ANALYTICAL APPROXIMATION OF SLIP DAMPING HYSTERESIS BY VELOCITY SQUARED DAMPING

an equivalent coefficient $\bar{C}_3\omega^2$ is obtained by equating the energy of each closed curve in Fig. (2.5).

Integrating the area enclosed by the slip damping curve in Fig. (2.5) yields

$$\Delta W/\text{cycle} = A^2(K - K_1) - A_1^2(K - K_1) \tag{2.4.3}$$

Setting this equal to Eq. (2.4.2) gives

$$\bar{C}_3 = \frac{3(A^2 - A_1^2)(K - K_1)}{8\bar{A}^3\omega^2} \tag{2.4.4}$$

the coefficient of the equivalent analytical representation of slip damping, $\bar{C}_3\dot{Q}^2(\text{sgn}\ \dot{Q})$. The amplitude $\bar{A}$ approaches A and the stiffness factor $\bar{K}$ approaches K for small damping.

2.5 Modal Versus Sub-System Damping.

In general the effects of damping are not investigated on the component or subsystem level, but are treated as overall, or modal, characteristics of the system. This approach to structural analysis generally yields valid information of gross system behavior, but it fails to define the contribution of each sub-system. Information of this nature is particularly important in design and control theory studies. In addition, the structural analyst often requires detailed knowledge of the vehicle response station-by-station along the vehicle.

Procedures that are particularly suited for dynamic response studies of complex systems, such as an aerospace vehicle, are documented by McTigue and Riley [6], Foss [7], and DaDeppo [8].

Methods presented by the authors of [6] and [7] are quite similar, in that they employ a matrix formulation of normal mode techniques to solve for the dynamic response of systems possessing linear damping. The contribution by Foss consists of a special coordinate transformation technique which enables the analysis of systems possessing mass, stiffness, and damping matrices that cannot be simultaneously diagonalized.

A method of constructing the viscous damping matrix for a freely vibrating system is given by DaDeppo [8]. This method assumes that the damping matrix can be expressed as a linear combination of matrices that depend only on mass and stiffness. Further, the method requires that experimentally determined damping ratios for the normal modes of vibration must be obtained before the uncoupled equations of motion can be solved.

The first phase of this modification and expansion has been developed by Koenig and Drain [9]. In this paper, a method of analyzing a lightly damped lumped-parameter system is presented in which the normal restrictions of proportional relationships between mass, stiffness, and damping are overcome. This method provides the basic approach used in formulating the linear analysis technique.

CHAPTER III

ANALYSIS OF TEST DATA AND LINEAR DAMPING FORCE

The test data available to the analyst contains information that is desirable for theoretical analysis and, in fact, contains additional experimental data not necessary for the analysis. It then becomes necessary to condition, or filter, this test data so that only the desired information is obtained. Such is the case when one attempts to produce only bending motion of the free-free vehicle in one plane, say the vehicle pitch plane. The test results shown in this chapter are a typical example. They are for the Saturn V Configuration I vehicle explained in Chapter II. The objective of this chapter is to show what analytical techniques can be applied to a typical set of experimental test data so that the modal damping and other modal parameters can be determined.

In the first section the experimental test data is investigated and an analytical technique for determining modal principle pitch and yaw frequencies, mass, and damping is shown. This technique for determining both pitch and yaw modal parameters from one test has obvious advantages. In the second section a technique for determining a linear viscous damping coefficient is illustrated for the Configuration I vehicle second mode. It is shown how this coefficient varies with frequency. An average equivalent linear viscous damping coefficient for each mode can be obtained.

3.1 Conditioning of Experimental Test Data.

As explained in the previous chapter, the test data is collected as accelerometer readings at different discrete frequencies for each nodal point along the vehicle axis. A record of the maximum accelerometer reading per unit input load versus frequency can be plotted as shown in Fig. (3.1). An attempt was made to keep the input force relatively constant at each frequency. The record shown is for the Configuration I vehicle.

Various deductions can be made by observing this data. These are as follows:

1) Yaw motion is excited with the force only in the pitch direction.

2) The resonant spikes appear to have a greater slope on the low frequency side.

3) The resonant frequencies, or modal frequencies, appear to be well defined.

4) Multiple peaks appear for some resonant spikes.

5) Modal coupling may occur between resonant frequencies.

6) Damping is very light causing the tall and narrow spikes.

In the course of this study each of the above items will be investigated for cause and effect relationships.

For further study, the response near the second mode; or second spike on Fig. (3.1), is observed in greater detail. Any other mode can be studied in the same way, as all are considered to have the same features. Converting from accelerations to displacements is accomplished by dividing the acceleration by the frequency squared (in radians per second) and multiplying by 386 (in. per sec. squared). This conversion is shown in Table 3.I. These values are shown for the vehicle tip (Station 4197) displacement; however, additional accelerometers are attached at other

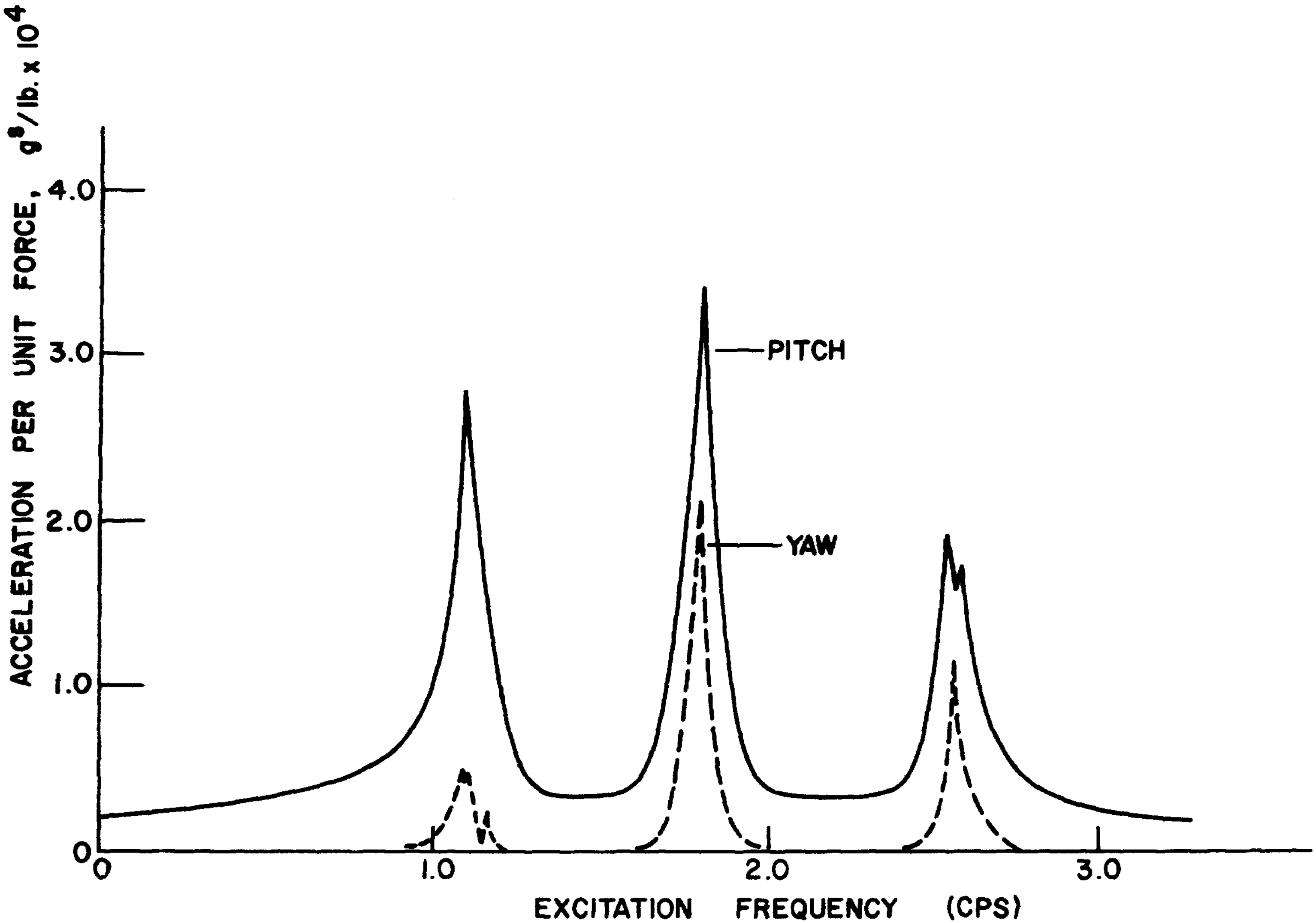

FIG. 3.1 ACCELEROMETER RECORD OF THE CONFIGURATION I VEHICLE TIP MOTION DURING PITCH TESTING

TABLE 3.I CONVERSION OF RAW TEST DATA TO NODAL DISPLACEMENTS

POINT	FREQUENCY cps. f	FREQUENCY rad./sec. ω	FORCE lb. F	TIP ACCELERATION		TIP DISPLACEMENTS		TAIL DISPLACEMENTS	
				Pitch Plane g^s/lb. x 10^4	Yaw Plane g^s/lb. x 10^4	Pitch Plane in., X	Yaw Plane in., Y	Pitch X_t in. x 10^2	Yaw Y_t in. x 10^2
1	1.778	11.17	942	.8992	.1021	.261	.0296	.858	.0974
2	1.783	11.20	952	1.014	.1178	.297	.0350	.978	.114
3	1.788	11.235	967	1.208	.1549	.358	.0459	1.250	.160
4	1.793	11.27	973	1.417	.2319	.419	.0687	1.503	.246
5	1.798	11.30	960	1.709	.3662	.497	.1065	1.824	.391
6	1.803	11.33	962	2.218	.5341	.641	.1595	2.45	.590
7	1.807	11.36	930	3.254	1.270	.904	.3530	3.63	1.42
8	1.813	11.39	922	3.507	2.062	.961	.5650	3.98	2.34
9	1.818	11.42	919	3.224	2.115	.877	.5760	3.67	2.41
10	1.823	11.455	928	3.213	1.939	.881	.5320	3.69	2.23
11	1.828	11.49	932	3.053	1.461	.830	.3970	3.56	1.70
12	1.833	11.52	941	2.692	.8750	.737	.2400	3.21	1.04
13	1.838	11.55	954	2.379	.6677	.657	.1845	2.88	.808
14	1.843	11.58	954	2.047	.4735	.563	.1775	2.52	.583
15	1.848	11.61	954	1.819	.4307	.500	.1183	2.27	.538

vehicle stations to record the pitch motion of the other nodal points. It will be shown later in this section how modal displacements are obtained from nodal values.

It is important to know the nodal displacements at the tail of the vehicle, Station 116. This is where the external sinusoidal forcing function is applied. Displacements for the tail node are also available from recorded data on acceleration. The computed tail displacements are also shown in Table 3.I. However, only pitch accelerometer readings were recorded for nodes other than the tip; and yaw values are obtained from

$$\text{Yaw Displ.} = \frac{\text{Tip Yaw Acc.}}{\text{Tip Pitch Acc.}} \times \text{Pitch Displ.} \qquad (3.1.1)$$

That is, the yaw mode shape is assumed to be the same as the pitch mode shape, only at a reduced amplitude. This is illustrated in Fig. 2.1.

The presence of both pitch and yaw motion, with the input force only in the pitch direction, indicates the vehicle has "Planar Coupling". There are two known causes for planar coupling in the Saturn V vehicle. These are both due to mass and stiffness not being axially symmetric. Such is the case with the (1) lunar module and (2) the command-service module interface. Below station 3100 the vehicle structure is symmetrical. The flight-type lunar module located in the service module possesses both mass and stiffness axial unsymmetry. The test vehicle, however, contained a symmetric component which simulated only the weight and C. G. of the lunar module. However, there is significant stiffness axial unsymmetry at the command module-service module interface. The interface structure is made up of six Bi-POD type supports which attach the command module to the service module. Three of these are attached to the command module by tension ties. The other three Bi-PODS rest on compression pads, but due to initial pretension loads, they are assumed to be effective in both tension and compression. In addition to the six Bi-POD supports, a torsion strut was added to one Bi-POD to give torsional strength to the interface. This strut is shown to be the primary stiffness coupler. Its effect on vehicle motion was that the vehicle tip subscribed an elliptic path. Thus, pitch excitation excited both modes lying in the principal major and minor vehicle planes. All sensor readings recorded during testing were the superposition of the two principal modes being excited. There is a slight difference in the frequency of the two modes, so their phase relationship varies considerably near resonance. A stiffness analysis was performed to determine the location of the principal major and minor planes. Major and minor planes of motion are inclined approximately 28^{o} from the vehicle pitch and yaw planes used in the dynamic test.

A plot of the tail displacement versus frequency is shown in Fig. (3.2). Many of the observations made from Fig. (3.1) are also possible in this Figure. The unsymmetrical, or warped, shape of the curve is obvious. Also, if one would connect the data points by the dashed line, two resonant peaks occur. The corresponding phase angle between the tail displacement and force is available from test data. This is shown in Fig. (3.3).

It might be assumed from Fig. (3.2) that the system exhibits a nonlinear soft spring characteristic. The amplitude versus frequency curve of such nonlinear systems are warped as in Fig. (3.2). However, the presence of two resonant peaks and the known presence of yaw motion leads one to believe that planar coupling is the cause of the warped curve. Also, the yaw maximum amplitude is at a higher frequency than for pitch.

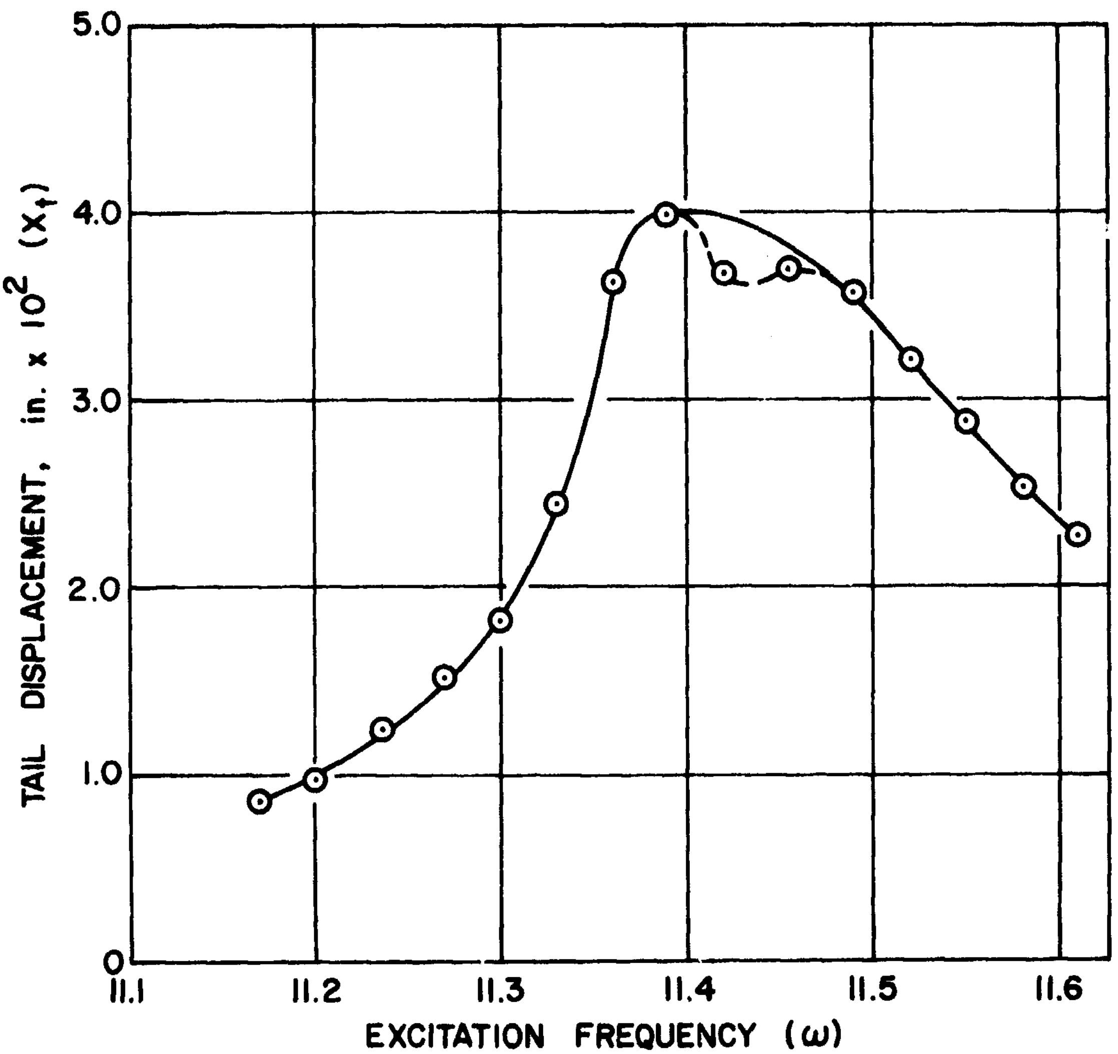

FIG. 3.2 TAIL DISPLACEMENT VERSUS FREQUENCY - SECOND MODE

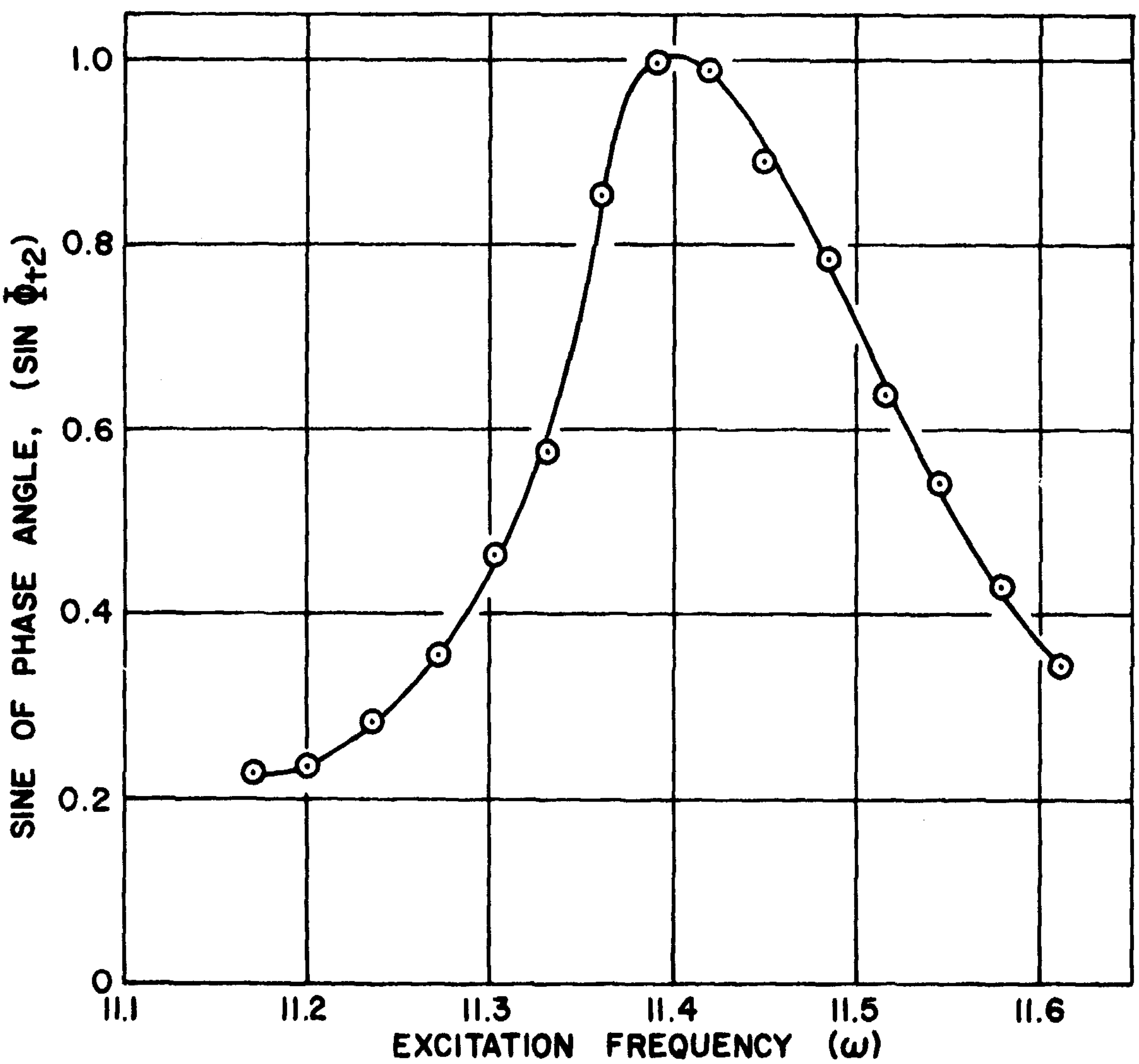

FIG. 3.3 SINE OF TAIL PHASE ANGLE VERSUS FREQUENCY - SECOND MODE

It is desirable to convert from nodal variables to modal variables before further investigation of the experimental data is attempted. The technique of converting from nodal variables (x_i) to the modal variables (Q_n) is explained in Section (2.2). That is, from Eq. (2.2.2)

$$\{x\} = [\phi]\{Q\} \tag{3.1.2}$$

where ϕ_{ij} is the displacement of the i^{th} mass at the resonant frequency of the j^{th} mode. Therefore,

$$x_i = \phi_{i1}Q_1 + \phi_{i2}Q_2 + \phi_{i3}Q_3 + \ldots \tag{3.1.3}$$

for the i^{th} node. For the tail displacement

$$x_t = \phi_{t1}Q_1 + \phi_{t2}Q_2 + \phi_{t3}Q_3 + \ldots \tag{3.1.4}$$

Any one of the modal displacements can be solved for in terms of the one nodal displacement and the remaining modal displacements. That is, for the second mode

$$Q_2 = \frac{x_t - \phi_{t1}Q_1 - \phi_{t3}Q_3 - \phi_{t4}Q_4}{\phi_{t2}} \tag{3.1.5}$$

where the influence of modes through the fourth mode are considered.

The modal displacements are obtained by solving the modal equations of motion

$$M_j\ddot{Q}_j + g_j(Q, \dot{Q}) + K_jQ_j = F_{ej}(t) \tag{3.1.6}$$

where the subscript j refers to the j^{th} mode, see Eq. (2.2.5). The solution of this equation with either nonlinear or linear damping can be represented as

$$Q_j = A_j \operatorname{Sin}(\omega t - \Phi_j) \tag{3.1.7}$$

where Φ_j is the phase angle with respect to the driving force. With a linear viscous damping force

$$g_j(Q, \dot{Q}) = C_j \dot{Q}_j$$

the amplitude becomes

$$A_j = \frac{|F_{ej}|}{M_j \omega_j^2 \left[(1 - r_j^2)^2 + (2\xi_j r_j)^2\right]^{\frac{1}{2}}} \tag{3.1.8}$$

where

$$F_{ej}(t) = F_e \operatorname{Sin} \omega t, |F_{ej}| = F_e \tag{3.1.9}$$

$$\left.\begin{aligned} \omega_j^2 &= \frac{K_j}{M_j} = \text{modal frequency squared} \\ r_j &= \frac{\omega}{\omega_j} = \text{frequency ratio} \\ \xi_j &= \frac{C_j}{2M_j\omega_j} = \text{damping factor} \end{aligned}\right\} \tag{3.1.10}$$

Furthermore, the modal force is related to the nodal force by

$$F_{ej}(t) = F(t)\phi_{tj} = \phi_{tj} F \operatorname{Sin} \omega t \tag{3.1.11}$$

when the load is applied at the tail (t).

The phase angle for the linear system is given by

$$\Phi_j = \tan^{-1} \frac{2\xi_j r_j}{1 - r_j^2} \tag{3.1.12}$$

When the forcing frequency is not near the modal frequency $(1 - r_j^2) \gg 2\xi_j r_j$

and

$$\Phi_j \doteq \begin{cases} 0, & r_j \ll 1 \\ \pi, & r_j \gg 1 \end{cases}$$

Substituting into Eq. (3.1.11) yields

$$\left.\begin{aligned} Q_j &\doteq A_j \operatorname{Sin} \omega t, \; r_j \ll 1 \\ Q_j &\doteq -A_j \operatorname{Sin} \omega t, \; r_j \gg 1 \end{aligned}\right\} \tag{3.1.13}$$

where

$$A_j \doteq \frac{\phi_{tj} F}{M_j \omega_j^2 \left| 1 - r_j^2 \right|} \tag{3.1.14}$$

Now one is prepared to solve for any modal displacement amplitude using Eq. (3.1.4). The second mode (j = 2) is of interest, so Eq. (3.1.5) with x_t for that mode is of interest. Substituting into Eq.(3.1.5) gives

$$A_2 \text{ Sin } (\omega t - \Phi_2) = \frac{x_t + (\phi_{t1}A_1 - \phi_{t3}A_3 - \phi_{t4}A_4) \text{ Sin } \omega t}{\phi_{t2}} \tag{3.1.15}$$

where the A_j values ($j \neq 2$) are the undamped amplitudes given in Eq. (3.1.14) with the modal parameters ϕ_{tj}, M_j, and ω_j available from test data. These values are shown in Table 3.II. Note that ϕ_{tj} is the relative displacement of tip to tail when $\omega = \omega_j$.

TABLE 3.II MODAL PARAMETERS FROM TESTS

MODE j	TAIL MODE FACTOR ϕ_{tj}	MODE MASS M_j, $\frac{\text{lb. sec.}^2}{\text{in.}}$	MODE FREQ. ω_j, rps.
1	.084	62.9	6.95
2	.041	21.0	11.39
3	.028	23.5	16.19
4	.086	245.0	21.58

Due to the method of support for the Configuration I vehicle there is a contribution to the nodal displacements from a "rigid-body rotation". The vehicle is essentially rotating about a fixed nodal point as shown in Fig. (3.4). It is supported by air bearings and hung like a pendulum, with lateral support given by springs as shown. The equation of motion can be written as

$$I\ddot{\gamma} + K_T\gamma = +RF \sin \omega t$$

where I is the vehicle moment of inertia about the fixed node. With some friction to dampen the free vibrations

$$\gamma(t) \doteq \frac{RF}{I(-\omega^2 + \omega_R^2)} \sin \omega t$$

where $\omega_R = 1.00$, the rigid-body frequency. Thus the tail displacement due to rigid body rotation is

$$x_t^R \doteq \frac{R^2F}{I(-\omega^2 + \omega_R^2)} \sin \omega t$$

or the amplitude

$$X_t^R = \frac{R^2F}{I\omega_R^2\left[1 - \left(\frac{\omega}{\omega_R}\right)^2\right]} \qquad (3.1.16)$$

This discussion leads one to conclude that further conditioning of the tail displacement amplitudes shown in Fig. (3.2) must be accomplished before they can be substituted into Eq. (3.1.15) as the amplitude of x_t. The tail displacement includes the vehicle bending displacement and the rigid-body displacement. Thus

$$x_t = x_t^B + x_t^R$$

where the superscript B refers to the bending. The bending displacements are those of interest and the ones to use in Eq. (3.1.15). Solving for the bending displacements

$$x_t^B = x_t - x_t^R$$

$$= x_t - X_t^R \sin \omega t$$

which are substituted for x_t in Eq. (3.1.15).

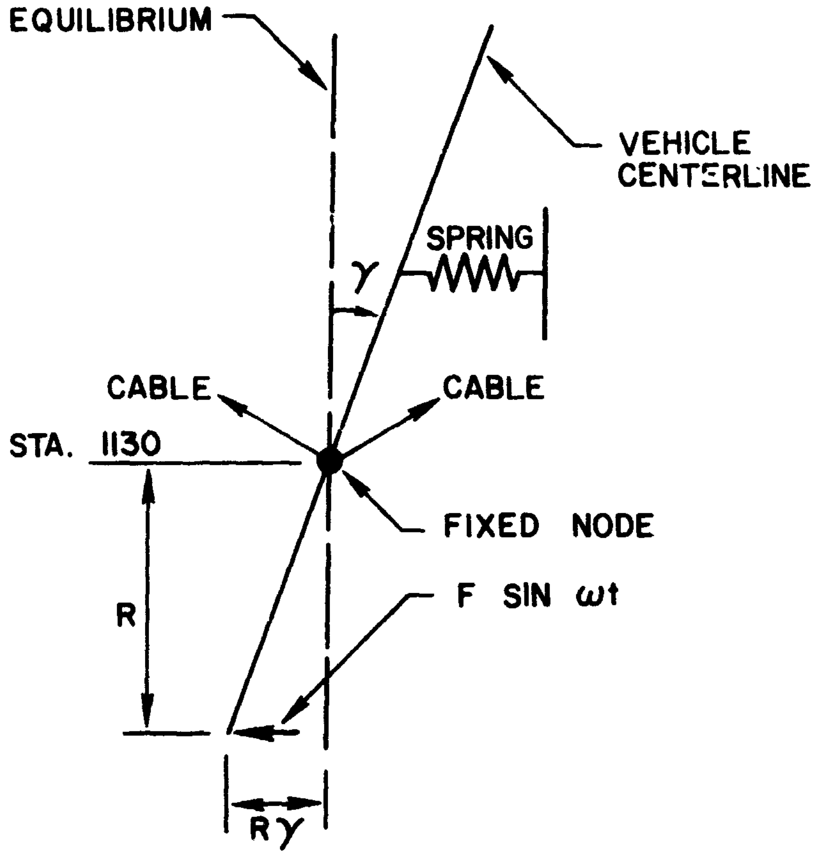

FIG. 3.4 RIGID-BODY ROTATION OF VEHICLE

Therefore,

$$A_2 \text{ Sin}(\omega t - \Phi_2) = \frac{x_t + (-X_t^R + \phi_{t1}A_1 - \phi_{t3}A_3 - \phi_{t4}A_4)\text{Sin } \omega t}{\phi_{t2}} \tag{3.1.18}$$

where the amplitude of x_t is given in Fig. (3.2). This equation may be written

$$A_2 \text{ Sin}(\omega t - \Phi_2) = \frac{x_t}{\phi_{t2}} + C_{t2} \text{ Sin } \omega t \tag{3.1.19}$$

where C_{t2} is the amplitude of the correction factor which accounts for rigid-body rotation and modes near the second mode for tail displacements. Thus,

$$C_{t2} = \frac{-X_t^R + \phi_{t1}A_1 - \phi_{t3}A_3 - \phi_{t4}A_4}{\phi_{t2}} \tag{3.1.20}$$

The motion of each nodal point undergoes harmonic motion; as observed during the tests. In other words

$$x_t = X_t \text{ Sin } (\omega t - \Phi_{t2}) \tag{3.1.21}$$

where the phase angle Φ_{t2} is that between the tail displacement and the input force. This is shown previously in Fig. (3.3). Substituting Eq. (3.1.21) into Eq. (3.1.19), expanding the trigonometric terms as the sum of sines and cosines, and equating coefficients of like trigonometric terms gives

$$A_2 \text{ Sin } \Phi_2 = \frac{X_t}{\phi_{t2}} \text{ Sin } \Phi_{t2}$$

and

$$A_2 \text{ Cos } \Phi_2 = \frac{X_t}{\phi_{t2}} \text{ Cos } \Phi_{t2} + C_{t2}$$

These equations may be solved for the desired modal amplitude and phase angle, which are:

$$\tan \Phi_2 = \frac{X_t \text{Sin } \Phi_{t2}}{X_t \text{ Cos } \Phi_{t2} + C_{t2}\phi_{t2}} \tag{3.1.22}$$

$$A_2 = \frac{X_t}{\phi_{t2}} \text{Cos } (\Phi_2 - \Phi_{2t}) + C_{t2} \text{ Cos } \Phi_2 \qquad (3.1.23)$$

The test data and computed modal values are shown in Table 3.III.

The values of Φ_2 and A_2 for the second mode are plotted in Fig. (3.5) and (3.6) respectively. The unsymmetrical warped shape of each curve indicates that rigid-body rotation and modal coupling were not the cause of the warped tail displacement curve. Thus, the warping is still considered to be due to planar, pitch and yaw, coupling.

With the modal amplitude and phase angle one essentially has single-degree-of-freedom response data for the vehicle pitch motion. With the response being a coupled planar motion one can represent the modal system as shown in Fig. (3.7). If the force was placed in the principle pitch ($\bar{p}$) direction no motion in the principle yaw ($\bar{y}$) direction would occur. The force applied to the Configuration I vehicle was not along either principle axis. Therefore, the vehicle has "planar coupling".

TABLE 3.III SECOND MODE AMPLITUDE & PHASE ANGLE

Point	Tail Amplitude X_t in.	Tail Phase Angle Φ_{t2} rad.	Mode Factor ϕ_{t2}	Rigid-Body and Yaw Correction C_{t2}	Mode Phase Angle Φ_2 rad.	Mode Correction $C_{t2}\mathrm{Cos}\ \Phi_2$	Modal Amplitude A_2 in.
1	.00858	.219	.041	+ .0625	.175	+ .0616	.271
2	.00978	.238		+ .0622	.189	+ .0610	.300
3	.01250	.287		+ .0620	.239	+ .0602	.365
4	.01503	.364		+ .0615	.313	+ .0585	.426
5	.01824	.479		+ .0608	.423	+ .0554	.500
6	.0245	.613		+ .0603	.559	+ .0512	.649
7	.0363	1.020		+ .0578	.967	+ .0328	.919
8	.0398	1.500		+ .0566	1.442	+ .0072	.978
9	.0367	1.726		+ .0559	1.663	- .0051	.891
10	.0369	2.047		+ .0566	1.989	- .0230	.878
11	.0356	2.237		+ .0559	2.185	- .0322	.836
12	.0321	2.450		+ .0556	2.402	- .0410	.742
13	.0288	2.571		+ .0561	2.525	- .0457	.657
14	.0252	2.697		+ .0556	2.654	- .0491	.566
15	.0227	2.792		+ .0561	2.753	- .0515	.502

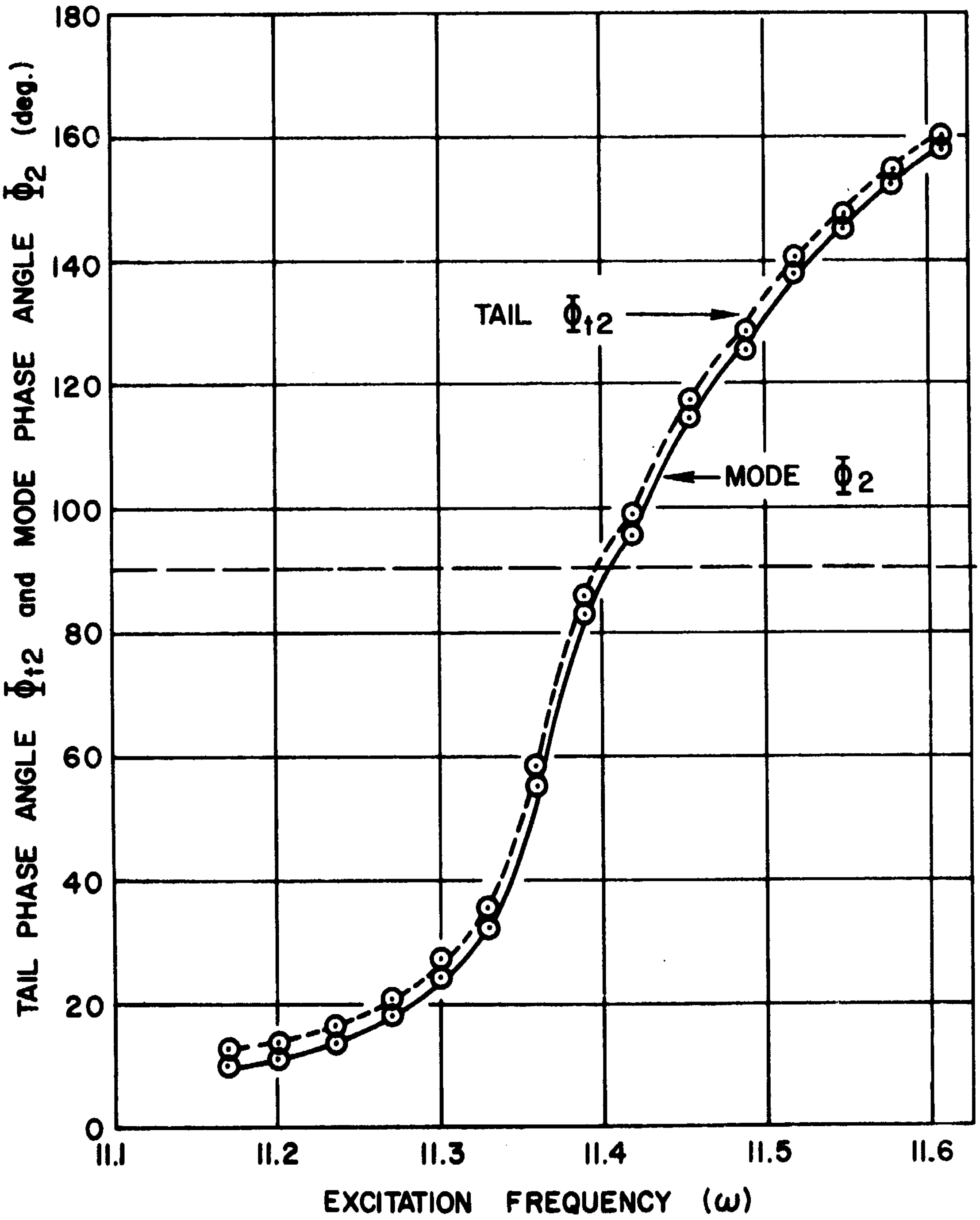

FIG. 3.5 TAIL NODE AND SECOND MODE PHASE ANGLES

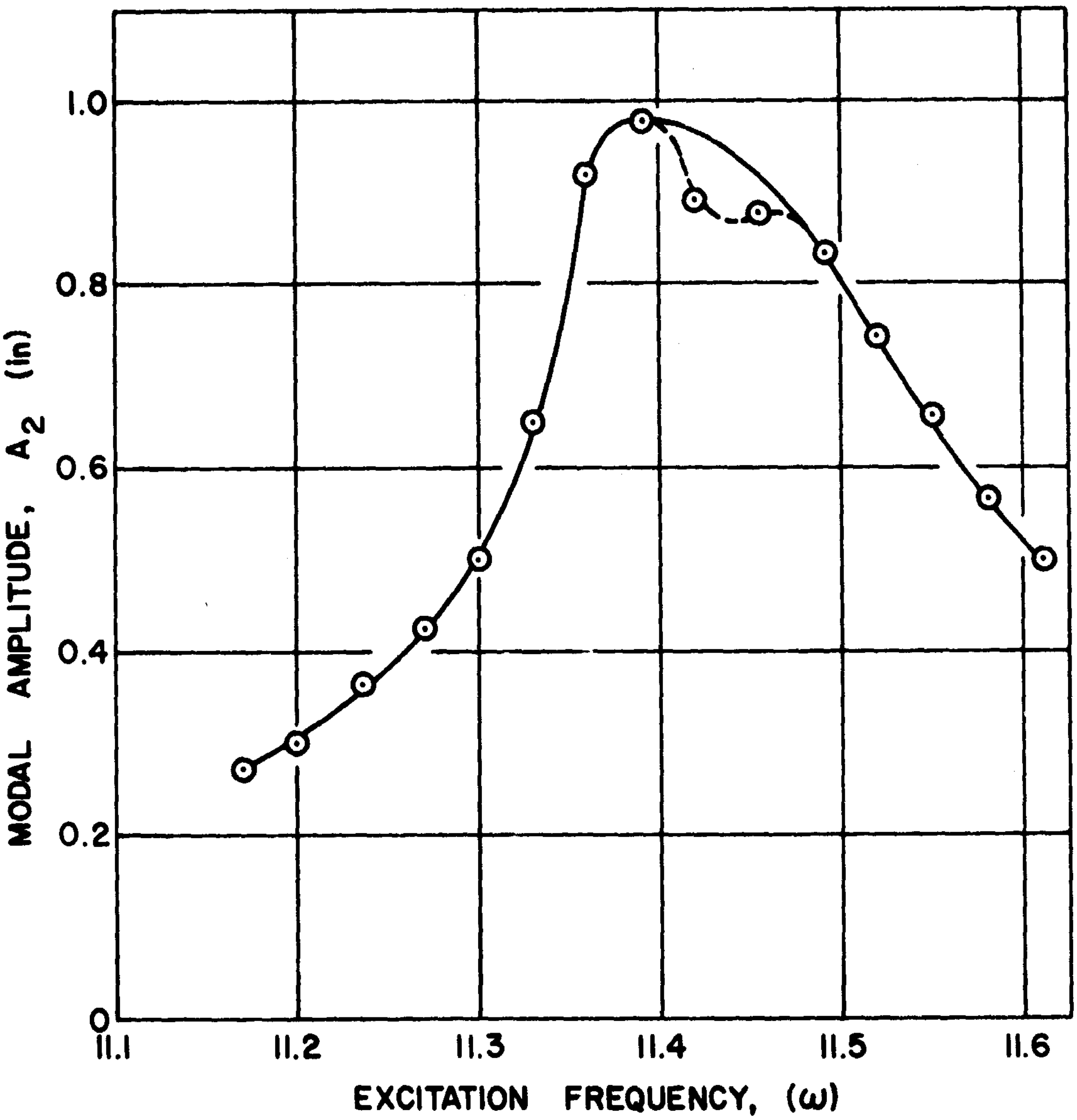

FIG. 3.6 MODAL AMPLITUDE VERSUS FREQUENCY - SECOND MODE

The system shown in Fig. (3.7) can be analyzed to predict what motion will occur along the vehicle pitch (p) direction. The modal pitch parameters are determined as a function of principle pitch and yaw parameters. The analytical results can be compared with the test results of Figs. (3.5) and (3.6). Thus, the principle pitch parameters and yaw parameters, as well as damping, can be determined that will reproduce test results

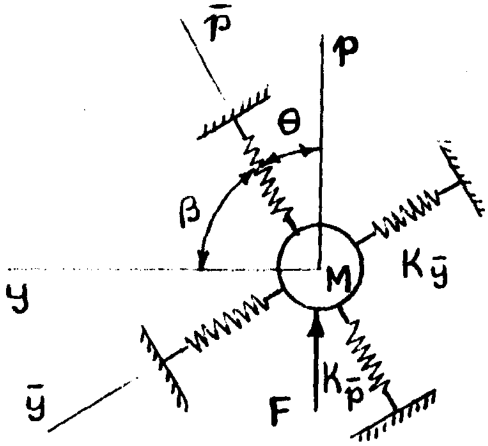

Figure 3.7 Single-Degree-of-Freedom Model with Planar Coupling

If mass M is given a displacement p, the deformation of springs $K_{\bar{p}}$ is p Cos θ, and the spring force is $K_{\bar{p}}(\text{Cos } \theta)p$. The p component of this force is

$$K_{\bar{p}}(\text{Cos}^2\ \theta)p$$

Considering the $K_{\bar{y}}$ springs, the force in the spring is $K_{\bar{y}}$ Sin θ p. The p component is

$$K_{\bar{y}}\ \text{Sin}^2\theta\ p$$

The total force in the p direction is

$$K_p\ p = (K_{\bar{p}}\ \text{Cos}^2\theta + K_{\bar{y}}\ \text{Sin}^2\theta)p$$

where

$$K_p = K_{\bar{p}}\ \text{Cos}^2\theta + K_{\bar{y}}\ \text{Sin}^2\theta \qquad (3.1.24)$$

and K_p is the equivalent spring constant. With the mass given a displacement in the y direction, the force in the y direction from the $K_{\bar{p}}$ spring is

$$K_{\bar{p}}\, y \mathrm{Cos}^2 \beta$$

and from the $K_{\bar{y}}$ spring is

$$K_{\bar{y}}\, y \mathrm{Sin}^2 \beta$$

Thus the total y force is

$$K_y\, y \;=\; (K_{\bar{p}} \mathrm{Cos}^2 \beta + K_{\bar{y}} \mathrm{Sin}^2 \beta) y$$

$$K_y \;=\; K_{\bar{p}} \mathrm{Sin}^2 \theta + K_{\bar{y}} \mathrm{Cos}^2 \theta \qquad (3.1.25)$$

For the total force in the y direction due to a p displacement

$$K_{yp}\, p \;=\; (K_{\bar{p}} \mathrm{Cos}\, \theta \,\mathrm{Cos}\, \beta \;-\; K_{\bar{y}} \mathrm{Sin}\, \theta \,\mathrm{Sin}\, \beta) p$$

Also, the total p force due to a y displacement is

$$K_{py}\, y \;=\; (K_{\bar{p}} \mathrm{Cos}\, \beta \,\mathrm{Cos}\, \theta \;-\; K_{\bar{y}} \mathrm{Sin}\, \beta \,\mathrm{Sin}\, \theta) y$$

and

$$K_{yp} \;=\; K_{py} \;=\; K_{\bar{p}} \mathrm{Sin}\, \theta \,\mathrm{Cos}\, \theta \;-\; K_{\bar{y}} \mathrm{Sin}\, \theta \,\mathrm{Cos}\, \theta \qquad (3.1.26)$$

The differential equations of motion for this single-degree-of-freedom linear system are

$$M\ddot{p} + K_p\, p + K_{py}\, y + C\dot{p} = F_p \mathrm{Sin}\, \omega t \qquad (3.1.27)$$

$$M\ddot{y} + K_y\, y + K_{yp}\, p + C\dot{y} = 0 \qquad (3.1.28)$$

where the damping factor "C" is considered to be the same in either direction (axially symmetric).

By solving the equations of motion for the steady-state response, the amplitude in the p-direction may be determined. Initial conditions are all zero. Thus, taking the Laplace transform of Eqs. (3.1.27) and (3.1.28) gives

$$(s^2 + \frac{C}{M} s + \frac{K_p}{M}) \, p(s) + \frac{K_{py}}{M} \, y(s) = \frac{F_p \, \omega/M}{s^2 + \omega^2}$$

$$(s^2 + \frac{C}{M} s + \frac{K_y}{M}) \, y(s) + \frac{K_{yp}}{M} \, p(s) = 0$$

In matrix notation using $\omega^2 = \frac{K}{M}$

$$\begin{bmatrix} s^2 + \frac{C}{M} s + \omega_p^2 & \omega_{py}^2 \\ \omega_{yp}^2 & s^2 + \frac{C}{M} s + \omega_y^2 \end{bmatrix} \begin{bmatrix} p(s) \\ y(s) \end{bmatrix} = \begin{bmatrix} \frac{F_p \, \omega/M}{s^2 + \omega^2} \\ \\ \end{bmatrix}$$

Solving for p(s) using Cramer's rule,

$$p(s) = \frac{\begin{vmatrix} \frac{F_p \, \omega/M}{s^2 + \omega^2} & \omega_{py}^2 \\ 0 & s^2 + \frac{C}{M} s + \omega_y^2 \end{vmatrix}}{\begin{vmatrix} s^2 + \frac{C}{M} s + \omega_p^2 & \omega_{py}^2 \\ \omega_{yp}^2 & s^2 + \frac{C}{M} s + \omega_y^2 \end{vmatrix}} = \frac{N(s)}{D(s)}$$

The characteristic equation describing the system is

$$\frac{1}{G(s)} = (s^2 + \frac{C}{M} s + \omega_p^2)\,(s^2 + \frac{C}{M} s + \omega_y^2) - \omega_{py}^2 \, \omega_{yp}^2$$

which has four roots. The result of Cramer's rule gives

$$p(s) = \frac{F_p \, \omega (s^2 + \frac{C}{M} s + \omega_y^2)}{M(s^2 + \omega^2) \left[(s^2 + \frac{C}{M} s + \omega_p^2)\,(s^2 + \frac{C}{M} s + \omega_y^2) - \omega_{py}^2 \omega_{yp}^2 \right]}$$

which has six terms in a partial fraction expansion. That is

$$p(s) = \frac{C_1}{s + j\omega} + \frac{C_2}{s - j\omega} + \frac{C_3}{s + s_3} + \frac{C_4}{s + s_4} + \frac{C_5}{s + s_5} + \frac{C_6}{s + s_6}$$

where s_3 through s_6 are the roots of the characteristic equation. Roots s_3 through s_6 are complex and there is no contribution from these last four terms to the steady-state motion. Thus

$$P_{ss}(s) = \frac{C_1}{s + j\omega} + \frac{C_2}{s - j\omega} \tag{3.1.29}$$

The first two coefficients of the partial fraction expansion are

$$C_1 = \lim_{s \to -j\omega} (s + j\omega)\, p(s)$$

$$C_2 = \lim_{s \to j\omega} (s - j\omega)\, p(s)$$

That is,

$$C_1 = \frac{F_p \left[-\omega^2 + (\frac{C}{M})(-j\omega) + \omega_y^2 \right]}{M(-2j)\left[(-\omega^2 - \frac{C}{M} j\omega + \omega_p^2)(-\omega^2 - \frac{C}{M} j\omega + \omega^2) - \omega_{py}^2 \omega_{yp}^2 \right]}$$

$$C_2 = \frac{F_p \, (-\omega^2 + \frac{C}{M} j\omega + \omega_y^2)}{M(2j)\left[(-\omega^2 + \frac{C}{M} j\omega + \omega_p^2)(-\omega^2 + \frac{C}{M} j\omega + \omega_y^2) - \omega_{py}^2 \omega_{yp}^2 \right]}$$

After much algebra

$$C_1 = \frac{(N_1N_3 + N_2N_4)j + N_1N_4 - N_2N_3}{N_3^2 + N_4^2} \quad \frac{F_p}{2M} \tag{3.1.30}$$

and C_2 is the conjugate of C_1, where

$$\left.\begin{aligned} N_1 &= -\omega^2 + \omega_{\bar{p}}^2 \sin^2\theta + \omega_{\bar{y}}^2 \cos^2\theta \\ N_2 &= -\frac{C}{M}\,\omega \\ N_3 &= (\omega_{\bar{p}}^2 - \omega^2)(\omega_{\bar{y}}^2 - \omega^2) - \left(\frac{C}{M}\right)^2 \omega^2 \\ N_4 &= -\frac{C}{M}\,\omega \left[(\omega_{\bar{p}}^2 - \omega^2) + (\omega_{\bar{y}}^2 - \omega^2)\right] \end{aligned}\right\} \tag{3.1.31}$$

Substituting C_1 and C_2 into Eq. (3.1.29) and taking the inverse Laplace transform gives the steady-state solution

$$p(t) = C_1 e^{-j\omega t} + C_2 e^{j\omega t} \tag{3.1.32}$$

This exponential solution can be expressed as a trigonometric solution

$$p(t) = A \sin(\omega t - \Phi) \tag{3.1.33}$$

where

$$A = \frac{\left[(N_1 N_4 - N_2 N_3)^2 + (N_1 N_3 + N_2 N_4)^2\right]^{\frac{1}{2}}}{N_3^2 + N_4^2} \frac{F_p}{M} \tag{3.1.34}$$

and

$$\tan\Phi = \frac{N_2 N_3 - N_1 N_4}{N_1 N_3 + N_2 N_4} \tag{3.1.35}$$

By substituting the values of N from Eqs. (3.1.31) into this equation the amplitude and phase angle are expressed in terms of principle values. That is, with the N_i values from Eqs. (3.1.31), the amplitude and frequency are in terms of the three parameters $\omega_{\bar{p}}$, $\omega_{\bar{y}}$, and $\frac{C}{M}$; or the four parameters $K_{\bar{p}}$, $K_{\bar{y}}$, C, and M.

The amplitude and phase angle of Eqs. (3.1.34) and (3.1.35) are the analytical values in the vehicle pitch direction. The corresponding experimental test values are shown in Figs. (3.5) and (3.6). At different frequencies (ω), values of amplitude $A = A_2$ and/or phase angle $\Phi = \Phi_{t2}$ are selected. Thus, the system parameters are determined by solving the resulting set of nonlinear algebraic equations.

It is not within the scope of this study to proceed further with the technique outlined above for finding the linear damping coefficient C. However, it is important to note that modal parameters for both pitch and yaw motion can be obtained from a single test. Thus, there may be a distinct advantage in the planar coupling which was originally considered to be an unfortunate oversight.

Rather than proceed with the coupled data it is considered a good approximation to uncouple the motion using a linearization technique which assumes that the system is linear and the principle pitch and yaw frequencies $\bar{\omega}_p$ and $\bar{\omega}_y$ are known. This is not a bad assumption because the two peaks observed in Fig. (3.2) indicate that

$$\bar{\omega}_p \doteq 11.40 \quad \text{rps.} \tag{3.1.36}$$

$$\bar{\omega}_y \doteq 11.50 \quad \text{rps.} \tag{3.1.37}$$

3.2 Linearized Data and Damping Coefficient.

In the previous section the accelerometer readings were used to obtain tail displacements and subsequently modal displacements and phase angles. Alternately one can assume a modal equation, or damping term in Eq. (2.2.5), and calculate the response in both the pitch and yaw directions independently; as if each is excited by a component of the actual force. Thus, Eqs. (3.1.7) through (3.1.12) are used for both the pitch and yaw motions with an assumed linear damping ξ_j and natural frequencies ω_j given by Eqs. (3.1.36) and (3.1.37). A control on the assumed damping is made by selecting one that makes the energy input per cycle in both the principle pitch and yaw directions sum to the total input energy per cycle.

Before the pitch and yaw response can be determined it is necessary to separate the input force into the pitch and yaw forces; as well as pitch and yaw energies, if energy loss per cycle is used to determine the damping coefficient. A sketch of the vehicle cross-section is shown in Fig. (3.8) where the barred axis refers to the principal (uncoupled) axis. As mentioned previously, the barred axes are $\theta = 28^{\circ}$ from the vehicle pitch and yaw axes.

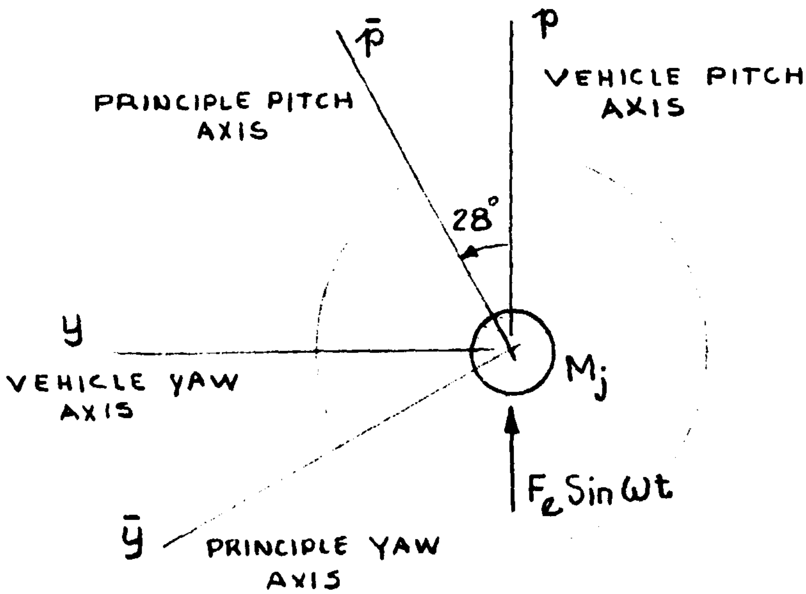

Figure 3.8 Rotation to Principle Pitch & Yaw Axes

To separate pitch and yaw motions the vehicle is considered to have two forces acting on it, one in the principle pitch direction and the other in principle yaw direction. That is, the modal forces are

$$F_{\bar{p}} = F_e \text{ Sin } \omega t \text{ Cos } \theta \tag{3.2.1}$$

$$F_{\bar{y}} = -F_e \text{ Sin } \omega t \text{ Sin } \theta \tag{3.2.2}$$

where the vehicle pitch force is

$$F_p = F \text{ Sin } \omega t \tag{3.2.3}$$

as given in Section (2.2). With the force applied at the tail node of the vehicle $F_e = \phi_{tj} F$

$$F_{\bar{p}} = \phi_{tj} F \text{ Sin } \omega t \text{ Cos } \theta \tag{3.2.4}$$

$$F_{\bar{y}} = -\phi_{tj} F \text{ Sin } \omega t \text{ Sin } \theta \tag{3.2.5}$$

for the j^{th} mode.

The energy loss per cycle for the damping force was discussed in Sections (2.3) and (2.4). Similarly for the external force

$$\Delta W/\text{cycle} = \int_{\text{cycle}} F(t)dx \tag{3.2.6}$$

where x is the displacement at the force or at the tail where

$$x_t = X_t \text{ Sin}(\omega t - \Phi_t) \tag{3.2.7}$$

as given in Eq. (3.1.21) for the second mode. Alternately one can write Eq. (3.2.6) as

$$\Delta W/\text{cycle} = \frac{1}{\omega} \int_{\Phi_t}^{2\pi+\Phi_t} F(t) \frac{dx_t}{dt} \, d(\omega t) \tag{3.2.8}$$

for the period of motion. Integrating this function gives

$$\Delta W/\text{cycle} = \pi X_t F \text{ Sin } \Phi_t \tag{3.2.9}$$

the energy input per cycle.

This energy input must be equal to the energy dissipation. The energy dissipation is discussed in Section (2.3) for different damping functions. In this section the modal damping is assumed to be linear viscous damping or (Case I)

$$g_j(\dot{Q}, Q) = C_{1j}\dot{Q} \tag{3.2.10}$$

The energy dissipation is given in Table 2.II as

$$\Delta W/\text{cycle} = \pi C_{1j} A_j^2 \omega$$

In terms of the damping factor used in the previous section ($C_{1j} = 2M_j\omega_j\xi_j$)

$$\Delta W/\text{cycle} = 2\pi M_j \omega_j \xi_j A_j^2 \omega \tag{3.2.11}$$

for the j^{th} mode.

There is energy dissipation in both the pitch and yaw modes. The amplitudes A_j are given in Eq. (3.1.8) for linear viscous damping. That is for the principle pitch amplitude

$$A_{j\bar{p}} = \frac{|F_{\bar{p}}|}{M_j\omega_{j\bar{p}}^2\left[(1 - r_{j\bar{p}}^2)^2 + (2\xi_j r_{j\bar{p}})^2\right]^{\frac{1}{2}}} \tag{3.2.12}$$

and similarly for the principle yaw amplitude. Substituting into (3.2.11) gives

$$\Delta W/\text{cycle}\Big|_{\bar{p}} = \frac{2\pi\left[\phi_{tj} F \cos\theta\right]^2 \xi_j\omega}{M_j\omega_{j\bar{p}}^3\left[(1 - r_{j\bar{p}}^2)^2 + (2\xi_j r_{j\bar{p}})^2\right]} \tag{3.2.13}$$

and for the principle yaw motion

$$\Delta W/\text{cycle}\Big|_{\bar{y}} = \frac{2\pi\left[\phi_{tj} F \sin\theta\right]^2 \xi_j\omega}{M_j\omega_{j\bar{y}}^3\left[(1 - r_{j\bar{y}}^2)^2 + (2\xi_j r_{j\bar{y}})^2\right]} \tag{3.2.14}$$

The input energy being made equal to the energy dissipation in each mode gives, from Eq. (3.2.9),

$$\pi X_t F \sin\Phi_t = \Delta W/\text{cycle}\Big|_{\bar{p}+\bar{y}} \tag{3.2.15}$$

where ξ_j is to be determined by trial and error.

Once again, numerical results for the Configuration I vehicle second mode will be used. The result is that ξ_2 will be determined for this vehicle. The known or assumed parameters for the second mode are

$$\left.\begin{aligned} \phi_{t2} &= 0.041 \\ \Theta &= 28 \text{ degrees} \\ M_2 &= 21.0 \text{ lbsec.}^2/\text{in.} \\ \omega_{2\bar{p}} &= 11.40 \text{ rps.} \\ \omega_{2\bar{y}} &= 11.50 \text{ rps.} \end{aligned}\right\} \qquad (3.2.16)$$

Those parameters which vary with frequency are F, X_t, Φ_t, and the frequency ratios $r_{j\bar{p}}$ and $r_{j\bar{y}}$. The left side of Eq. (3.2.15) can be plotted as a function of frequency using numerical values in Table 3.I and Fig. (3.3). This plot is shown in Fig. (3.9).

Actually the damping coefficient ξ can be found with only one value of ω. Substituting Eqs. (3.2.13) and (3.2.14) into Eq. (3.2.15), and selecting a frequency and input energy from Fig. (3.9), one can solve for the damping factor ξ. For example with $\omega \doteq \omega_{\bar{p}} = 11.39$

$$114.5 = \frac{2\pi[.041(922)(.883)]^2\xi(11.39)}{21.0(11.40)^3[(1-.999)^2 + 4\xi^2(.999)^2]}$$

$$+ \frac{2\pi[.041(922)(.469)]^2\xi(11.39)}{21.0(11.50)^3[(1-.991)^2 + 4\xi^2(.991)^2]}$$

Solving for ξ by trial and error gives

$$\xi = .0059$$

which represents approximately .6 percent of critical damping. Consequently the amount of energy dissipated in the principle pitch direction is 106.1 inch pounds compared with 8.40 inch pounds in the principle yaw direction when $\omega = 11.39$. The corresponding amplitudes at this frequency are $A_{2\bar{p}} = 1.025$ inches and $A_{2\bar{y}} = .286$ inches.

At each value of ω for which the input energy and force is known a damping factor is obtained and a set of amplitudes and energy losses per cycle are calculated. The results are shown in Table 3.IV. Note that a considerable variation in the linear damping coefficient ξ occurs. This coefficient is shown to vary with frequency; having the largest value near the resonant frequencies. The average, or equivalent, linear damping coefficient for this second mode is $\xi = .005$. Therefore, the average damping coefficient is

$$c_1 = \frac{2M}{m} \sum_{i=1}^{m} \omega_i \xi_i = 2.30 \tag{3.2.18}$$

where m = 15, the number of data points. The average linear second mode(s) Configuration I vehicle damping force defined by Eq. (3.2.10) is

$$\boxed{g_s(Q, \dot{Q}) = 2.30\, \dot{Q}} \tag{3.2.19}$$

A plot of the principal pitch and yaw amplitudes is shown in Fig. (3.10). With the exception of two data points for the pitch amplitudes the curves are symmetrical. Checking these two points (6 & 9) in Figs. (3.2) and (3.3), it is noted that experimental values for these points are sensitive to slight variations in frequency. For the further studies in Chapter V the amplitude at point six is taken as .885 and at point nine is taken as 1.010 to eliminate experimental errors (see Table 3.IV). One can conclude from Fig. (3.10) that the principle cause of the unsymmetry shown in the modal amplitude of Fig. (3.6) is pitch and yaw coupling.

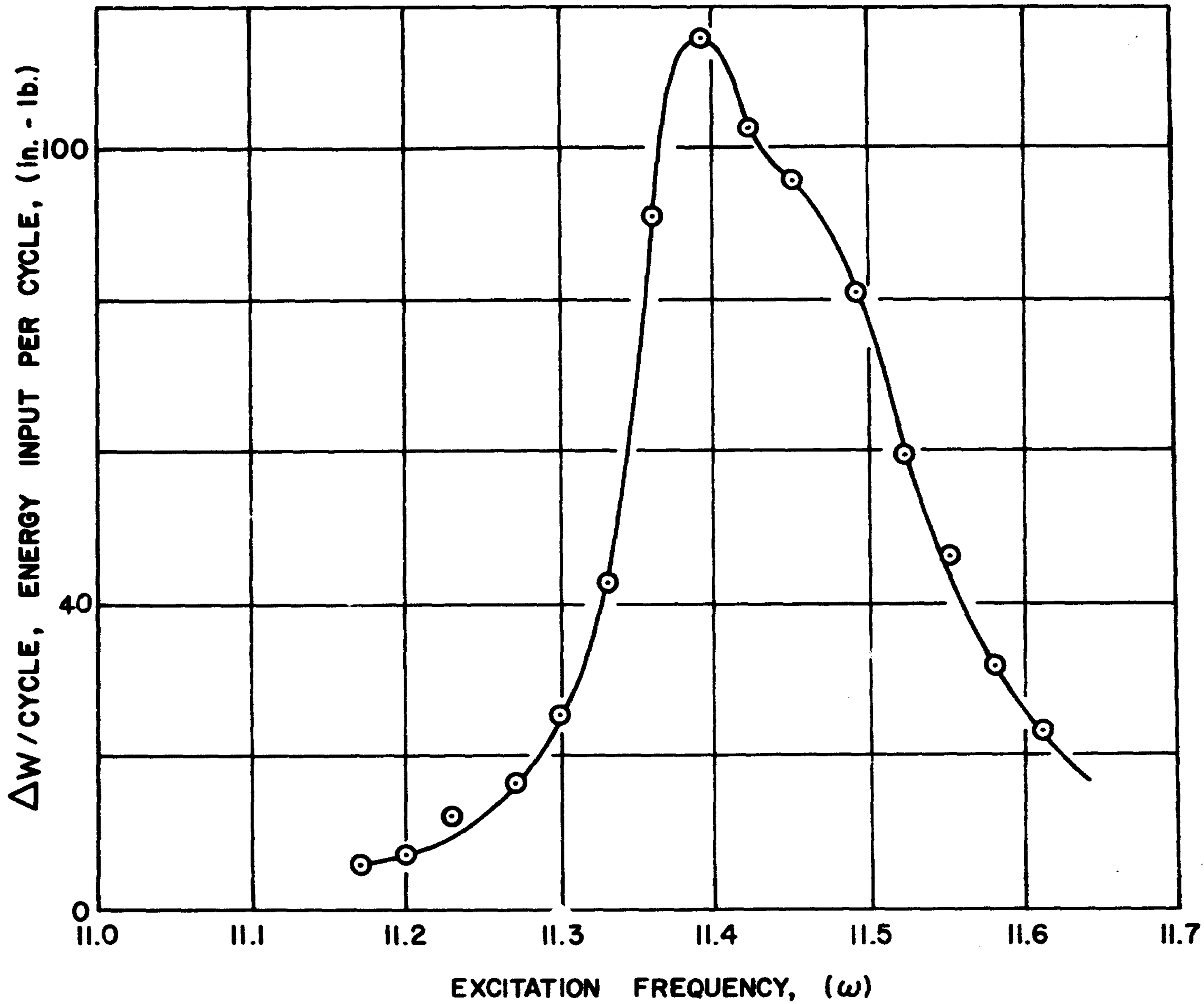

FIG. 3.9 ENERGY INPUT PER CYCLE - SECOND MODE

TABLE 3.IV LINEAR DAMPING COEFFICIENT AND PITCH & YAW SECOND MODE VALUES

POINT	INPUT FREQUENCY ω	ENERGY INPUT* ΔW/cycle	LINEAR DAMPING** ξ	PITCH MODE PARAMETERS A_{2p}- in.	PITCH MODE PARAMETERS ΔW/cycle	YAW MODE PARAMETERS A_{2y}- in.	YAW MODE PARAMETERS ΔW/cycle
1	11.17	5.75	.00328	.310	5.05	.115	.70
2	11.20	6.87	.00276	.364	6.11	.127	.76
3	11.235	10.6	.00296	.438	9.55	.146	1.05
4	11.27	16.3	.00290	.552	14.90	.169	1.40
5	11.30	25.8	.00300	.690	24.0	.190	1.80
6	11.33	43.0	.00250	.990	40.6	.224	2.40
6+	11.33	53.8	.00378	.885	50.6	.217	3.16
7	11.36	91.0	.0053	.974	85.5	.245	5.50
8	11.39	114.5	.0059	1.025	106.1	.286	8.40
9	11.42	104.7	.0063	.935	93.2	.341	12.6
9+	11.42	113.0	.0058	1.010	100.5	.350	12.5
10	11.455	95.8	.0050	.923	73.5	.487	20.6
11	11.49	81.0	.00330	.719	29.4	.948	51.6
12	11.52	59.4	.00430	.546	22.2	.703	37.3
13	11.55	46.0	.0070	.421	21.6	.379	20.7
14	11.58	31.9	.0092	.343	18.80	.286	13.1
15	11.61	23.6	.0082	.310	13.75	.259	9.85

* See Table 3.I for parameters.

** Second mode constants are in Eq. (3.2.16).

+ Corrected for experimental error.

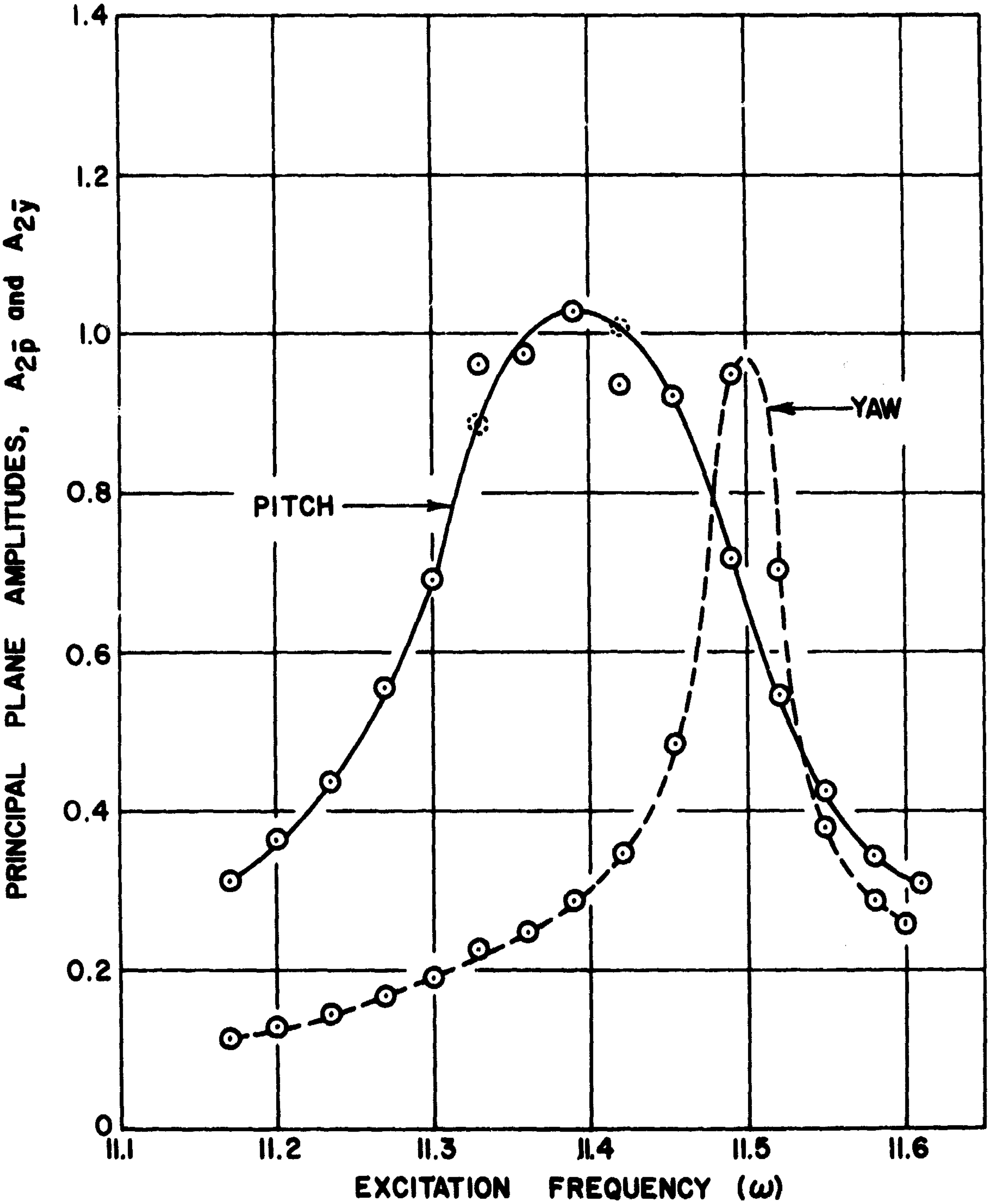

FIG. 3.10 PRINCIPAL PITCH AND YAW MODAL AMPLITUDES VERSUS FREQUENCY - SECOND MODE

CHAPTER IV

DETERMINATION OF A NONLINEAR DAMPING FORCE

The purpose of this chapter is to permit the damping force to be a nonlinear function of modal amplitudes and velocities. The analytical techniques for obtaining this modal damping force are discussed in detail. Once again the techniques are limited by the type and accuracy of the experimental test data.

In general the computed values of linear viscous damping change as the amplitude of motion changes. This indicates that the viscous damping coefficient is not a constant in the modal equations of motion. To predict what damping coefficient to use for amplitudes outside the range of test values is only a hazardous guess. However, with a nonlinear damping force one can obtain a constant damping coefficient which has a much better chance of predicting responses outside the range of test values. Furthermore, response amplitude versus frequency plots can be approximated more accurately.

Experimental data on the Configuration II vehicle, discussed in Chapter II, provides enough necessary information for analytical studies. In this test data, three amplitude versus frequency sweeps were conducted over the first and second modes. This additional information provides the extra data necessary to calculate what type of damping force should be used, as well as the constant coefficient of this damping term, or terms.

4.1 From Variable Linear Damping Coefficients.

The modal equation of motion given by Eq. (2.2.5) is

$$\ddot{Q} + \frac{1}{M}g[Q, \dot{Q}] + \omega_n^2 Q = \frac{F_e}{M} \text{Sin } \omega t$$

where $g(Q, \dot{Q})$ is the modal damping force. With linear viscous damping

$$g(Q, \dot{Q}) = C_1\dot{Q} \tag{4.1.1}$$

which is Case I in Table I. Thus

$$\ddot{Q} + \frac{C_1}{M}\dot{Q} + \omega_n^2 Q = \frac{F_e}{M} \text{Sin } \omega t \tag{4.1.2}$$

which is a linear differential equation. The coefficient of the damping term can be written

$$\frac{C_1}{M} = 2\zeta_1\omega_n$$

where

$$\xi_1 = \frac{C_1}{2M\omega_n} \tag{4.1.3}$$

Values of ξ_1 have been computed by The Boeing Company [2] for the Configuration II vehicle for three different resonant amplitudes and for the first and second modes. A procedure for calculating these ξ_1 values is discussed below.

The steady state solution of Eq. (2.1.2), with the input frequency the same as the modal frequency (resonance at $\omega = \omega_n$), becomes

$$Q_{ss} = \frac{F_e}{2M\omega_n^2\xi_1} \text{Cos } \omega_n t \tag{4.1.4}$$

Thus, the maximum amplitude at resonance becomes

$$A_m = \frac{F_e}{2M\omega_n^2\xi_1} \tag{4.1.5}$$

which shows that the amplitude varies linearly with the input force amplitude. Solving for the damping coefficient

$$\zeta_1 = \frac{F_e}{2M\omega_n^2 A_m} \tag{4.1.6}$$

or

$$C_1 = \frac{F_e}{\omega_n A_m} \tag{4.1.7}$$

The dynamic parameters of the mode necessary to calculate the damping parameters are obvious from Eq. (4.1.6). These parameters were available directly from test data and strip charts. However, some of the accelerometer readings were obviously in error and were not averaged in with the others. The dynamic parameters of the first and second mode are shown in Table 4.I for the three different force levels used in each sweep of frequency.

The modal amplitude A_m is computed from Eq. (4.1.5) and the damping coefficient C_1 is computed using Eq. (4.1.7) with $\omega_n = 2\pi f_n$. These results are shown in Table 4.II. The results show that the damping coefficient changes. This should not be true if the natural frequency does not change and the system is linear (A_m directly proportional to F_e); see Eq. (4.1.7).

The damping coefficient C_1 as a function of A_m for the first mode is shown in Fig. (4.1) and for the second mode is shown in Fig. (4.2). These curves along with the additional system parameters of energy dissipation can be used to obtain a new damping force $g(Q, \dot{Q})$ with appropriate constant damping coefficients. For the average linear damping coefficient, the damping force for the first (F) mode is

$$\left.\begin{aligned}&\boxed{g_F(Q, \dot{Q}) = 1.643\,\dot{Q}}\\&\text{and for the second(s) mode is}\\&\boxed{g_s(Q, \dot{Q}) = 5.797\,\dot{Q}}\end{aligned}\right\}\quad(4.1.8)$$

TABLE 4.I 500-D VEHICLE YAW TESTS (CONFIGURATION II)

Sweep/Test Info.	First Mode	Second Mode
"A"		
F = Force	675 lb.	970
f_n = Modal Frequency	1.66882 cps.	2.72468
M = Generalized Mass	48.7921 lb.sec.^{2}/in.	33.0058
ζ_1 = Average Damping	.00146946	.00465191
ϕ_r = Displ. at Load Pt.	.028685	.028415
F_e = Modal Force = $\phi_r F$	19.37 lb.	27.35
"B"		
Force	875	1426
Modal Frequency	1.66577	2.71952
Generalized Mass	49.2457	37.2351
Average Damping	.00160711	.00455892
Displ. at Load Pt.	.028521	.028272
Modal Force	24.95	40.35
"C"		
Force	1035	1944
Modal Frequency	1.66401	2.71573
Generalized Mass	50.7830	33.5607
Average Damping	.00166541	.00552947
Displ. at Load Pt.	.028006	.028725
Modal Force	28.98	55.80

From previous work shown above

$$\frac{\Delta W}{\text{cycle}} = \pi A_m^2 \omega C_1$$

for linear viscous damping, see Table 2.II. However, the damping coefficient, C_1, in linearly dependent on amplitude, A_m as shown in Fig. (4.1) and (4.2).

TABLE 4.II DAMPING COEFFICIENT, AMPLITUDE, AND ENERGY LOSS

Mode/Sweep	C_1 = linear damping coeff.	A_m = modal amplitude	ΔW/cycle = energy loss per cycle
1^{st}			
A	1.504 $\frac{\text{lb. sec.}}{\text{in.}}$	1.229 in.	74.76 in. lb.
B	1.657	1.439	112.79
C	1.768	1.567	142.69
2^{nd}			
A	5.257	.3061	26.49
B	5.801	.4071	51.60
C	6.333	.5164	90.52

That is,

$$C_1 = C_{01} + C_{11}A_m \tag{4.1.9}$$

where C_{01} is the value of C_1 at $A_m = 0$ and C_{11} is the average slope of the two line segments (practically the same for each segment). Thus

$$\left.\begin{aligned} C_1 &= .506 + .800A_m \quad \text{"First Mode"} \\ C_1 &= 3.715 + 5.127A_m \quad \text{"Second Mode"} \end{aligned}\right\} \tag{4.1.10}$$

Substituting Eq. (4.1.9) into Eq. (4.1.8) shows in general for the first two modes

$$\frac{\Delta W}{\text{cycle}} = \pi A_m^2 \omega C_{01} + \pi A_m^3 \omega C_{11} \tag{4.1.11}$$

where C_{01} and C_{11} are constant for all A_m values. As shown in Table 2.II, the second term on the left is the typical form for the energy loss per cycle when the damping term in Eq. (4.1.2) is

$$g(Q, \dot{Q}) = C_3|Q|\dot{Q} \qquad (4.1.12)$$

That is, for this damping term

$$\frac{\Delta W}{\text{cycle}} = \frac{4}{3} A_m^3 \omega C_3$$

and from Eq. (4.1.11)

$$C_3 = \frac{3}{4} \pi C_{11} \qquad (4.1.13)$$

Also, some linear viscous damping is present as indicated by the first term on the left in Eq. (4.1.11). Thus, the damping force for the first (F) mode becomes

$$\boxed{g_F(Q, \dot{Q}) = .506\,\dot{Q} + 1.886|Q|\dot{Q}} \qquad (4.1.14)$$

and for the second (s) mode becomes

$$\boxed{g_s(Q, \dot{Q}) = 3.715\,\dot{Q} + 12.08|Q|\dot{Q}} \qquad (4.1.15)$$

These results indicate that a better expression for the modal equation of motion to replace Eq. (4.1.2) is

$$\ddot{Q} + \frac{C_1}{M}\dot{Q} + \frac{C_3}{M}|Q|\dot{Q} + \omega_n^2 Q = \frac{F_e}{M}\sin \omega t \qquad (4.1.16)$$

for the Configuration II vehicle being studied. Because of the limited experimental data this must be considered as a first-order correction to the damping term. With additional experimental data one may find that the equivalent linear damping coefficient is a function of amplitude to a higher power than that obtained above. Also, one may find a dependence of the linear damping coefficient on frequency as amplitude is held constant.

The main objective of this study was to show a method with which one can obtain a better damping term than the commonly used linear viscous damping by using experimental data based on linear damping. This was done with the limited data available on the Configuration II vehicle. The same procedure may be followed on other missile configurations. It is recommended that such studies be conducted with much more experimental data being made available.

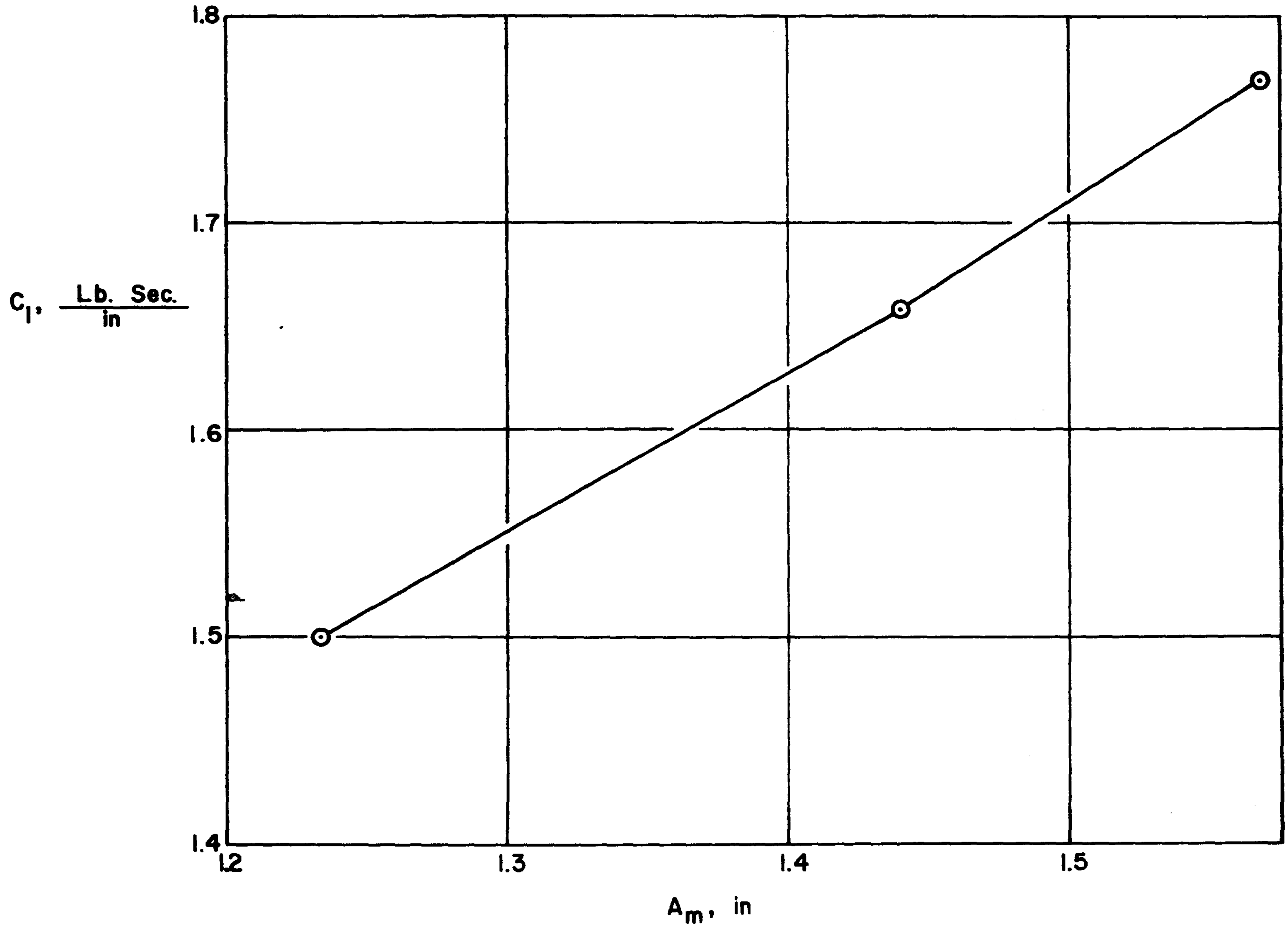

FIG. 4.1 LINEAR DAMPING COEFFICIENT AS A FUNCTION OF RESONANT AMPLITUDE - FIRST MODE

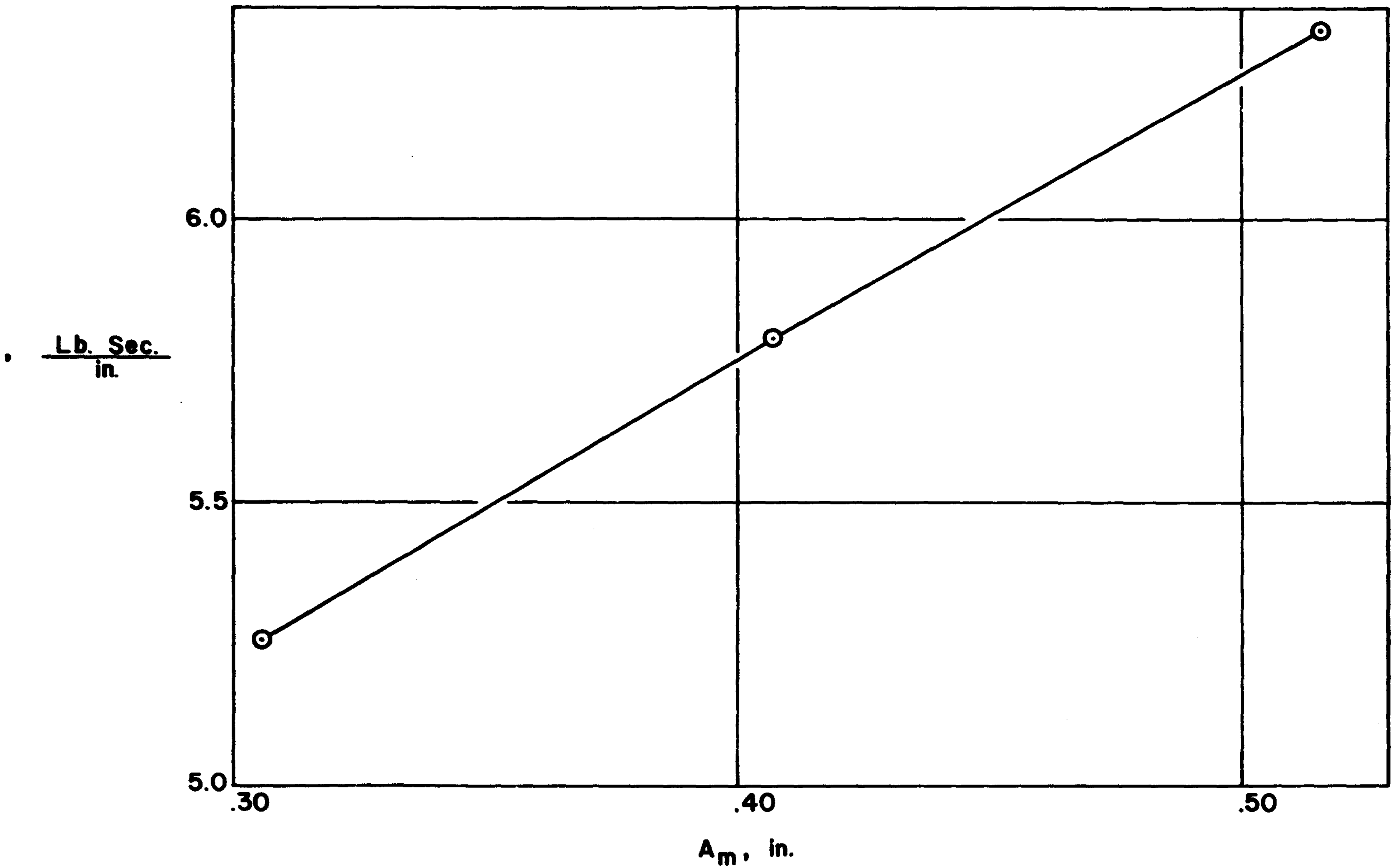

FIG. 4.2 LINEAR DAMPING COEFFICIENT AS A FUNCTION OF RESONANT AMPLITUDE - SECOND MODE

4.2 From Amplitude Versus Frequency Plots.

Normally the test information is displayed as an amplitude versus frequency plot at each vehicle station. The corresponding modal displacement versus frequency is obtained as shown in Chapter III, Section 3.2. If the experimental data is of sufficient accuracy the shape of the amplitude-frequency curve will indicate the type or types of damping present. Coeffients of the damping functions are once again determined from resonant amplitudes.

To use this method requires one to obtain an approximate solution of the nonlinear differential equations of motion. All five cases of damping will be considered by substituting into Eq. (2.2.5).

The method preferred by this author to solve the nonlinear modal equations of motion for systems having a steady-state response is the Ritz Averaging Method [10]. Solving the modal equation of motion

$$\ddot{Q} + \frac{1}{M} g[Q, \dot{Q}] + \omega_n^2 Q = \frac{F_e}{M} \text{Sin } \omega t \qquad (2.2.5)$$

given previously, with different cases of damping (see Table 2.I) forms a basis for comparing these cases. Furthermore, a direct link between the methodology of this section and energy loss per cycle is possible. For a review of the Ritz Averaging Method, the following discussion is included.

Galerkin says to expand the solution Q(t) into a series

$$Q(t) = \sum A_n \psi_n(t)$$

If the series is the exact one, when substituted into Eq. (2.2.5)

$$S[Q] = \ddot{Q} + \frac{1}{M} g(Q, \dot{Q}) + \omega_n^2 Q - \frac{F_e}{M} \text{Sin } \omega t = 0$$

However, an exact series is rarely known, so one is faced with an approximate solution series $\overline{Q}(t)$ and

$$S[\overline{Q}] = \ddot{\overline{Q}} + \frac{1}{M} g(\overline{Q}, \dot{\overline{Q}}) + \omega_n^2 \overline{Q} - \frac{F_e}{M} \text{Sin } \omega t \neq 0$$

The object is to make the error

$$S[\overline{Q}] - S[Q] = S[\overline{Q}]$$

a minimum. Ritz says make $\psi_n(t)$ harmonic functions and minimize the error over one cycle. Using the first two terms of Fourier series

$$\overline{Q}(t) = A_1 \text{ Cos } \omega t + A_2 \text{ Sin } \omega t = A \text{ Cos } (\omega t - \Phi) \qquad (4.2.1)$$

The idea is to minimize the integral error squared or

$$I_n = \sum_{n=1}^{2} \frac{\partial}{\partial A_n} \int_{t_o}^{t_1} \left\{ S[\overline{Q}] - S[Q] \right\}^2 dt = 0$$

With two constants

$$I_n = \int_0^{2\pi} S[\overline{Q}] \frac{\partial S[\overline{Q}]}{\partial A_n} d(\omega t) = 0, \; n = 1, 2$$

Substituting $\overline{Q}(t)$ from Eq. (4.2.1) into this equation yields

$$I_1 = -\left(\frac{\omega}{\omega_n}\right)^2 \text{Cos } \Phi + G(A, \omega) + \text{Cos } \Phi - \frac{F_e}{M\omega_n^2 A} = 0$$

$$I_2 = -\left(\frac{\omega}{\omega_n}\right)^2 \text{Sin } \Phi - G(A, \omega) + \text{Sin } \Phi = 0$$

where

$$G(A, \omega) = \frac{4}{\pi \omega_n^2 MA} \int_0^{2\pi} g(\overline{Q}, \dot{\overline{Q}}) \text{ Sin } (\omega t - \Phi) d(\omega t) \qquad (4.2.2)$$

The phase angle Φ is determined from I_2 as

$$\Phi = \text{arc tan } \frac{G(A, \omega)}{1 - \left(\frac{\omega}{\omega_n}\right)^2} \qquad (4.2.3)$$

Klotter found that by combining I_1 and I_2 in a particular way that a simple expression can be obtained. That is, with $\eta^2 = \left(\frac{\omega}{\omega_n}\right)^2$

$$(1 - \eta^2)^2 + [G(A, \omega)]^2 = \left(\frac{F_e}{M\omega_n^2 A}\right)^2 \tag{4.2.4}$$

The amplitude versus frequency curve is easily obtained by plotting this equation in parts. First, the first term on the left side is plotted, then the forcing term on the right is added to obtain an undamped curve. Then the damping term is added and the final A versus η^2 curve is obtained for a particular modal mass M, frequency ω_n, and equivalent force F_e (See Fig. 4.3). Different curves are obtained for each damping case $g(Q, \dot{Q})$ used in Eq. (4.2.2) or Eq. (4.2.4). Differences can be used to evaluate the representation of damping, and to determine which one is best if accurate experimental amplitude frequency curves are available.

A very important relationship is found to exist between energy losses per cycle, as given in Table 2.II, and the damping term in Eq. (4.2.4), as given by Eq. (4.2.2). That is

$$G_i(A, \omega) = \frac{\mathcal{L}_i}{C_i \pi A^2 \omega_n} \cdot \quad \Delta W/\text{cycle} \tag{4.2.5}$$

where $\mathcal{L}_i$ is the normalized damping coefficient normalized with respect to critical linear viscous damping (note that $\mathcal{L}_1 \equiv \xi_1$ shown in Eq. (4.1.3))

$$\mathcal{L}_i = \frac{C_i}{2M\omega_n} \tag{4.2.6}$$

Table 4.III is a summary of the five cases of damping studied previously and shows the damping force, energy loss per cycle, and damping term. One should further note that the denominator on the right side of Eq. (4.2.5) is similar to the energy loss for viscous damping.

The best method to show differences in amplitude versus frequency for various damping cases is to observe the horizontal difference, δ , and the

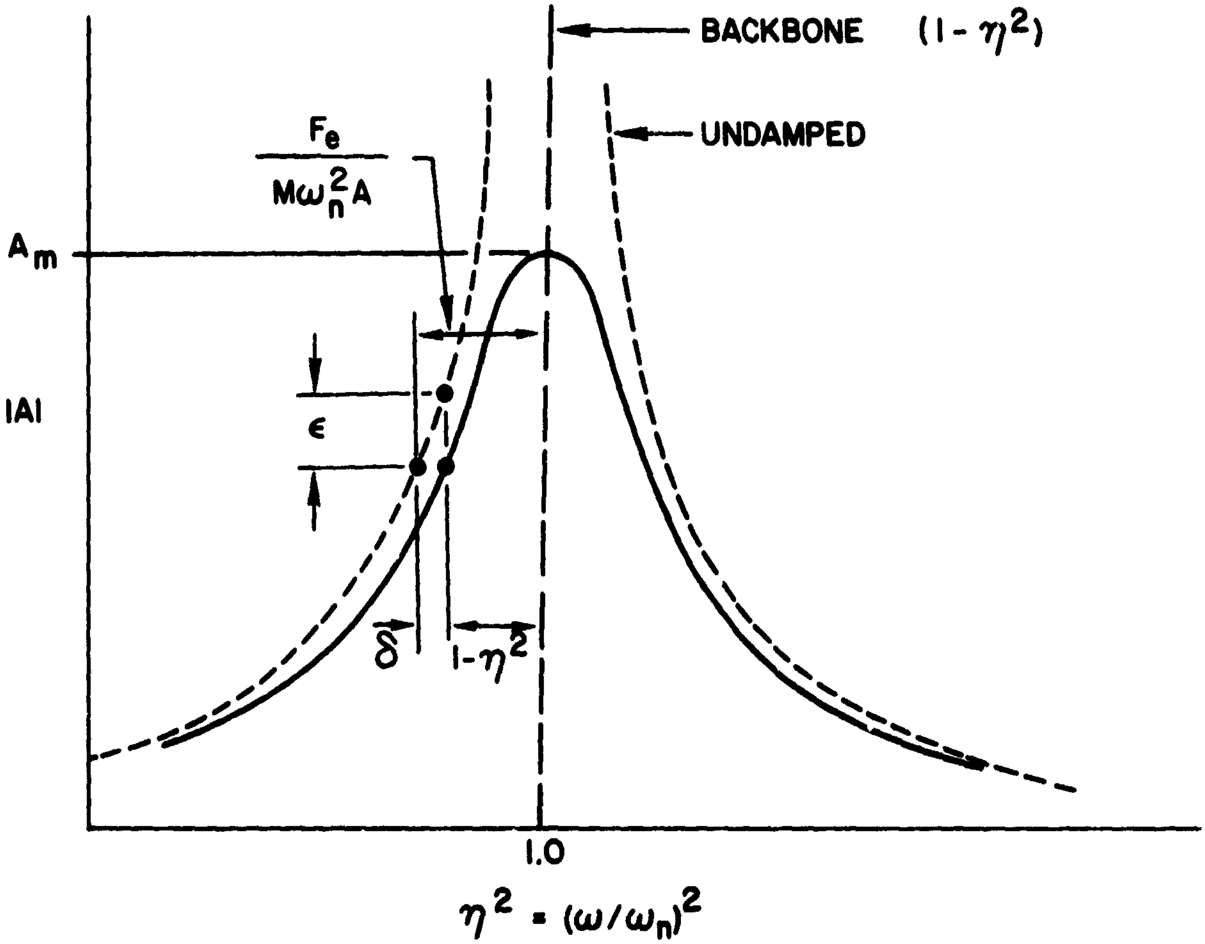

FIG. 4.3 TYPICAL AMPLITUDE VERSUS FREQUENCY RATIO CURVE

vertical difference, ϵ , between the undamped and damped curves, as shown in Fig. (4.3). Numerical results for the bending of the Saturn V vehicle show that the most narrow spike for the first mode results from Cases I and II, and Cases III and IV yield the widest spike. Case V can be made narrow or wide depending on the free parameter α. Furthermore, damping can be neglected except for a narrow band of frequencies near resonance ($\eta^2 = 1$). This helps justify the statements of Chang [3] quoted and used in obtaining the modal equations of motion, Eq. (2.2.5).

TABLE 4.III DAMPING TERM FOR DIFFERENT CASES OF DAMPING

Case	Damping Force $g(\bar{Q}, \dot{Q})$ lb.	Energy Loss/Cycle ΔW/cycle	Damping Term $G(A, \omega)$
I	$C_1 \dot{Q}$	$C_1 \pi A^2 \omega$	$2\mathcal{L}_1 \frac{\omega}{\omega_n}$
II	$C_2 \lvert Q \rvert (\mathrm{sgn}\ \dot{Q})$	$2C_2 A^2$	$4\mathcal{L}_2 \frac{1}{\pi \omega_n}$
III	$Q_3 (\dot{Q})^2 (\mathrm{sgn}\ \dot{Q})$	$\frac{8}{3} C_3 A^3 \omega^2$	$\frac{16}{3} \mathcal{L}_3 \frac{A\omega^2}{\pi \omega_n}$
IV	$C_4 \lvert Q \rvert \dot{Q}$	$\frac{4}{3} C_4 A^3 \omega$	$\frac{8}{3} \mathcal{L}_4 \frac{A\omega}{\pi \omega_n}$
V	$C_1(\dot{Q} + \alpha Q^2 \dot{Q})$, $C_1 \alpha = C_5$	$C_1 \pi A^2 \omega (1 + A^2 \frac{\alpha}{4})$	$2 \mathcal{L}_1 \frac{\omega}{\omega_n} (1 + A^2 \frac{\alpha}{4})$

The undamped curve is the same for all cases. The difference between the damped and undamped curves is a function of the type of damping in the system. This is represented by a horizontal difference δ(or $1 - \eta^2$) at a particular amplitude, or by a vertical difference ϵ at a particular frequency ratio, see Fig. (4.3). The different curves for different damping cases can be compared with experimental data and the curve which fits the data best is the single one that should be used for the system. Similar conclusions are possible by using the phase angle, Φ, versus frequency ratio, η^2.

One must know the dynamic parameters to plot amplitude versus frequency ratio curves. Given the generalized mass M, natural modal frequency ω_n, and equivalent modal force F_e, the various damping coefficients $\mathcal{L}_n$, n = 1, 2, 3, 4, 5, are calculated knowing the resonant modal amplitude A_m. To illustrate, the values given in Table 4.I, as obtained for the Saturn V Configuration II first mode vehicle tests (Sweep C), are used as follows:

$$M = 50.7838 \frac{\text{lb. sec.}^2}{\text{in.}}$$

$$f_n = 1.66401 \text{ cps.}$$

$$F_e = 28.98 \text{ lb.}$$

$$A_m = 1.567 \text{ in.}$$

The undamped curve is obtained using the first three values. The damping coefficients $\mathcal{L}_n$ are obtained when $\eta^2 = 1$, or $\omega = \omega_n$, and $A = A_m$. Thus for each case

$$\left.\begin{aligned} \mathcal{L}_1 &= \frac{F_e}{2M\omega_n^2 A_m} \\ \mathcal{L}_2 &= \frac{\pi F_e}{4M\omega_n A_m} \\ \mathcal{L}_3 &= \frac{3\pi F_e}{16M\omega_n^3 A_m^2} \end{aligned}\right\} \qquad (4.2.7)$$

$$\left.\begin{aligned} \mathcal{L}_4 &= \frac{3\pi F_e}{8M\omega_n^2 A_m^2} \\ \mathcal{L}_1 &= \frac{F_e}{2M\omega_n^2 A_m} \times \frac{4}{4 + \alpha A_m^2}, \ \mathcal{L}_1 \alpha = \mathcal{L}_5 \end{aligned}\right\} \quad (4.2.7)$$

For the last case $\mathcal{L}_1$ is given if the damping coefficient α is known. Furthermore, with two terms and two coefficients representing the damping $g(\overline{Q}, \dot{\overline{Q}})$, an additional degree of freedom exists. Thus, the curve can be made to fit another data point; say at $\eta^2 = \eta_1^2$, or $\omega = \omega_1$, where $A = A_1$. This allows for $\mathcal{L}_1$ and α to be solved for simultaneously. In general, one could have "k" damping terms and coefficients which could be made to fit "k" data points.

Figures (4.4) are for the experimental data given above. In Fig. (4.4) one curve is for the undamped case and the other two curves are for Cases I through IV. Figure (4.5) is for Case V with $\alpha = 1.0$ and $\alpha = 100.0$. Case I has the narrowest spike and Case IV is the widest spike. Case III lies slightly inside Case IV and Case II lies slightly outside Case I. Case V is the same as Case I with $\alpha = 0$ but wider than Case IV when $\alpha = 100.0$. Curves for the phase angle Φ, as given by Eq. (4.2.3), as a function of frequency ratio, complement the amplitude versus frequency curves. Figure (4.6) shows all cases superimposed on a single coordinate system.

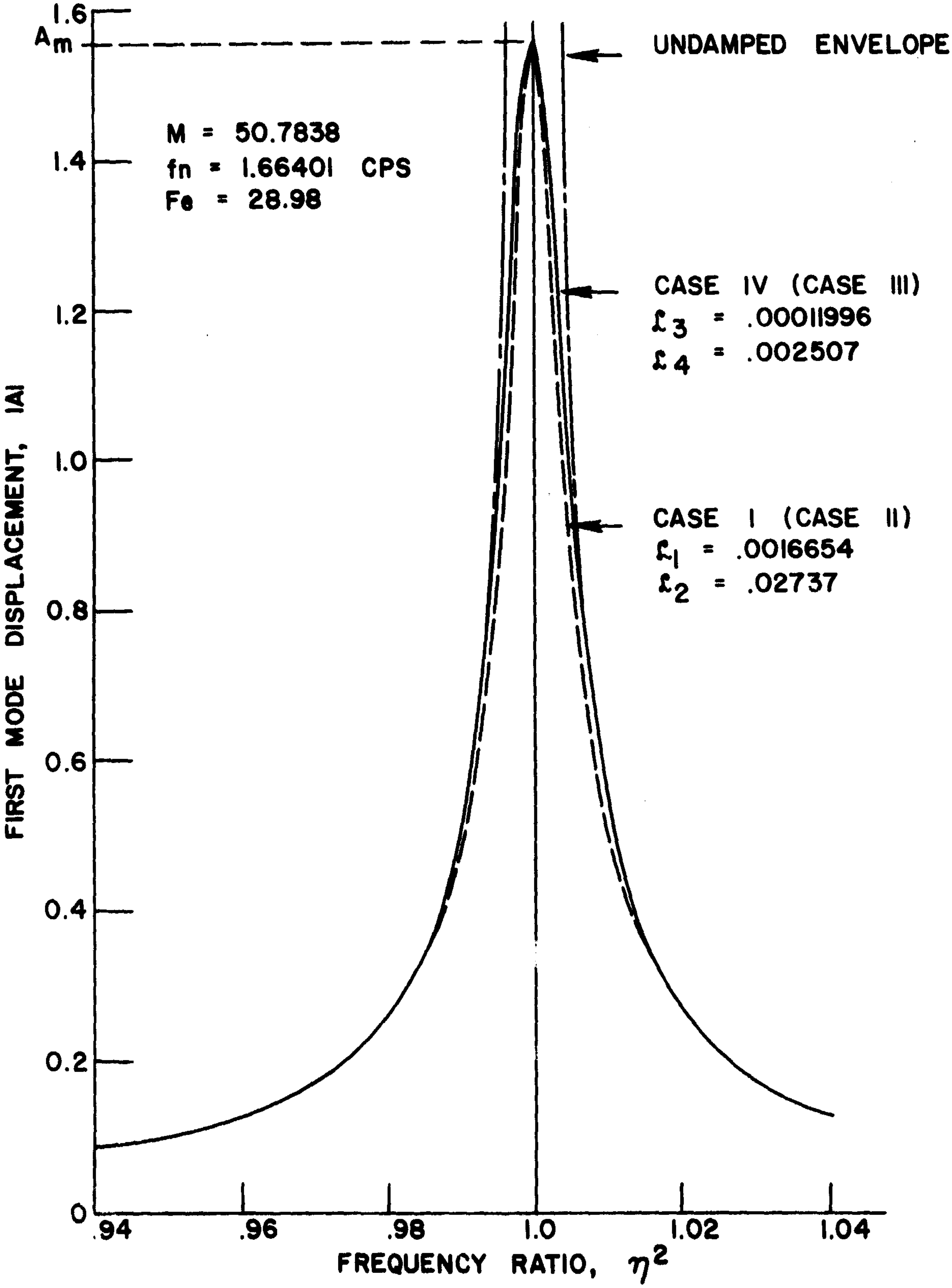

FIG. 4.4 DISPLACEMENT VERSUS FREQUENCY RATIO SQUARED, CASES I-IV

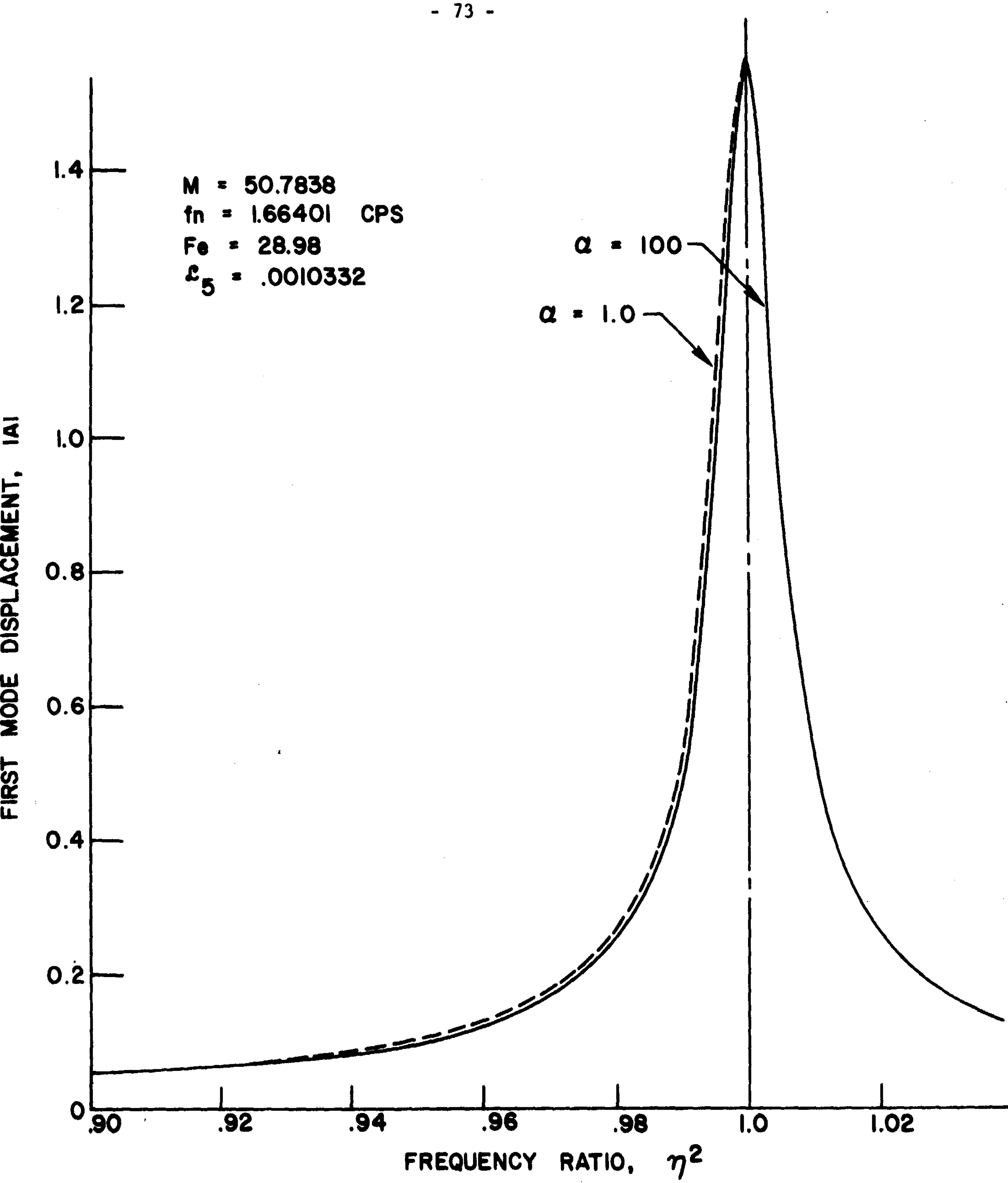

FIG. 4.5 DISPLACEMENT VERSUS FREQUENCY RATIO SQUARED, CASE V

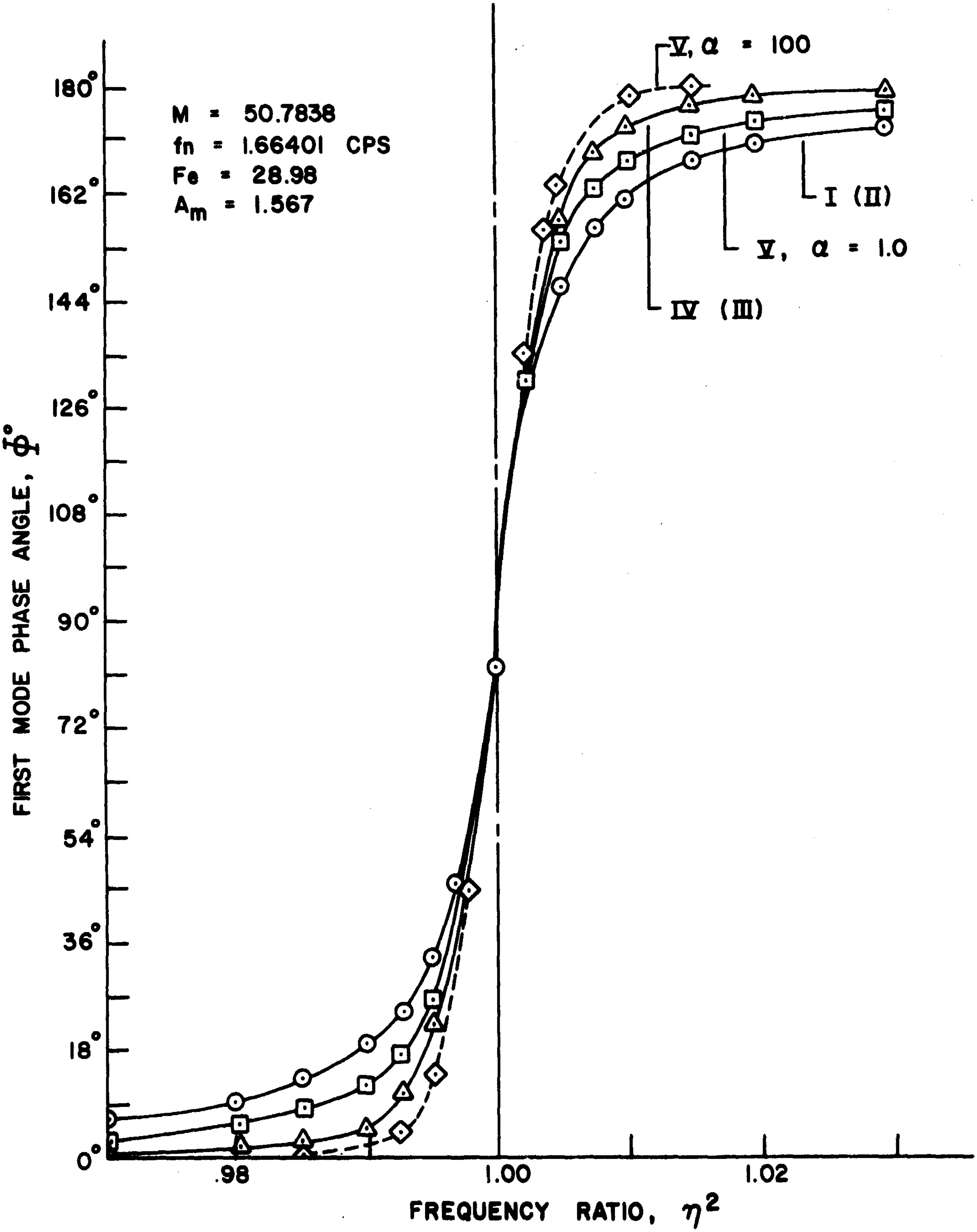

FIG. 4.6 PHASE ANGLE VERSUS FREQUENCY RATIO SQUARED

From the above amplitude versus frequency curves it is hard to distinguish differences between each damping case. A better indicator is the difference between the damped and undamped curves both horizontally (δ) and vertically (ϵ), as indicated previously. Figure (4.7) shows the horizontal difference δ as a function of amplitude A. Figure (4.8) shows the vertical difference ϵ as a function of amplitude A. From these curves one can distinctly see differences between the various representations of damping. Note that ϵ versus A is only useful for small values of A. Experimental data points can also be plotted on these difference curves if the curve envelope defining by the undamped system is determined. As shown previously, the undamped curve lies at a distance

$$\pm \frac{F_e}{M\omega_n^2 A}$$

from the backbone ($\eta^2 = 1$) curve. Therefore,

$$\frac{F_e}{M\omega_n^2 A} - (1 - \eta^2) = \delta_e, \ \eta^2 < 1 \qquad (4.2.8)$$

where A and η are data points and δ_e is the experimental δ. It then becomes a simple observation to see what curve or damping representation is the best fit for the data. Thus, the best representation of damping is known. Difficulty in implementing this procedure for finding the best damping term is discussed below.

After further investigation it becomes apparent that the horizontal difference, δ, is very small compared with the distance from the backbone to the undamped curve, $F_e/M\omega_n^2 A$, for small values of amplitude. The maximum distance from the undamped curve (δ) occurs for Case I damping.

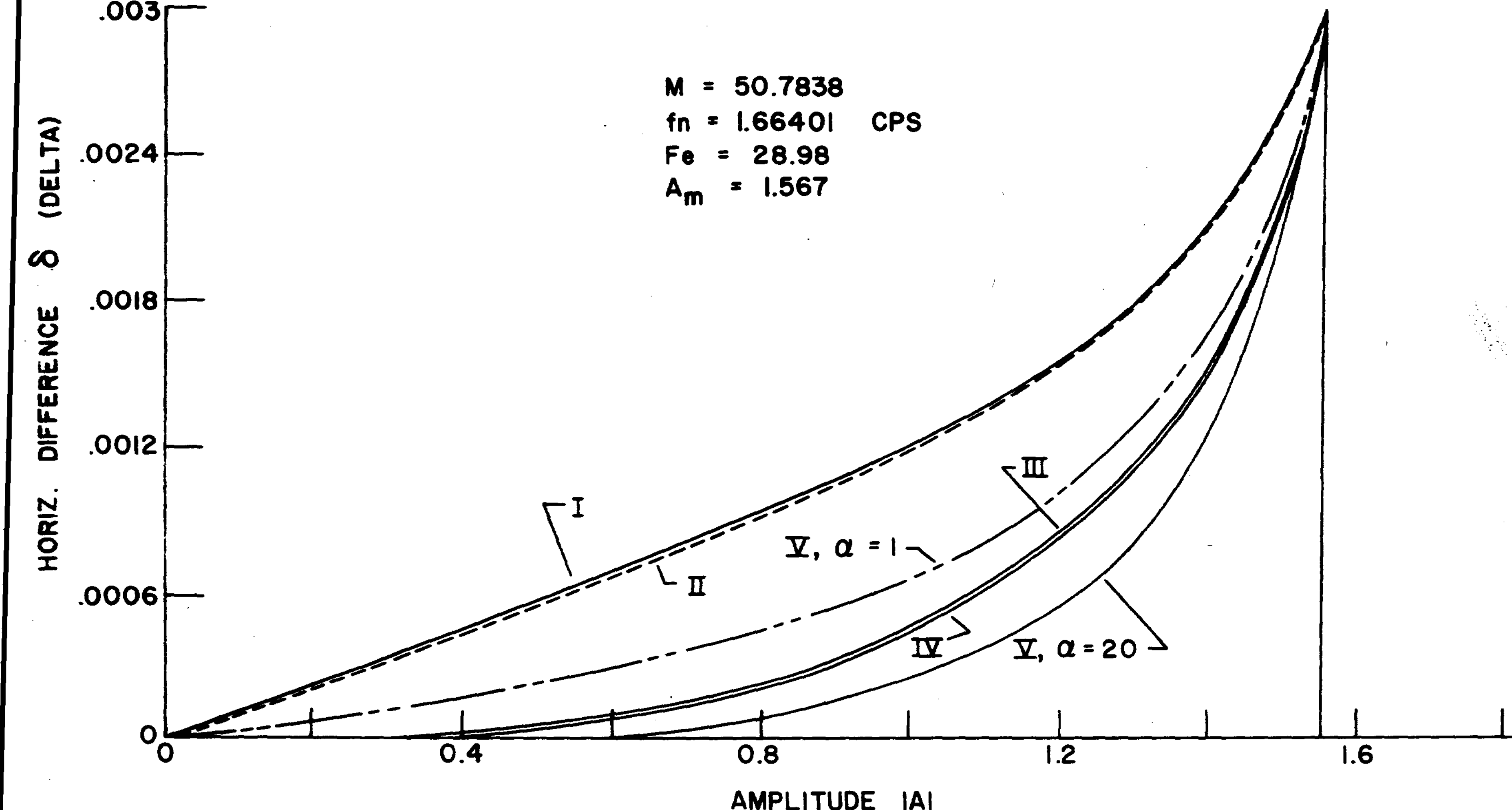

FIG. 4.7 HORIZONTAL DIFFERENCE (δ) VERSUS AMPLITUDE - FIRST MODE

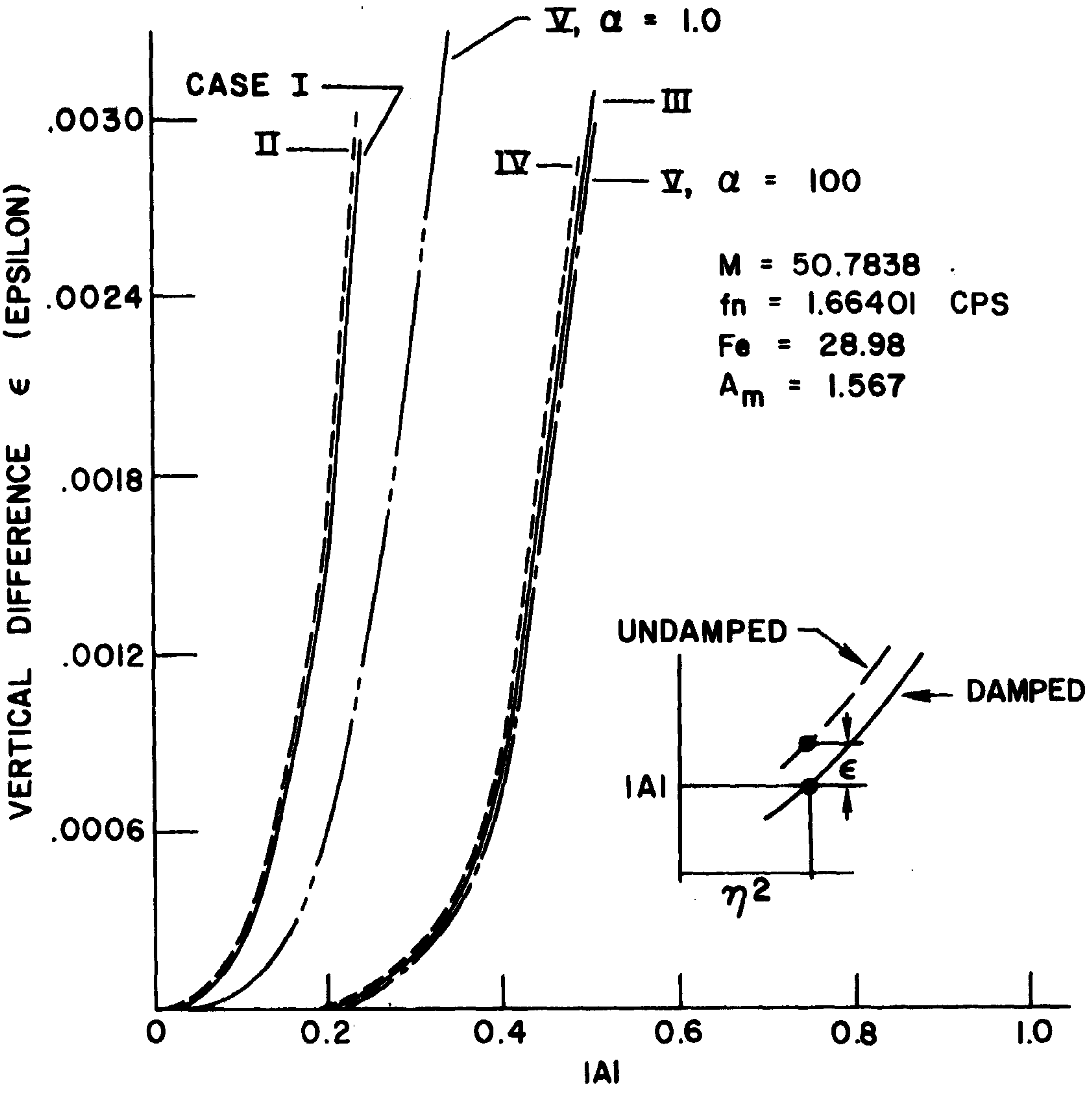

FIG. 4.8 VERTICAL DIFFERENCE (ε) VERSUS AMPLITUDE - FIRST MODE

Therefore,

$$\frac{F_e}{M\omega_n^2 A} \doteq 1 - \eta^2, \; A << A_m \qquad (4.2.9)$$

For example, with A = 1.01 and Case I damping; δ = .001209, where the distance to the undamped curve is .005404 for Configuration II first mode Sweep C. Thus, the conclusion is that the system can be considered undamped for $A << A_m$. Figure (4.9) illustrates the maximum percent error (Case I) in using the undamped curve for different amplitude ratios. A practical limit of $A/A_m = .5$ for neglecting damping represents a maximum error of 14 percent when Eq. (4.2.9) is used instead of Eq. (4.2.4) with linear viscous damping.

For $A < .5A_m$ the experimental data is not accurate enough to distinguish the damped from the undamped curves. Thus, only in a very narrow band of frequency ratio (say $.992 < \eta^2 < 1.008$) is damping a significant factor. However, with amplitudes near maximum, the damping is very significant. That is, as $A \to A_m$ one has $1 - \eta^2 \to 0$ and $\delta \to F_e/M\omega_n^2 A$. Given accurate experimental data near the maximum amplitude, A_m, the most appropriate damping case may be determined.

Sufficient data near A_m was not available from the amplitude versus frequency sweeps for the Configuration I vehicle or the Configuration II vehicle. An illustration of this is shown in Section 3.1 for Configuration I. There are many factors that affect the amplitude versus frequency curves more than the type of system damping. However, those amplitudes near a modal or resonant frequency are greatly influenced by damping; the most influence being at resonance. More data points at or near resonance are desired, for this analytical technique.

One concludes from the above discussion that the three resonant amplitudes of Configuration II vehicle, shown in Table 4.II, can be used as data in lieu of different points on one amplitude versus frequency curve. Figures (4.6) and (4.7) are of no value for this data but Eqs. (4.2.7) can be used to select damping coefficient and the most appropriate modal damping case. A damping case is selected based on (1) its ability to predict maximum amplitudes and (2) the minimum precent variation in each calculated damping coefficient.

Consider the Configuration II vehicle in its first mode (Sweeps A, B, and C, see Table 4.II). In Table 4.IV the damping coefficients $\mathcal{L}_n$ were obtained for Sweep C using Eqs. (4.2.7). Using these same damping coefficients, along with experimental data for M, F_e, and ω_n for Sweeps A and B, the maximum amplitudes A_m' is computed using Eqs. (4.2.7). A comparison of the computed amplitude and actual amplitude is shown in Table 4.IV with the percent error being

$$\frac{A_m' - A_m}{A_m} \times 100 = \text{percent error}$$

Indications are that Case V with $\alpha = 1.0$, or

$$g(Q, \dot{Q}) = C_1(\dot{Q} + Q^2\dot{Q}) \qquad (4.2.10)$$

is the best damping case from the five possibilities studied. The coefficient

$$C_1 = 2\,\mathcal{L}_1 M\omega_n = 0.5486 \text{ and}$$

$$\boxed{g_F(Q, \dot{Q}) = 0.5486\ (\dot{Q} + Q^2\dot{Q})} \qquad (4.2.11)$$

is obtained, which agrees with previous results where Case I plus Case IV was used in Section 4.1.

An alternate method exists for evaluating which case of damping is most appropriate using the three sweeps. With the modal amplitude A_m known, a set of damping coefficients, $\mathcal{L}_n$, can be calculated for each Sweep A, B, and C. These results are shown in the Table 4.V. The coefficient with least percent variation determines the most appropriate damping term. The same conclusions as above are obtained.

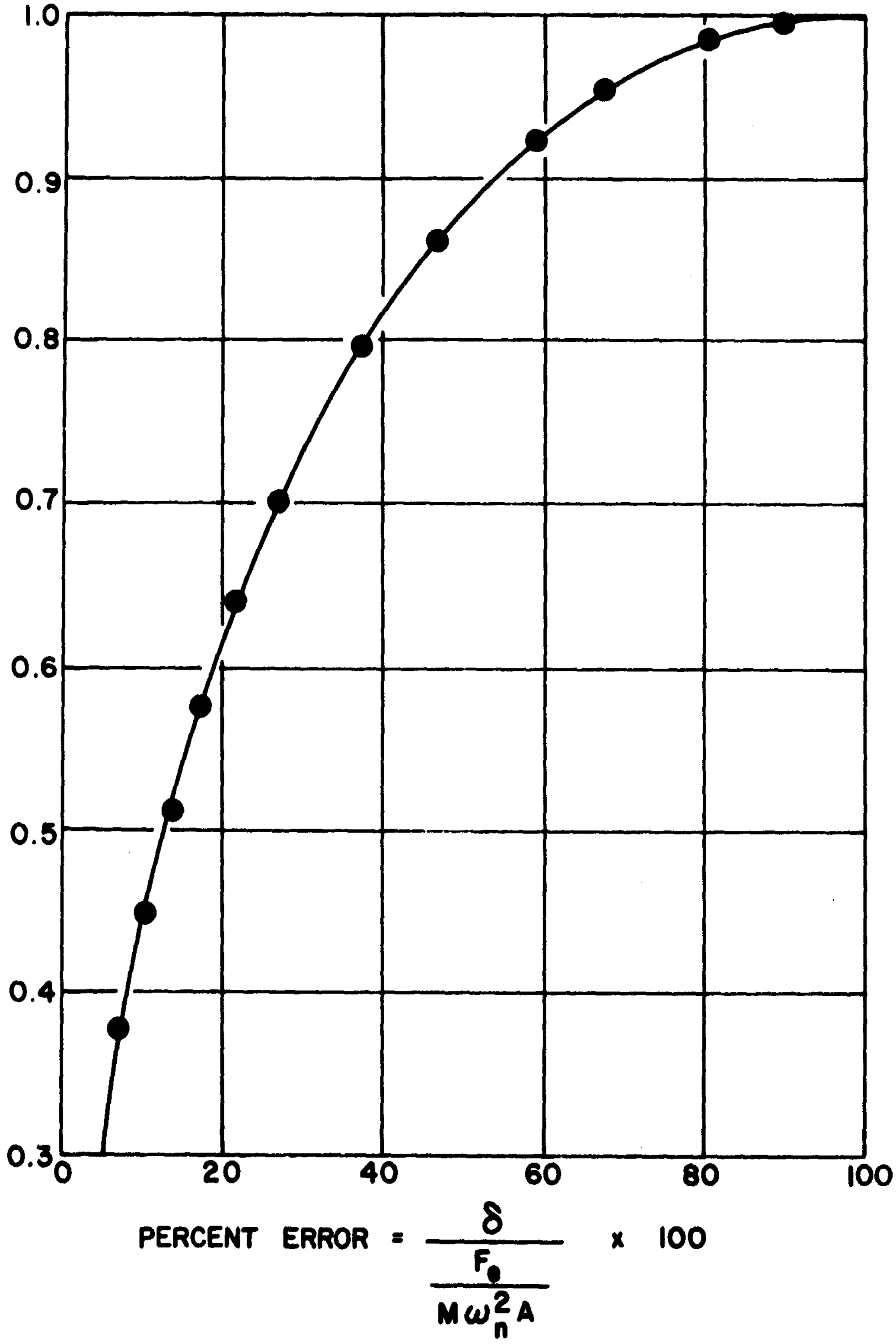

FIG. 4.9 MAXIMUM PERCENT ERROR AT CONSTANT AMPLITUDE BETWEEN DAMPED AND UNDAMPED CURVES

TABLE 4.IV ERRORS IN USING DAMPING COEFFICIENTS OBTAINED FROM ONE SWEEP TO PREDICT OTHER AMPLITUDES - FIRST MODE

PERCENT ERROR IN MAXIMUM AMPLITUDE							
Case	$\mathcal{L}_n^*$	M	F_e	ω_n	A'_m	A_m	% Error
I	.0016654	48.79	19.37	1.6688	1.085	1.229	- 11.7
II	.02737				1.087		- 11.5
III	.00011996		SWEEP "A"		1.301		+ 5.8
IV	.002507				1.303		+ 6.0
V (α = 1)	.0010332				1.255		+ 2.1
I	.0016654	49.24	24.95	1.6657	1.390	1.439	- 3.4
II	.02737				1.390		- 3.4
III	.001196		SWEEP "B"		1.474		+ 2.4
IV	.002507				1.475		+ 2.5
V (α = 1)	.0010332				1.461		+ 1.5

*Obtained from Sweep C where A_m = 1.567

TABLE 4.V PERCENT VARIATION IN DAMPING COEFFICIENTS CALCULATED FROM VARIOUS SWEEPS - FIRST MODE

VARIATIONS IN DAMPING COEFFICIENTS				
System Parameter	Experimental Data & Computed Damping			Maximum Percent Variation
	Sweep A	Sweep B	Sweep C*	
M	18.79	49.24	50.78	
F_e	19.37	24.95	29.90	
ω_n	1.6688	1.6657	1.6640	
A_m	1.229	1.439	1.567	
$\mathcal{L}_1$	.0014695	.0016071	.0016654	- 11.8%
$\mathcal{L}_2$	.02421	.02643	.02737	- 11.5%
$\mathcal{L}_3$	.0013450	.00012490	.0011996	+ 12.1%
$\mathcal{L}_4$	.002819	.002634	.002507	+ 12.4%
$\mathcal{L}_5$ ($\alpha = 1.0$)	.0010674	.0010600	.0010332	+ 3.3%

*This case was used for $\mathcal{L}_n$ values in the Table 4.IV.

4.3 From an Equivalent Energy Dissipation Function.

From Table 2.II in Chapter II the energy loss per cycle, or energy dissipation, is given as

$$\Delta W/\text{cycle} = C\pi A^2\omega \qquad (4.3.1)$$

with a linear viscous modal damping force $g(Q, \dot{Q}) = C\dot{Q}$ and a steady state amplitude $Q = A \sin(\omega t - \phi)$. The modal damping coefficient as determined in Section 4.I is

$$C_j = \frac{F_e}{\omega_n A_m} \qquad (4.3.2)$$

where the subscript j refers to the j^{th} mode. This equation can also be obtained from the first equation of Eqs. (4.2.7).

After investigating the first four cases of damping in Table 2.I, it is noted that they may be represented by either

$$g(Q, \dot{Q}) = \alpha\left|\frac{dQ}{dt}\right|^p(\text{sign }\dot{Q}),\ p > o \qquad (4.3.3)$$

or

$$g(Q, \dot{Q}) = \alpha|Q|\left|\frac{dQ}{dt}\right|^p(\text{sign }\dot{Q}),\ p > o \qquad (4.3.4)$$

In Cases I through IV the exponent "p" is an even integer. This restriction on the exponent can be relaxed to make these functions even more general. The object is to equate the energy dissipation of Eq. (4.3.1) to that computed for the damping forces above.

The energy dissipation for equation (4.3.3) is

$$\Delta W/\text{cycle} = \int_{\text{cycle}} g(Q, \dot{Q})dQ$$

$$= \frac{1}{\omega}\int_{\text{period}} g(Q, \dot{Q})\dot{Q}d(\omega t) \qquad (4.3.5)$$

Eqs. (4.3.3) and (4.3.4) are substituted into Eq. (4.3.5) with a one term approximation of the nonlinear response as $Q = A \sin(\omega t - \Phi)$. The results for Eq. (4.3.3) is

$$\Delta W/\text{cycle} = 2\sqrt{\pi}\,\alpha A^{p+1}\,\omega^p\,\frac{\Gamma\left(\frac{p+2}{2}\right)}{\Gamma\left(\frac{p+3}{2}\right)} \qquad (4.3.6)$$

and for Eq. (4.3.4) is

$$\Delta W/\text{cycle} = 2\alpha\, A^{p+2}\omega^{p}\, \frac{\Gamma\left(\frac{p+2}{2}\right)}{\Gamma\left(\frac{p+4}{2}\right)} \tag{4.3.7}$$

where Γ refers to Gamma Functions. These are referred to as Energy Dissipation Functions.

The technique to determine the coefficient α and exponent p is to equate energies of the linear damping case to either one of the nonlinear cases at different values of the input force for each mode. Necessary experimental information is available on the Configuration II vehicle first and second modes to allow this technique to be applied.

First, consider the nonlinear damping force to be that of Eq. (4.3.3). Equating the energy dissipation function of Eq. (4.3.1) to that of Eq. (4.3.6) gives

$$\alpha = \beta\, \frac{C}{\omega^{p-1}A^{p-1}}$$

where

$$\beta = \frac{\sqrt{\pi}}{2}\, \frac{\Gamma\left(\frac{p+3}{2}\right)}{\Gamma\left(\frac{p+2}{2}\right)} = \beta(p) \tag{4.3.8}$$

Substituting for the linear damping coefficient, C, as given in Eq. (4.3.2) requires that the energy dissipation be evaluated at the natural modal frequency, $\omega = \omega_n$, where the amplitude is a maximum $A = A_m$. Thus,

$$\alpha = \beta\, \frac{F_e}{\omega_n^{p}A_m^{p}} \tag{4.3.9}$$

There are available at each resonant frequency, or mode, three sets of data for amplitude and force. Letting the subscript r denote each set corresponding to Sweeps A, B, and C.

$$\alpha = \alpha_r = \beta\, \frac{F_{er}}{\omega_n^{p}A_{mr}^{p}}\,, \quad r = 1,2,3 \tag{4.3.10}$$

A properly chosen value of the exponent p will make the damping coefficient α_r relatively constant for any r value. Because β and ω_n^p only vary with p, it is desirable to make

$$\frac{F_{er}}{A_{mr}^p} = \text{constant}, \; r = 1,2,3 \tag{4.3.11}$$

The value of p that does this is the desired exponent in Eq. (4.3.3).

Test data for the first mode is available in Tables 4.I and 4.II. That is,

$$\left.\begin{array}{lll} r = 1, & F_{e1} = 19.37, & A_{m1} = 1.229 \\ r = 2, & F_{e2} = 24.95, & A_{m2} = 1.439 \\ r = 3, & F_{e3} = 28.98, & A_{m3} = 1.567 \end{array}\right\} \tag{4.3.12}$$

Plotting log (F_{er}) versus log (A_{mr}), the slope of this curve is the exponent p. Such a plot is shown in Fig. (4.10). The slope of this straight line is the exponent

$$p = 1.859 \tag{4.3.13}$$

With the exponent known the coefficient α is computed from Eq. (4.3.10) using any r and β calculated from Eq. (4.3.8). That is, with $\omega_n = 10.47$

$$\beta = 1.155$$

and

$$\alpha = 0.1917$$

The damping force for the first (F) node of the Configuration II vehicle can be represented as

$$\boxed{g_F(Q, \dot{Q}) = .1917 \left| \frac{dQ}{dt} \right|^{1.859} (\text{sign } \dot{Q})} \tag{4.3.14}$$

The data for the second mode is also plotted in Fig. (4.10). Following the same procedure as above, the slope of this straight line is

$$p = 1.342 \tag{4.3.15}$$

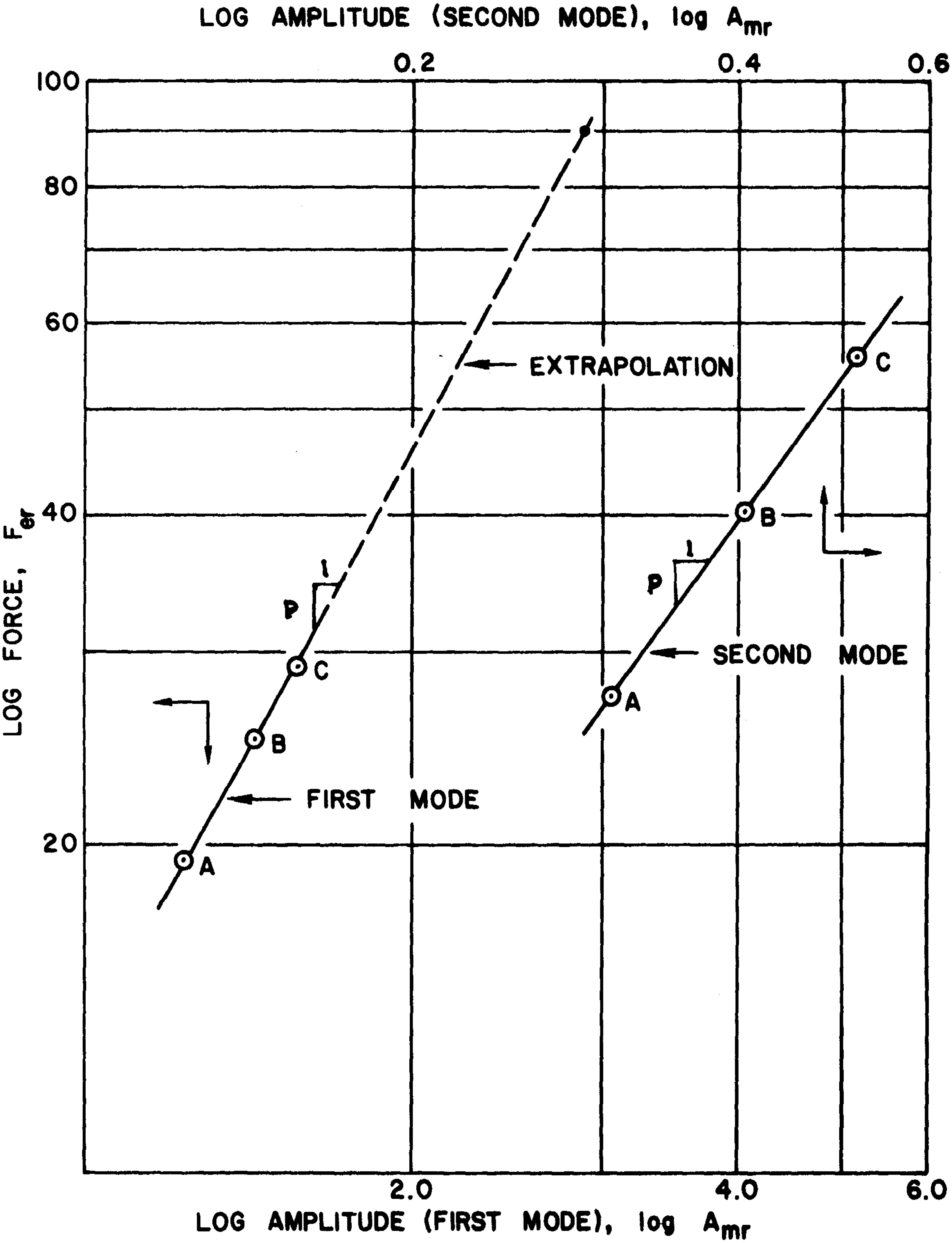

FIG. 4.10 RESONANT FORCE VERSUS AMPLITUDE

The corresponding values of ω_n, β and α are

$$\omega_n = 17.09$$

$$\beta = 1.064$$

$$\alpha = 3.005$$

Thus, the damping force for the second (s) mode of the Configuration II vehicle can be represented as

$$\boxed{g_s(Q, \dot{Q}) = 3.01 \left| \frac{dQ}{dt} \right|^{1.342} (\text{sign } \dot{Q})} \tag{4.3.16}$$

In the above paragraphs the force given by Eq. (4.3.3) was used to describe damping. The same procedure may be followed for Eq. (4.3.4). Equating energy dissipation functions of Eqs. (4.3.1) and (4.3.7) yields

$$\alpha = B \frac{C}{\omega^{p-1} A^p} \tag{4.3.17}$$

where

$$B = \frac{\pi}{2} \frac{\Gamma\left(\frac{p+4}{2}\right)}{\Gamma\left(\frac{p+2}{2}\right)} \tag{4.3.18}$$

Considering the force and amplitudes of resonance, Eq. (4.3.2) is used to substitute for C in Eq. (4.3.17). Therefore

$$\alpha = B \frac{F_e}{\omega_n^p A_m^{p+1}} \tag{4.3.19}$$

For different forces and amplitudes at resonance

$$\alpha_r = B \frac{F_{er}}{\omega_n^p A_{mr}^{p+1}}, \quad r = 1,2,3$$

to correspond to sweeps A, B, and C. Once again a value of the exponent p is chosen so that

$$\frac{F_{er}}{A_{mr}^{p+1}} = \text{constant}, \quad r = 1, 2, 3 \tag{4.3.20}$$

Comparing this equation with Eq. (4.3.11), one notes that P + 1 is now what p was before. Thus, the value of p for the first mode is

$$p = .865$$

and for the second mode is

$$p = .342$$

Calculating the coefficients B using Eq. (4.3.18), and ω_n^p for the same ω_n values as before, gives

$$\alpha = 3.89 \quad \text{FIRST MODE} \tag{4.3.21}$$

$$\alpha = 59.4 \quad \text{SECOND MODE} \tag{4.3.22}$$

Thus, the damping force for the first (F) and second (s) modes of the Configuration II vehicle can be represented as

$$\boxed{g_F(Q, \dot{Q}) = 3.89 \, |Q| \, \left| \frac{dQ}{dt} \right|^{.865} (\text{sign } \dot{Q})} \tag{4.3.23}$$

and

$$\boxed{g_s(Q, \dot{Q}) = 59.4 \, |Q| \, \left| \frac{dQ}{dt} \right|^{.342} (\text{sign } \dot{Q})} \tag{4.3.24}$$

No apparent advantage seems to exist for using Eqs. (4.3.14) and (4.3.16) rather than Eqs. (4.3.23) and 4.3.24). Either set will yield the resonant amplitudes equally well. However, their influence on energy dissipation is different, as shown by Eqs. (4.3.6) and (4.3.7). The relative influence of an amplitude change on energy dissipation is greater than for a frequency change in Eq. (4.3.7) ($A^{p+2}\omega^p$ relative to $A^{p+1}\omega^p$). Where the damping greatly affects the amplitudes is in a narrow band of frequencies near resonant modes, as shown in Section 4.2. Thus, the range of ω is also smaller than the range of A. Therefore, using the equations where energy dissipation is more sensitive to amplitude, A, one should use Eqs. (4.3.23) and (4.3.24).

The amplitude of the resonant response for forces above those used in the experimental test can be obtained by extrapolation. From the equations for the damping coefficients one can solve for A_m as a function of the force F_e. Thus, from Eq. (4.3.9), for example,

$$A_m = \sqrt[p]{\beta \frac{F_e}{\omega_n^p \alpha}} = \frac{1}{\omega_n} \sqrt[p]{\frac{F_e \beta}{\alpha}} \qquad (4.3.25)$$

Only when $p = 1.0$ does amplitude increase linearly with force. For the first mode $p = 1.859$, so the amplitude will not increase as rapidly as the force does. To illustrate this influence on extrapolation, consider the modal force to be 90.0 lbs. For a constant coefficient linear viscous damping ($p = 1.0$) the amplitude $A_m = 4.84$. Extrapolation in Fig. (4.10) shows $A_m = 2.90$. This represents a 67% error in the predicted amplitude. Thus, a grossly overdesigned vehicle may result.

CHAPTER V

AN EMPIRICAL METHOD TO DETERMINE DAMPING FORCE

In the previous chapters the damping force was determined by analytical techniques. The different techniques utilized different parts of the test data. In general, only one or two terms were used to describe the damping force. In this chapter an empirical method is introduced that permits many damping forces to be considered for each mode. The final selection of a few terms to represent damping is based on systematic elimination of many possibilities. As much test data as desired can be used to make the selection.

The method is based on a set of data points for amplitude, A, frequency, ω, and energy loss or input, E. A polynomial in amplitude and frequency is chosen to represent the energy loss of the system. Coefficients of the polynomial are obtained from a computer program. That is, a three dimensional surface that contains or approximates the data points is obtained. Each term in the energy loss polynomial is related to an analytical representation of damping. Also, statistical data on how accurately each term and each set of terms approximate the data is obtained from the computer program.

Data used for this empirical method is that for the Configuration 1 vehicle shown in Chapter III. Numerical results show good agreement with analytical techniques.

5.1 The Polynomial Representation of Energy Loss per Cycle.

The energy loss per cycle or energy dissipation due to different modal damping forces was discussed previously in Section (2.3). Due to the complexity of the Saturn V vehicle, it is likely that many sources of damping are present. To say that the modal damping force can be represented by a single term is to say that this source of damping is predominant and other sources are relatively insignificant. Whatever the damping may be, an empirical method can decide what the modal force or forces should be.

Investigating Table 2.II, it is obvious that authors are attempting to make energy loss per cycle dependent on different powers of modal amplitude (A) and frequency (ω). As a result, the analytical representations of damping have resulted as shown in Table 2.I. The result of all sources or cases of damping being present is that energy loss per cycle is an albegraic sum of each. Furthermore, the energy loss per cycle, ΔW/cycle, due to damping equals the external input energy supplied to the system by the external force, or as discussed in Section (3.2),

$$\Delta W/\text{cycle} = E = \int_{\text{cycle}} \frac{F_c}{M} \sin \omega t \, dQ \qquad (5.1.1)$$

If enough damping terms are present one can complete the spectrum on powers of amplitude and frequency as follows:

$$\Delta W/\text{cycle} = a_1A^2 + a_2A^2\omega + a_3A^2\omega^2$$

$$+ \; a_4A^3 + a_5A^3\omega + a_6A^3\omega^2 + \ldots = E(A,\omega) \qquad (5.1.2)$$

Each term on the left results from a certain representation of modal damping force $g(Q, \dot{Q})$.

The coefficients a_i in Eq. (5.1.2) can be determined emperically if sufficient data points are available. Experimental data is obtained for each mode, as shown in Section 3.1, and the amplitude A, frequency ω (near resonance), and energy input, E are calculated. Thus, points (A, ω, E) are obtained on a three-dimensional plot. The object is to fit a surface describing energy as a polynomial in amplitude and frequency, E(A, ω), Eq. (5.1.2), to the set of data points. The relative magnitude of the coefficients a_i will show what terms in Eq. (5.1.2) are significant. A computer program has been obtained and modified for the Univac 1108. The original program, obtained from SHARE program catalog, was called "Multivariate Regression Program I" and is discussed in the following section. The input to this program is the set of data points (A, ω, E) and the form of the polynomial E(A, ω) to represent the left side of Eq. (5.1.2). Thus, E(A, ω) is made to fit the data points. First, the program tries to fit the data with each single term in E(A, ω) and orders the terms based on a statistical goodness-of-fit. Next the program fits the data with the total polynomial E(A, ω) and selects coefficients of each term for a best fit. The order of importance of the terms are given based on a statistical T-ratio test. Finally, a table is given to show the percent error in fitting the surface E(A, ω) to the data points (A, ω, E).

Figure 5.1 shows the energy surface as a function of amplitude and frequency E(A, ω) where fifteen data points (A, ω, E) are fitted with zero error. Energy losses, available from experimental tests, for five amplitude values at each frequency near or at resonance are shown. The energy loss function is selected and the curve fit program yields coefficients of the damping terms. Table 5.I shows the conversion factors from the coefficients of energy terms to the damping force coefficient; for the five cases shown in Table 2.I.

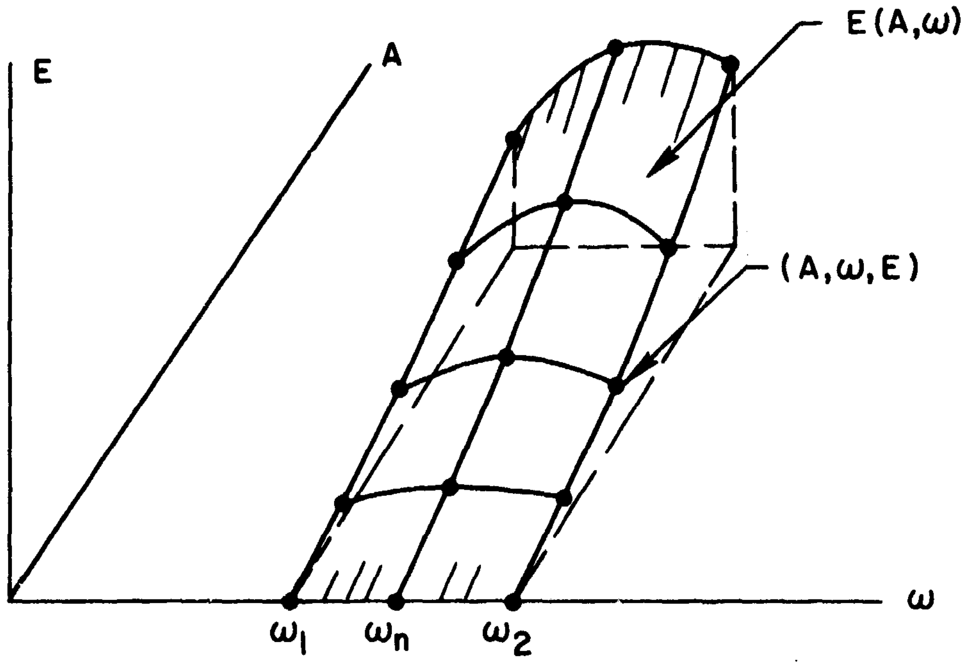

FIG. 5.1 ENERGY LOSS VERSUS AMPLITUDE AND FREQUENCY

TABLE 5.I DAMPING COEFFICIENTS FROM ENERGY TERMS

CASE	DAMPING FORCE $g(Q, \dot{Q})$	ENERGY TERMS IN $E(A, \omega)$	DAMPING COEFFICIENT C_i
I	$C_1\dot{Q}$	$a_1A^2\omega$	$C_1 = a_1/\pi$
II	$C_2\lvert Q\rvert(\text{sign }\dot{Q})$	a_2A^2	$C_2 = a_2/2$
III	$C_3(\dot{Q})^2(\text{sign }\dot{Q})$	$a_3A^3\omega^2$	$C_3 = 3a_3/8$
IV	$C_4\lvert Q\rvert\dot{Q}$	$a_4A^3\omega$	$C_4 = 3a_4/4$
V	$C_5Q^2\dot{Q}$	$a_5A^4\omega$	$C_5 = 4a_5/\pi$

One could also invent other damping forces $g(Q, \dot{Q})$ to complete the spectrum of the polynomial $E(A, \omega)$. Also, if fractional powers were used, the damping terms of Eqs. (4.3.3) and (4.3.4) could be obtained.

In the following section the details of the curve fitting program are discussed. The statistical tests used to evaluate the results of the curve fit are also briefly discussed.

5.2 Program to Compute Damping Coefficients.

The object of this program is to define a surface, which is described by a sum of terms each being a function of the independent variables, which will best contain a given set of data points. For this study, the data points are energy loss values as a function of amplitude (A) and frequency (ω). The terms $[\phi_k(A,\omega)]$ are energy loss functions each due to a different source of damping being present. The object is to obtain the best fit of the sum of terms (energy losses).

$$\sum_{k=1}^{n} a_k \phi_k(A,\omega) \tag{5.2.1}$$

to the set of data points obtained experimentally.

To satisfy this objective program SDA 3104 from the Share Program Library has been obtained. This program was prepared by the Department of Navy, David Taylor Model Basin, and is entitled, "Multivariate Regression Program I." However, this program was much too extensive, required computing hardware not available, and was written in Fortran II language. Thus, considerable revision in this program has been required. In the following paragraphs the main features of the revised program are discussed.

The program must be given a series of m observations which have been made on p variables X_i, $i = 1, 2, \ldots, p$, where an "observation" is an ordered p-tuple of observedly coincident values of the variables. Hence, the j^{th} observation is

$$(X_{1j}, X_{2j}, X_{3j}, \ldots, X_{pj}) = Q_j \qquad (5.2.2)$$

A series of transformations are to be made on each observation so that

$$I = [\phi_1(Q_j), \phi_2(Q_j), \ldots, \phi_n(Q_j), E(Q_j)] \qquad (5.2.3)$$

The transformation $E(Q_j)$ is to be distinguished from the $\phi(Q_j)$ because E is considered to be the "dependent" variable; that is, fixed for given values of the "independent"variables ϕ_k. The variable $\overline{E}(Q_j)$ represents the exact $E(Q_j)$ obtained from the j^{th} observation.

The program then determines $A = (a_1, a_2, \ldots, a_n)$ such that

$$\sum_{j=1}^{m} \left\{ \sum_{k=1}^{n} a_k \phi_k(\dot{Q}_j) - \overline{E}(Q_j) \right\}^2 = \text{minimum} \qquad (5.2.4)$$

The program prints out and evaluates the resultant curve fit according to several criteria. The program also optionally prints out certain by-products of the computation including the correlation coefficients for all possible pairs of the transformed variables. Plots of the deviations vs. any of the variables may be made. Provision is made for ease in fitting the same curve on a number of data sets or in fitting a number of curves on the same data set.

For the purpose of a statistical evaluation of the curve fit the program gives the following information:

$$\sum_{j=1}^{m} \phi_i(Q_j) \quad . \qquad \text{"Sum"}$$

$$\bar{\phi}_i(Q_j) = \frac{1}{m}\ (\text{sum})$$ "Average value"

$$\sigma_{\phi i} = \sqrt{\frac{1}{m} \sum_{j=1}^{m} [\phi_i(Q_j) - \bar{\phi}_i(Q_j)]^2}$$ "Standard Deviation"

$$\sum_{j=1}^{m} \phi_i^2(Q_j)$$ "Sum of Squares"

A comparison of the significance of one term fits is also obtained. This is a listing in decreasing order of importance the variables ϕ_i and their significance as an indicator of E when taken by themselves. The program also tries to fit a plane to the data points and independent variables read in.

Furthermore, a "goodness-of-fit" table is printed out containing such information as

$$\sum_{j=1}^{m} [E(Q_j)]\ , \quad \sum_{j=1}^{m} [\bar{E}(Q_j)]\ , \quad \sum_{j=1}^{m} [E(Q_j) - \bar{E}(Q_j)]$$

$$\sum_{j=1}^{m} [E(Q_j)]^2, \quad \sum_{j=1}^{m} [\bar{E}(Q_j)]^2, \quad \sum_{j=1}^{m} [E(Q_j) - \bar{E}(Q_j)]^2$$

and so on. The values of a_k, the regression coefficients of ϕ_k, are printed out along with their standard error. Another list is also made where the variables ϕ_k are printed out in decending order of importance as measured by the T-ratio test. A number of other criteria of the regression are calculated and printed out. They are:

a) Root-mean-square error
b) The average absolute deviation
c) The average absolute precent of deviation
d) The standard error of the regression
e) The largest absolute deviation

f) The largest absolute percent of deviation
g) The square of the correlation coefficient
h) The correction coefficient, fitted curve versus observed curve
i) A table breaking down the observations by number and by percent.

For the damping study of the Saturn V missile system, certain dependent and independent variables are defined for the above general curve-fit program. There are two variables X_i, $i = 1,2$. which are the amplitude (A) and frequency (ω). Thus, for Eq. (5.2.2) $X_1 = A$ and $X_2 = \omega$ giving

$$(A, \omega) = Q_j$$

The transformations on these observations $\phi_k(A, \omega)$ represent the energy loss per cycle. This is,

$$\phi_1 = A^2$$

$$\phi_2 = A^2\omega$$

$$\phi_3 = A^3\omega$$

$$\phi_4 = A^3\omega^2$$

represent a set of transformations previously obtained for typical systems. Logically other terms could be added to this set as studies of the vehicle system may indicate. The dependent variable is the energy loss per cycle; a linear combination of ϕ functions. Thus, as shown by Eq. (5.2.1.),

$$E(A, \omega) = a_1\phi_1 + a_2\phi_2 + a_3\phi_3 + \ldots \qquad (5.2.5)$$

makes the set of functions shown in Eq. (5.2.3) complete.

The m observations of the two variables (A, ω) and the total energy loss E are input data obtained from experimental studies. With this input the coefficients a_k are calculated according to Eq. (5.2.4). These coefficients are in turn linearly related to the coefficients of the damping term in the equation of motion for the system, see Table 5.I.

The program proceeds to fit the sum of functions given by Eq. (5.2.1) to the experimental data. It evaluates this fit by performing statistical studies. Of significant importance in these studies is a comparison of one-term fits and a listing in order of importance the ϕ_k variables. Another result of these studies shows ϕ_k variables in descending order of importance.

For future efforts in checking this program, a set of reasonable data with known results will be selected and the curve-fit program executed. The results that the program should yield will be known in advance, and whether these results are reproduced or not will be the check. Furthermore, numerical results for the Configuration I vehicle are obtained with data available from Chapter III.

A printout of the computer program, instructions for input data, and the output format will be provided by the University of Alabama in Huntsville Research Institute upon request.

5.3 Numerical Results for Empirical Damping

To check-out the computer program, a fictitious set of experimental data is calculated and two polynomials in amplitude and frequency are used to approximate this data. For the first step, a set of 14 energy loss values, $E(A, \omega) = E$, were calculated from

$$1.571\ A^2\omega + 1.067\ A^3\omega = E$$

with increasing ω and a bell-shaped distribution for A. The program was asked to fit these data points (E, A, ω) with the true energy loss expression

$$E(A, \omega) = a_1\phi_1 + a_2\phi_2 \qquad (5.3.1)$$

where the transformations or polynomials are

$$\phi_1 = A^2\omega$$

$$\phi_2 = A^3\omega$$

The results of the regression program, or curve-fit program, gave

$$a_1 = 1.571$$

$$a_2 = 1.066$$

which agrees with the calculated input data. Furthermore, the significance of one-term fits showed ϕ_1 to be more significant than ϕ_2; with the same ordering for the T-ratio test.

If the same set of data points is used, and the five term expression for energy loss per cycle

$$E(A, \omega) = a_1\phi_1 + a_2\phi_2 + a_3\phi_3 + a_4\phi_4 + a_5\phi_5 \tag{5.3.2}$$

is used to fit this data, with ϕ_1 and ϕ_2 the same and

$$\phi_3 = A^3\omega^2$$

$$\phi_4 = A^2$$

$$\phi_5 = A^4\omega$$

the results are similar. However, coefficients a_1 and a_2 are reduced and the other coefficients are given some small value. That is, the computer program shows the following order of significance and corresponding coefficient values

$$E(A, \omega) = 1.455\ A^2\omega + .827\ A^3\omega + .1179\ A^3\omega^2 + .222\ A^2 + .0223\ A^4\omega \tag{5.3.3}$$

The coefficients should be $a_1 = 1.571$, $a_2 = 1.067$ and the remaining coefficients zero. This illustrates the inaccuracy in assuming energy losses that are actually not present in the system; a fact that will be recorded for later interpretation. However, it is concluded that the curve-fit program is functioning properly, and can predict the damping. It should be noted that the percent error in fitting the data points using the second (not accurate) polynomial was more than twice what it was using the true polynomial. Thus, the polynomial which yields the greatest accuracy indicates the damping terms which should be included in the modal equation of motion. Table 5.II shows the data (ω, A, E) and the percent deviation in E using Eq. (5.3.3). The percent deviation is small even with the less accurate polynomial.

TABLE 5.II NUMERICAL RESULTS FOR CHECK-OUT DATA

ω	A	E	$E(A,\omega)^*$	% DEVIATION
1.500	.800	2.329	2.324	.221
1.520	.860	2.790	2.792	-.057
1.540	.920	3.320	3.318	.061
1.560	.970	3.830	3.816	.377
1.580	1.020	4.360	4.361	-.015
1.600	1.040	4.940	4.958	-.357
1.620	1.120	5.610	5.609	.014
1.640	1.180	6.450	6.453	-.053
1.660	1.230	7.230	7.234	.085
1.680	1.170	6.480	6.479	.008
1.700	1.110	5.770	5.768	.026
1.720	1.060	5.220	5.221	-.018
1.740	1.010	4.690	4.700	-.223
1.760	.950	4.110	4.104	.139

*From Eq. (5.3.3)

With the computer program checked-out, the numerical results for the Saturn V Configuration I vehicle will be obtained. The experimental test data for this vehicle are shown in Chapter III. Furthermore, this data is for the second bending mode.

First, the modal amplitude values obtained directly from the tail displacements X_t in Table 3.I as

$$\bar{A}_2 = \frac{X_t}{\phi_{t2}} = \frac{X_t}{0.041} \tag{5.3.4}$$

are used. This is similar to Eq. (3.1.23) but does not allow for corrections due to phase changes, rigid body motion, and adjacent modes. The input frequency, ω, and energy, $E = \Delta W/\text{cycle}$, are given in Table 3.IV . The energy loss polynomial, $E(A, \omega)$, is now chosen to be used in the computer program as

$$E(A, \omega) = \sum_{k=1}^{n} a_k \phi_k(A, \omega) \tag{5.3.5}$$

The program yields the most significant energy loss terms and their corresponding coefficients, a_k.

At this point it is helpful to discuss the selection of Eq. (5.3.5) in more detail. The most general polynomial used was as follows:

$$\begin{aligned} E(A, \omega) &= a_1 A^2 \omega + a_2 A^2 + a_3 A^3 \omega^2 \\ &+ a_4 A^3 \omega + a_5 A^4 \omega + a_6 A \\ &+ a_7 A^3 + a_8 A^4 + a_9 A^2 \omega^2 \end{aligned} \tag{5.3.6}$$

The first five terms are for the damping forces shown in Table 2.I, or Table 5.I, and the remaining are considered to complete a spectrum of powers on A and ω. When attempting to use the nine term polynomial to the very rough data discussed above, negative coefficients resulted. However, the program gives two indications of those terms which best fit the data. By repeating the procedure with the few terms of most significance a new set of improved results occur. Repeating this again one can obtain a good energy loss polynomial with only one or two terms in it. Furthermore, a danger exists in including energy losses in the polynomial which do not exist in the system. This was illustrated in the check-out data.

For the roughly calculated modal amplitudes given by Eq. (5.3.4) it is desirable to assume an energy loss polynomial with only one or two terms. That is, there are many things, such as modal coupling, that are affecting the amplitude more than damping. However, it is interesting to compare results on this very rough data with the analytical results for linear viscous damping of Chapter III, and the results for improved or conditioned data shown below. For this purpose, two energy loss polynomials

$$E_1(A, \omega) = a_1 A^2 \omega + a_4 A^3 \omega \tag{5.3.7}$$

$$E_2(A, \omega) = a_1 A^2 \omega \tag{5.3.8}$$

are considered. The computer results of this study are shown in Table 5.III. The computer program gave the energy polynomials.

$$\left.\begin{aligned} E_1(A, \omega) &= 5.221\ A^2\omega + 5.538\ A^3\omega \\ E_2(A, \omega) &= 9.942\ A^2\omega \end{aligned}\right\} \tag{5.3.9}$$

with the $A^2\omega$ term in E_1 being more significant than $A^3\omega$. The percent deviation for E_2 is shown to be fairly good near frequencies where damping is important.

TABLE 5.III COMPUTED ENERGY LOSS AND PERCENT DEVIATION FOR ROUGH MODAL DATA

ω	$\overline{A}_2$	E	$E_1(A,\omega)$	$E_2(A,\omega)$	% DEVIATION for E_2
11.17	.209	5.75	3.11	4.85	21.76
11.20	.239	6.87	4.18	6.36	14.05
11.235	.305	10.6	7.22	10.39	17.53
11.27	.367	16.7	11.08	15.17	9.14
11.30	.445	25.8	17.20	22.25	13.77
11.33	.598	43.0	34.57	40.28	6.32
11.36	.886	91.0	90.06	88.46	2.79
11.39	.971	114.5	113.82	106.77	6.75
11.42	.896	102.7	93.10	90.95	11.44
11.455	.901	95.8	94.43	92.04	3.92
11.49	.868	81.0	86.81	86.06	- 6.25
11.52	.783	59.4	67.50	70.21	- 18.21
11.55	.7025	46.0	51.93	56.66	- 23.19
11.58	.614	31.9	37.64	43.40	- 34.79
11.61	.553	23.6	29.41	35.30	- 52.15

The corresponding damping forces for the energy loss polynomials in Eq. (5.3.9) can be obtained from Table 5.I. Thus, for the Configuration I vehicle second mode

$$\boxed{g_s(Q,\ \dot{Q}) = 1.66\ \dot{Q} + 4.15|Q|\dot{Q}} \qquad (5.3.10)$$

or

$$\boxed{g_s(Q,\ \dot{Q}) = 3.165\ \dot{Q}} \qquad (5.3.11)$$

is the empirically determined damping force. Surprisingly, the damping force of Eq. (5.3.11) compares very well with the results of Section (3.2) given by Eq. (3.2.19).

Finally, an improved set of experimental data is used to obtain empirical equations for damping. The data shown in Table 5.IV, for the Configuration I vehicle second mode, has been corrected for pitch and yaw coupling assuming that the linear damping factor varies with frequency. The computer program may be used to obtain the energy loss polynomial which approximates the data points ($A_{2\bar{p}}$, ω, $E_{\bar{p}}$) for the principle pitch motion. Based on rough data, the amplitude squared times frequency term was shown to be reasonably accurate. Thus, the two polynomials from Eq. (5.3.6) used to approximate the energy loss are

$$E_3(A, \omega) = a_1 A^2 \omega + a_3 A^3 \omega^2 \qquad (5.3.12)$$

$$E_4(A, \omega) = a_3 A^3 \omega^2 \quad \text{(DATA POINTS 4 THRU 12 ONLY)} \qquad (5.3.13)$$

which allows for the dependence of damping force on velocity squared. Table 5.IV shows the results of the computer program. The smallest percent deviations shown in the table were for E_4 near the resonant frequency.

The computer program gave

$$E_3(A, \omega) = 1.17\, A^2 \omega + .604\, A^3 \omega^2 \qquad (5.3.14)$$

$$E_4(A, \omega) = .707\, A^3 \omega^2 \qquad (5.3.15)$$

with the $A^3\omega^2$ term being more significant in the E_3 polynomial. The damping forces can be obtained by the conversion factors shown in Table 5.I. Thus, for the Configuration I vehicle second mode

$$\boxed{g_s(Q, \dot{Q}) = 0.373\, \dot{Q} + 0.230\, (\dot{Q})^2 (\text{sign}\ \dot{Q})} \qquad (5.3.16)$$

or

$$\boxed{g_s(Q, \dot{Q}) = 0.265 (\dot{Q})^2 (\text{sign}\ \dot{Q})} \qquad (5.3.17)$$

is the empirically determined damping force. Results show that Eq. (5.3.17) yields the most accurate results. To compare with the results of Section 3.2 where $g_s(Q, \dot{Q}) = 2.30\ \dot{Q}$, the computer program gave $g_s(Q, \dot{Q}) = 2.39\ \dot{Q}$ which is in good agreement. However, deviations were much larger than for Eq. (5.3.17).

Other modes and vehicle configurations can be studied by this empirical method. The computer program is easily applied and has considerable flexibility in choosing the most appropriate damping terms.

TABLE 5.IV COMPUTED ENERGY LOSS AND PERCENT DEVIATION FOR PRINCIPLE PITCH DATA

ω	$A_{2\bar{p}}$	E	$E_3(A,\omega)$	$E_4(A,\omega)$	% DEVIATION for E_4
11.17	.310	5.05	3.50		
11.20	.364	6.11	5.40		
11.235	.438	9.55	8.94		
11.27	.552	14.90	16.93	15.11	- 1.4
11.30	.690	24.00	31.65	29.67	- 23.6
11.33†	.885	50.60	64.16	62.94	- 24.4
11.36	.974	85.50	88.70	88.58	- 2.1
11.39	1.025	106.10	98.44	98.83	6.8
11.42†	1.010	100.50	94.84	95.05	5.4
11.455	.923	73.50	73.78	73.00	0.7
11.49	.719	29.40	36.61	34.71	- 18.1
11.52	.546	22.20	17.08	15.28	10.1
11.55	.421	21.60	8.14		
11.58	.343	18.80	4.86		
11.61	.310	13.75	3.73		

†corrected experimental data

CHAPTER VI

SUMMARY AND CONCLUSIONS

Although each chapter and section contains its own summary, it is desirable to collect all results into one summary. Different analytical techniques for different Saturn V - Apollo vehicles are used. These are discussed and referenced for ease in referring to detailed discussions. Also, a new and very useful empirical method is summarized. In each case the experimental test data influences the amount and type of information possible for determining the damping force. The type of test data available is summarized and a discussion of desired test results is given.

It is concluded that nonlinear damping is present in the Saturn V vehicle and it can be predicted.

6.1 Modal Damping Force Summary.

Modal damping forces have been obtained using different analytical techniques as well as an empirical method. These forces are to be used in the modal equation of motion given by Eq. (2.2.5). Only the first and second modes of the 500-D Saturn V dynamic test vehicle were investigated. However, the methodology may be applied to higher modes without modification.

Both the Configuration I and Configuration II vehicles were studied. These configurations are discussed in Chapter II. Not all techniques were used on each configuration. Some dependence of analytical technique on the type and amount of test data exists. This dependence will be discussed in the following section. Hysteretic or structural damping can be represented by velocity squared damping (see Section 2.4).

A summary of the modal damping forces are as follows:

Configuration I vehicle - second mode

$$g_s(Q, \dot{Q}) = 2.30\,\dot{Q} \tag{3.2.19}$$

$$g_s(Q, \dot{Q}) = 1.66\,\dot{Q} + 4.15|Q|\dot{Q} \tag{5.3.10}$$

$$g_s(Q, \dot{Q}) = 3.165\,\dot{Q} \tag{5.3.11}$$

$$g_s(Q, \dot{Q}) = .373\,\dot{Q} + .230\,(\dot{Q})^2(\text{sign}\,\dot{Q}) \tag{5.3.16}$$

$$g_s(Q, \dot{Q}) = .265(\dot{Q})^2\,(\text{sign}\,\dot{Q}) \tag{5.3.17}$$

Configuration II vehicle - first and second modes

$$g_F(Q, \dot{Q}) = 1.643\,\dot{Q} \tag{4.1.8}$$

$$g_F(Q, \dot{Q}) = .506\,\dot{Q} + 1.886|Q|\dot{Q} \tag{4.1.14}$$

$$g_F(Q, \dot{Q}) = .5486\,\dot{Q} + .5486\,Q^2\dot{Q} \tag{4.2.11}$$

$$g_F(Q, \dot{Q}) = .1917|\dot{Q}|^{1.859}(\text{sign}\,\dot{Q}) \tag{4.3.14}$$

$$g_F(Q, \dot{Q}) = 3.89\,|Q|\,|\dot{Q}|^{.865}(\text{sign}\,\dot{Q}) \tag{4.3.23}$$

$$g_s(Q, \dot{Q}) = 5.797\,\dot{Q} \tag{4.1.8}$$

$$g_s(Q, \dot{Q}) = 3.715\,\dot{Q} + 12.08|Q|\dot{Q} \tag{4.1.15}$$

$$g_s(Q, \dot{Q}) = 3.01|\dot{Q}|^{1.342}(\text{sign}\,\dot{Q}) \tag{4.3.16}$$

$$g_s(Q, \dot{Q}) = 59.4|Q|\,|\dot{Q}|^{.342}(\text{sign}\,\dot{Q}) \tag{4.3.24}$$

Damping forces for the Configuration I vehicle were obtained in Chapters III and V. In Chapter III the vehicle was assumed to have linear viscous damping, and great care was observed in obtaining an error free average damping coefficient (ξ = .005) for the second mode. Actually, the linear coefficient was found to vary with frequency. Variations with amplitude, or force, may also be present, but data was not available to evaluate this possible variation. In Chapter V an empirical method to determine first mode damping was used. With this method the damping force, or forces, are selected so that the energy dissipation equals the input energy. A very general expression of modal damping may be assumed, and the computer program that equates energies is used to decide which damping forces are significant.

Damping forces for the Configuration II vehicle are obtained in Chapter IV. In this chapter three analytical techniques are used which permit the damping force to be nonlinear. Each method utilizes the input energy and the peak resonant amplitudes at different force levels. In the first method of Section 4.1 an amplitude dependent linear damping coefficient is substituted into the energy dissipation function. This results in a constant coefficient energy dissipation function that would result from a linear plus a nonlinear damping force. In the second method of Section 4.2 the shape of the amplitude versus frequency curve is shown to change with different damping forces. Also, relationships between the maximum modal peak or resonant amplitudes and the damping coefficients for different damping forces were obtained. The damping force that predicts the resonant amplitudes with least variation in this coefficient is the best one to use. The third method of Section 4.3 assumes a nonlinear damping force which is either the velocity raised to an unknown power or amplitude times velocity to an unknown power. The coefficient and exponent of the damping force is chosen knowing the energy dissipation and resonant amplitudes.

Damping force of the velocity squared type was detected. Thus, one concludes that slip damping is a major contributor at the amplitudes tested.

6.2 Experimental Test Data Summary.

The object of this section is to summarize the type of test data that was available and its utilization in determining the modal damping forces. The test data was made available by The Boeing Company through the cooperation of the sponsor, and by graduate students at U.A.H. who were employed by The Boeing Company.

The types of test data that are utilized in obtaining the modal damping force are summarized as follows:

1. The resonant amplitudes and corresponding modal frequencies.
2. The energy dissipation and energy input per cycle.
3. The shape of the modal amplitude versus frequency curves.

Furthermore, to convert from nodal output data to modal parameters, the mode shape factors ϕ_{ij} are utilized. The modal mass M_j may be either calculated or determined from test data. The types of test data are listed in decreasing order of importance as utilized in this study.

Modal test data may contain extraneous information that is undesirable when attempting to determine the damping force. This is illustrated in Chapter III, Section 3.1. In this section the nodal displacements of the Configuration I vehicle tail were converted to modal displacements and corrected for rigid body rotations and adjacent modal displacements. However, the results still contained the influence of planar pitch and yaw coupling. The natural modal frequency in pitch is different than in yaw, and the coupling produces an unsymmetrical or warped amplitude versus frequency curve.

However, once the principle pitch and yaw modal frequencies are known the motion can be uncoupled. A method for determining principle pitch and yaw frequencies and the damping coefficient is shown. Actually the planar coupling may be used to advantage; as principle pitch and yaw modal parameters can be determined from one test.

It may be concluded from the discussion above that rigid body rotation, adjacent modes, and planar coupling have a significant influence on the amplitude versus frequency curve shape. In Chapter IV, Section 4.2 , the influence of damping on the shape of this curve is investigated. It is shown that damping is only significant near each modal frequency and that accurate test data is required to be able to tell what damping force should be used. The test data available was not considered accurate enough, but may become accurate when planar coupling is removed.

The test data available for the Configuration II vehicle was much more useful than for the Configuration I vehicle. That is, many more data points were available near each resonant mode. This was due to the fact that three frequency sweeps were made at three different force levels. This modal test data is shown in Chapter IV, Table 4.I. However, modifications in the raw data accelerometer readings were necessary to obtain this data. These accelerometer readings were considered to be good if they had their maximum values at the resonant frequency; regardless of what that reading was. For two accelerometers out of the approximately twenty that were averaged to obtain modal parameters, the readings were obviously in error. The modal damping was predictable and logical after these readings were removed.

A general observation of the test data shows that tests were conducted at what appears to be quite low bending amplitudes. Whether calculated results for modal damping can be used to accurately predict near resonant amplitudes above those used to obtain the damping is speculative. If the same sources of damping are present at the same relative magnitudes, no problem exists.

6.3 Conclusions.

It is concluded that damping of the Saturn V vehicle can be predicted with reasonable accuracy. Different analytical techniques may be used to obtain the damping force. Each has its own advantages and disadvantages depending on the experimental test data available, east of application, accuracy of results, and its ability to be extended. An empirical method is also used which has a broad application; capable of permitting many sources of damping to occur simultaneously. Conclusions concerning the test data, each analytical technique, the empirical method, and the results for linear and nonlinear damping are discussed below.

The type of experimental test data most useful is amplitude and energy input values at or near each resonant modal frequency. Only near these resonant frequencies is damping a major contributor to the amplitudes (see Section 4.2). Different force levels should be used; as the relationship between force and amplitude is an indication of linear or nonlinear damping, as well as stiffness. With only a single amplitude versus frequency curve, the presence of nonlinear modal damping is difficult to detect. Furthermore, with the bending not being coplanar, the test data is complicated by the presence of planar coupling (see Section 3.1). This coupling is undesirable if pure amplitude versus frequency curves are desired, but may be desirable in obtaining both principle pitch and yaw modal parameters from a single test.

Presently used analytical techniques assume linear viscous damping. This can only yield an equivalent damping coefficient. Many sources of damping such as material damping, fuel sloshing, and slip damping are nonlinear functions. Thus, the linear damping coefficient is not constant and may vary with modal resonant amplitude and/or frequency (see Section 3.2). Each analytical representation of damping has a known energy loss per cycle value; which is a function of amplitude and frequency to different powers (see Section 2.3). Energy loss functions along with the amplitude and frequency dependent linear damping coefficient can be used to derive a constant coefficient nonlinear damping force (see Section 4.1). Similarly, a single term damping force with an unknown coefficient and exponent of the modal velocity or amplitude can be used. The exponent is found so that resonant amplitudes are obtained and the coefficient is selected based on energy dissipation (see Section 4.3).

The empirical method simply assumes energy dissipation to be a polynomial in amplitude and frequency (see Section 5.1). With the input energy equal to the energy dissipation, the coefficients of the polynomial are selected using a computer program (see Section 5.2). The results are that each term in the polynomial is related to a damping force (see Section 5.3). Statistical information from the computer program indicates which damping force or forces best fits the data. It is concluded that this method allows the most freedom in selecting the appropriate damping force, but a danger exists in permitting too many forces to occur. This method is relatively easy to apply once the energy input values are obtained.

The Saturn V Configuration I vehicle has about .5 percent critical damping for its second mode. Both the average linear coefficient and the empirical method gave these results (2.3 $\dot{Q}$). Amplitude dependence could be observed with the test data available; therefore, the best results indicated the damping force $.230|Q|^2(\text{sign } \dot{Q})$ should be added to the linear viscous damping force $.373\ \dot{Q}$.

The Saturn V Configuration II vehicle has about .16 percent critical damping for its first mode, and about .5 percent critical damping for its second mode. These are based on an average linear viscous damping coefficient. Sufficient data was available for this vehicle to permit one to determine a nonlinear damping force. It was determined that either the form $|Q|\dot{Q}$ or $Q^2\dot{Q}$ should be added to the linear damping term $\dot{Q}$. Typical results give for the first mode damping force $.506\ \dot{Q} + 1.886|Q|\dot{Q}$. The best results for a single term nonlinear damping force are: $.1917|\dot{Q}|^{1.859}(\text{sign } \dot{Q})$ for the first mode and $3.01|\dot{Q}|^{1.342}(\text{sign } \dot{Q})$ for the second mode.

It is further concluded that an equivalent viscous damping coefficient cannot be used to accurately predict resonant amplitudes at force levels above those of the experimental test. The result is that the predicted nodal amplitudes will be much higher than actual amplitudes. Fortunately, this is a conservative prediction when stresses are considered. However, the vehicle is overdesigned for stress with nonlinear damping present. A typical example, for the Configuration II vehicle first mode, shows that amplitudes 67 percent larger than actual amplitudes are predicted using linear damping when test results are extrapolated to force levels three times those of the test.

REFERENCES

[1] "Dynamic Test Vehicle Test-Analysis Correlation," Boeing Document D5-15722, November, 1967.

[2] Lowe, J. W., "500-D Vehicle, Yaw Testing, Time Point 11," The Boeing Co. Flash Report No. 35, May, 1967.

[3] Chang, C., "Damping in Multi-Beam Vibration Analyses, Part II - Damping Properties of Saturn I Dynamic Test Vehicle SAD-6," Lockheed Missile and Space Co., TM 54/20-12, November, 1964.

[4] Reed, R. R., "Survey on the Representation of Damping in Structural Dynamics," NASA/MSFC Internal Note, P. & V.E.-S-66-8, July, 1966.

[5] Lazan, B. J., Damping of Materials and Members in Structural Mechanics, Pergamon Press, New York, N. Y., 1968.

[6] McTigue, L. D., and Riley, G. F., "Saturn V DTV Pretest Analysis Methods," The Boeing Co., Document D5-15204, November, 1964.

[7] Foss, K. A., "Co-ordiantes Which Uncouple the Equations of Motion of Damped Linear Dynamic Systems," Journal of Applied Mechanics, Vol. September, 1956.

[8] DaDeppo, D. A., "Damping in Discrete Linear Elastic Systems," Journal of the Engineering Mechanics Division, ASCE, Vol. 89, April, 1963.

[9] Koenig, H. J., and Drain, D. I., "Method of Relating Modal Damping to Local Dampers in Lumped-Parameter Systems," NASA TN D-3637, Lewis Research Center, December, 1966.

[10] Klotter, K. K., "Nonlinear Vibration Problems Treated by the Averaging Method of W. Ritz," First U. S. National Congress of Applied Mechanics, 1951.